DESIGN PRINCIPLES FOR USING DIELECTRIC ELASTOMER TRANSDUCERS APPLIED TO POWERED PROSTHETICS AND ORTHOTICS

by

David P. Allen

APPROVED BY SUPERVISORY COMMITTEE:

Robert D. Gregg, Chair

Walter Voit, Co-Chair

Arif Malik

Yonas Tadesse

Soli Deo gloria

DESIGN PRINCIPLES FOR USING DIELECTRIC ELASTOMER TRANSDUCERS APPLIED TO POWERED PROSTHETICS AND ORTHOTICS

by

DAVID P. ALLEN, BS, MS

DISSERTATION

Presented to the Faculty of

The University of Texas at Dallas

in Partial Fulfillment

of the Requirements

for the Degree of

DOCTOR OF PHILOSOPHY IN

MECHANICAL ENGINEERING

THE UNIVERSITY OF TEXAS AT DALLAS

May 2020

ACKNOWLEDGMENTS

The single name on the title page of this dissertation does not tell the whole story. To borrow from Sir Isaac Newton, "If I have seen further, it is by standing on the shoulders of teammates." Thanks to:

The Polymer Actuation Team for uncounted hours designing, programming, building, and testing the hardware and software for this work.

VSA *phase 1*	VSA *phase 2*	AFO
Alexandre Leboucher	Sophie Farmer	Joshua Laube
Vinnicius Rocha de Lima	Wayne Henricks	Ryan Little
Jorge Cossio	Hannah "Zel" Barber	Jeremy Warren
		Andrew Glick

Edgar Bolívar for helping design the DET VSA and build its testbed. More than that, thanks for being a good friend who happily double-checked my ideas and made them better.

My advisors, Dr. Robert Gregg and Dr. Walter Voit, for believing in me, guiding me through the graduate school process, and providing me resources to complete my work.

Gregory Ellson and Xavier Carrier for polymer design and fabrication in VSA phase 1.

My other labmates in the LocoLab and APRL for being my friends and making my graduate school days pleasant.

My funding sources, the Burroughs Wellcome Fund and the National Science Foundation (award number 1830360).

Forever Faithful Photography for the pictures in Chapter 3.

Cynthia A. Brewer for providing plot color schemes through
`http://www.colorbrewer2.org`

Faith Allen for helping me through the ups, downs, and long nights of graduate school. You were my reason for going to school in the morning, and my reason to come home at night. You are my wife, my love, and my best friend.

My Heavenly Father, the giver of all good things and the ultimate source of my skills and accomplishments.

March 2020

DESIGN PRINCIPLES FOR USING DIELECTRIC ELASTOMER TRANSDUCERS

APPLIED TO POWERED PROSTHETICS AND ORTHOTICS

David P. Allen, PhD
The University of Texas at Dallas, 2020

Supervising Professors: Robert D. Gregg, Chair
Walter Voit, Co-Chair

The advancement of powered prostheses and orthoses is restricted by the shortcomings of available actuator technologies such as electric motors, hydraulics, and pneumatics. Dielectric elastomer transducers (DETs) are a kind of artificial muscle that promises to overcome the shortcomings of the actuators commonly used in powered prostheses and orthoses. However, while much research has investigated how to design DETs themselves for optimal performance, little guidance is available for designing the devices that use DETs in their actuation systems. This work addresses this lack of guidance by reexamining the fundamental principles of DET operation, and then explains four design principles based on those fundamentals. The usefulness of these principles is demonstrated in two example designs that are proofs-of-concept for solutions to actuation challenges. The first design is a variable-stiffness actuator that uses dielectric elastomers to create variable stiffness without the mechanical complexity that plagues state-of-the-art variable-stiffness actuator designs. The second design is an ankle-foot orthosis that uses a dielectric elastomer transducer to provide toe lift assistance for foot drop patients without the drawbacks of current foot drop solutions.

TABLE OF CONTENTS

ACKNOWLEDGMENTS iv
ABSTRACT v
LIST OF FIGURES viii
LIST OF TABLES xiii
LIST OF ABBREVIATIONS xiv
CHAPTER 1 INTRODUCTION 1
1.1 Actuation of powered prostheses and orthoses 1
1.2 Dielectric elastomer transducers 3
1.3 Overview 4
CHAPTER 2 DESIGN PRINCIPLES 5
2.1 How dielectric elastomer transducers work 5
2.2 Derivation and statement of design principles 16
CHAPTER 3 VARIABLE-STIFFNESS ACTUATOR 28
3.1 Introduction 28
3.2 Design 30
3.3 Modeling of variable-stiffness module 35
3.4 Results and discussion 39
3.5 Conclusions 48
3.A Materials and Methods 48
CHAPTER 4 ANKLE-FOOT ORTHOSIS 52
4.1 Background on foot drop remedies 52
4.2 Analysis of application requirements 53
4.3 Implementation 63
4.4 Experimental methods 66
4.5 Results and discussion 70
4.6 Conclusion 77
CHAPTER 5 CONCLUSION 78
5.1 Benefits of artificial muscles 78

5.2 Challenges of using DETs 80
5.3 The path forward 86
BIBLIOGRAPHY 87
BIOGRAPHICAL SKETCH 99
CURRICULUM VITAE

LIST OF FIGURES

2.1 The fundamental element of a DET is an elastomer film sandwiched between a pair of stretchable electrodes. When charged, it actuates (converts electrical energy to mechanical energy) as it expands and generates (converts mechanical energy to electrical energy) as it contracts. 6

2.2 A DET has two energy storage systems (U_e and U_m) that are connected through the transduction work (W_t) done by electrostatic forces on its electrodes. 7

2.3 In the width-constrained configuration, a DET element is loaded with force F along its length l_1, its width l_2 is held constant, its thickness l_3 is constrained by the elastomer film's constant volume, and charge Q is stored on the electrodes corresponding to voltage V across the electrodes. 8

2.4 The spring curve for a width-constrained DET shifts down and to the right when the DET is charged. It stiffens (steeper slope) when the DET has a constant charge, but it softens (shallower slope) when the DET has a constant voltage. These curves are based on a width-constrained DET with linear elasticity. 8

2.5 If a DET is loaded with a constant force F_A, then applying a voltage will cause the length change $l_b - l_a$. If the DET is held at a constant displacement l_a, then applying a voltage will cause the force change $F_A - F_B$. 9

2.6 These schematic symbols, consisting of a spring that is compressed by capacitor plates, represent DETs with voltage-induced displacements of interest in the plane of the elastomer (spring axis parallel to plates) and through the thickness of the elastomer (spring axis perpendicular to plates). 10

2.7 In the reference state, the DET element is undeformed and discharged. In a current state, it is deformed and may have charge stored on its electrodes. . . . 11

2.8 A DET is biased when it is loaded in the direction of its voltage-induced displacement (to the right in this illustration). 17

2.9 Biasing uses a DET's stiffness change to enhance its voltage-induced displacement. The biased displacement is equal to the unloaded displacement (left of the gap) plus a contribution due to stiffness change (right of the gap) 18

2.10 A DET can have an elastic bias with stiffness k_b. In this diagram, both the DET and the elastic bias are in tension. 19

2.11 One limitation of biasing is that in order to achieve a bounded enhancement of voltage-induced displacement, the bias stiffness must not be either too greatly positive or too greatly negative. 20

2.12 Another limitation of biasing is that positive stiffness and constant force biases will not enhance voltage-induced displacement if a stiffening control method such as constant charge is used. 21

2.13 DETs are often built with bias mechanisms, such as the spring depicted here. The spring is compressed and then connected to the DET, so it holds the DET in tension providing a bias to enhance its voltage-induced displacement. This arrangement is implemented in spring roll actuators.[56] 21

2.14 Pressure, weight, and elastic loads can bias a DET if they are oriented correctly. 22

2.15 For a given load and displacement range, a DET with a bias load can be smaller than a DET with a bias mechanism because the former does not include the mass and volume of the bias mechanism or that of the extra DET material needed to counteract the bias mechanism's force. 23

2.16 Loads like these cannot bias a DET. Damping opposes DET motion, and inertial loads do not load the DET. Load types that could bias a DET (such as the weights shown here) do not do so if they are oriented opposed to DET motion or are too small. 23

2.17 A DET can bear more force (F) than voltage can induce on it (ΔF), and can displace farther ($l_b - l_r$) than its voltage-induced displacement (Δl). 24

2.18 Because of design principle 3, a DET could be used as a variable-stiffness element that transmits large forces from a motor to a load. 25

2.19 Antagonistic configurations have no equilibrium position shift because the voltage-induced displacements of their constituent DETs cancel, and they can bear tension and compression loads if the DETs have pre-stretch or out-of-plane displacement. 26

3.1 Working principle of a dielectric elastomer transducer (DET). A DET, consisting of a thin film of dielectric elastomer coated with stretchable electrodes, softens when a constant voltage V is applied across its electrodes due to electrostatic forces that tend to expand it in area and compress it in thickness. . . . 31

3.2 Cone diaphragm DET configuration. The DETs used in this work were cone diaphragm modules as depicted in photograph on the right. When a module's center disk is displaced, the elastomer film deforms into the curved cone shape depicted by the dashed lines in the left diagram. For modeling purposes, the deformed shape is approximated as a straight sided cone depicted by the solid outline in the left diagram. 32

3.3 Our DET variable-stiffness actuator (VSA). This actuator has only one component motion in its variable-stiffness mechanism: the relative translation of the DET modules' center disks and outer frames. The modules' center disks are connected to the input components (blue), which are driven by the VSA's motor and ball screw (yellow). The modules' outer frames are connected to the actuator's load by the output components (orange). Both the input and output components are constrained to linear motion by the linear-bearing guide-rod system. The variable-stiffness mechanism consists of thirty-two DET modules (thirty active, and two insulating) though the diagram shows only ten for clarity. The variable-stiffness mechanism softens when the DET modules are charged with constant voltage. 33

3.4 Electrical model of a DET. The electrical behavior of a DET is modeled in this work by a capacitance C that represents the charge storage of the DET that changes as the DET deforms, with a series resistance R_s that represents the resistance in the DET's electrodes, and a parallel resistance R_p that represents the current leakage path through the dielectric elastomer. Schematic redrawn and modified from reference [33]. 36

3.5 Our DET VSA can independently modulate its stiffness and equilibrium position as seen in this plot of the load applied to the DET VSA and its output point displacement. It has the same range of stiffnesses after the actuation motor shifted the equilibrium position from equilibrium position 1 to equilibrium position 2. 40

3.6 The VSA's variable-stiffness mechanism softens when charged with a constant voltage, as seen in these tensile test results with a displacement rate of 1 mm/s. The loops progress in a clockwise direction. The light gray curves are data from the other voltage levels given for context. 41

3.7 Our DET VSA softened approximately quadratically with the applied voltage up to 53 %. These values were calculated from the rising tension portion of the third cycles of the trajectories shown in Figure 3.6 by dividing the force at [5, 15, 25] mm by the corresponding displacement. Because the DET stiffness is quadratically dependent on voltage, quadratic fits using only a quadratic term and a constant term equal to the initial point are plotted for comparison with the experimental data. 41

3.8 The DET VSA changed stiffness rapidly while charging to 5 kV with only three DET modules installed and the variable-stiffness mechanism's displacement fixed at [5, 15, 25] mm. 43

3.9 The viscoelasticity of the DET modules caused them to exert more force and have more hysteresis when the variable-stiffness mechanism was displaced more rapidly. The force-displacement trajectories settled towards a steady-state response producing peak forces of less magnitude on each subsequent cycle. The loops progress in a clockwise direction, so the hysteresis is dissipative. 44

3.10 Our DET VSA absorbed more and returned less mechanical energy at faster displacement rates. Thus, it dissipated more mechanical energy at faster displacement rates. These values were calculated by integrating the third tension cycle of the 0 kV curves in Figure 3.9. 44

3.11 Much of the electrical energy used to charge the DET modules was stored in the modules and could be recovered to increase the efficiency of stiffness changing. These values are the energy used to change stiffness during relaxation tests. The stored energy values calculated from Equation (3.1) are marked with hollow markers connected by dashed lines, and experimental values are shown with circular markers connected by solid lines. 45

3.12 Current leakage through the dielectric causes our DET VSA to draw continuous electrical power while holding reduced stiffness as determined from measurements of the leakage current through five DET modules connected in parallel. The leakage power we measured was not consistent with the power dissipated through a constant resistance value (shown by the gray curves). The leakage power decreased over time while the DETs were held at constant voltage. . . 46

3.13 The custom universal testing machine (UTM) used for testing is depicted here with the DET VSA connected and the 200 N load cell installed. 49

4.1 The DET AFO provides dorsiflexion support to relieve foot drop symptoms by stiffening during swing and loading response, and it avoids impeding push off by softening during push off. To increase battery life, the DET AFO's charge recovery system recovers charge from the DET at the start of swing and returns it at the start of foot flat. 55

4.2 The core of our DET AFO design is a DET strap that lifts the toes. To determine actuation stretch required from the DET, the geometry of the DET AFO is modeled by a triangle with sides a and b representing the distances from the strap's attachment points to the ankle and side c representing the length of the DET. To determine the force required from the DET, the DET's loading is modeled as foot weight W and DET tension T acting on the lever arm b. 56

4.3 The selection of $a = 35\,\text{cm}$ and $b = 5\,\text{cm}$ for the connection placements achieves a compromise between minimizing actuation stretch and force requirements. 59

4.4 The DET AFO's high-voltage power system features a charge recovery system to reduce the amount of energy needed from the high-voltage DC-DC converter to charge the DET. The charge recovery system recovers charge from the DET by closing S_{ch}, and it returns charge to the DET by closing S_{dch}. The system can also drain the DET by closing S_{dr}. 60

4.5 Our DET AFO prototype consists of a DET strap that connects a shoe to a knee brace. The control and power electronics (not shown here) would be worn in a waistpack. 64

4.6 A width-constrained DET of the type used in the DET AFO has polyimide fibers that maintain a 400 % width prestretch of the VHB 4905 elastomer film. The DET is pictured on a storage frame. 65

4.7 The AFO's power and control electronics. 66

4.8 The DET AFO's testbed connected to the DET with pin joints [5 and 35] cm from the ankle joint to use the geometry selected during analysis. The motion of the lever arm was constrained by hard stops to approximately −20° to 10°. The DET was loaded by a 7.8 N weight connected to the lever arm 6 cm from the ankle joint. 68

4.9 The DET assembly raised the weighted lever arm after it was manually lowered during the dorsiflexion tests, so the AFO can provide dorsiflexion support. When the DET assembly was charged to 2.8 kV during the plantarflexion test, it lowered the weighted lever arm to −22.2°, so charging the DET assembly reduces the effort that would be required from the plantarflexor muscles to stretch the DET assembly. The left panels show the first 2 s of the tests, and the right panels show the whole tests. 71

4.10 In the gait cycle tests, the voltage and ankle angle trajectories followed regular patterns. The voltages converged to the trajectories depicted here after the first four cycles. The ankle angle crept downward (lower angle) with subsequent cycles, but the ankle angle change was fairly consistent across cycles. Results from trials with a 5 s gait period are shown on the left, and results from trials with a 1 s gait period are shown on the right. CR means charge recovery. . . . 73

LIST OF TABLES

3.1 Dimensions of our DET VSA and its DET modules 34
3.2 How module dimensions affect the performance of cone diaphragm modules 39
4.1 Parameters used for calculating AFO specifications 58
4.2 Mass of DET AFO components 64
4.3 Energy consumed per cycle in the gait cycle tests with 5 s gait period, and resulting battery life assuming a 10 W h battery capacity 74
4.4 Energy used to charge the DET in the gait cycle tests with a 5 s gait period . . 75

LIST OF ABBREVIATIONS

AFO	Ankle-foot orthosis
DET	Dielectric elastomer transducer
UTM	Universal testing machine
VHB	Very high bond. A line of adhesive tapes produced by 3M
VSA	Variable-stiffness actuator

CHAPTER 1

INTRODUCTION

The advancement of powered prosthesis and orthosis technology is hindered by the shortcomings of state-of-the-art actuators. When used in powered prostheses and orthoses, these actuators, including electric motors, pneumatics, and hydraulics, tend to result in designs that are heavy, bulky, and energy inefficient. One way to overcome these shortcomings is to use a new actuator technology called dielectric elastomer transducers (DETs). However, there is little information available that is usable for designing actuation systems that use DETs. This work begins to fill that gap by contributing design principles for incorporating DETs into actuation systems, and contributing two applications of those principles that solve problems in the field of powered prostheses and orthoses.

1.1 Actuation of powered prostheses and orthoses

The development of powered lower-limb prostheses and orthoses is a great advance for the field of prosthetics and orthotics. Though state-of-the-art unpowered prostheses and orthoses have certainly enriched the lives of many people with disabilities, these passive prostheses and orthoses can never fully restore natural limb functions. These devices can only support their users; they cannot supply power to replace missing or weak muscles. In contrast, powered prostheses and orthoses can restore natural limb motor function because they have motors or other actuators.

Electric motors in various forms are common prosthesis and orthosis actuators.[1,2] These motors are typically paired with high-reduction transmissions to amplify their torque to the levels required for human joints. These transmissions have backlash and friction that complicate force control. These devices also lack the compliance that human muscles and tendons have, and research shows that this compliance is key to achieving natural and efficient gait.[3,4] Some powered prostheses and orthoses use series elastic actuators to obtain the benefits of compliance.[1,2,5,6] This approach allows them to store and return energy efficiently and respond compliantly to impacts enhancing user safety and actuator durability.[7,8] Some powered prostheses and orthoses take this approach further by using variable-stiffness actuators (VSAs) that can adapt their compliance to changes in gait parameters.[9] To circumvent the issues of backlash and friction and add compliance, some recent designs use high-torque motors with low reduction transmissions.[10–12]

Though convenient and easily controlled, electric motors have shortcomings for use in powered prostheses and orthoses. Electric motors with high power-to-weight ratios typically deliver that performance at high speeds, so they need high-reduction transmissions to drive human joints. These transmissions add considerable weight and bulk to a prosthesis or orthosis reducing the benefit of the high power-to-weight ratio. Motors and transmissions spinning at high speeds produce considerable amounts of noise, which is obtrusive for daily use prostheses and orthoses. Compliant elements add additional weight, volume, and complexity to motors, especially for variable stiffness mechanisms. High-torque-density motors can mitigate the noise and compliance issues by using low-reduction transmissions or directly driving joints, but their energy consumption may be high because they draw high currents to create their high torques and they consume power during standing (their ability to regenerate energy from negative work during gait offsets this drawback).[10,13] Finally, electric motors are typically used with rigid frames that add weight and bulk to orthoses making them more obtrusive to their users.

For use in prostheses and orthoses, pneumatics and hydraulics have some advantages over electric motors, but they have significant shortcomings also. Pneumatics and hydraulics can provide muscle-like force and stroke, and they can have high power-to-weight ratios,[2] so they usually directly drive joints without the need for a gearbox.[14–16] Further, the compressibility of gases gives pneumatic mechanisms an inherent compliance. However, hydraulics require bulky, noisy pumps, and fluid friction hurts their efficiency.[2] Pneumatics also rely on pumps or bulky compressed gas cylinders, and their valve actions make noise. They also have hysteresis that makes them difficult to control.[17]

Artificial muscles[18,19] are a promising option for powering prostheses and orthoses because they can avoid the shortcomings of electric motors.[20] Artificial muscles are actuators that produce a stable displacement change in response to an input such as light, heat, or electricity.[21] In many applications, they do not need reduction transmissions because their force, stroke, and velocity characteristics are suitable for direct drive operation. They are typically inherently compliant, so they do not need additional mechanisms to introduce compliance. Because of their inherent compliance and direct drive ability, they may be able to operate without the rigid frames that electric motors require. The elimination of reduction transmissions, additional compliant mechanisms, and rigid frames combine to reduce the weight, bulk, and complexity of devices powered by artificial muscles. Further, artificial muscles (except for those that use pneumatics or electric motors) operate silently so they can be less obtrusive than electric motors. Finally, some types of artificial muscles have efficient energy transduction mechanisms,[19,20] so

they may be able to achieve equal or greater energy efficiency than electric motors in powered prostheses and orthoses.

1.2 Dielectric elastomer transducers

Among the many types of artificial muscles, DETs stand out as a good choice for powering prostheses and orthoses.[22,23] Powered prostheses and orthoses require energy efficient actuators in order to achieve acceptable battery life. Most types of artificial muscle have energy conversion efficiencies of less than 50 %, including thermally actuated artificial muscles (such as shape memory alloys, shape memory polymers, and coiled semicrystalline polymers), ionic artificial muscles (such as ionic polymer metal composites, conducting polymers, and carbon nanotube actuators), and pneumatic artificial muscled (such as soft fluidic actuators, McKibben artificial muscles, and pleated pneumatic artificial muscles).[18,19] Artificial muscles for powered prostheses and orthoses should have actuation strain of at least 10 % so that they can be used without mechanical amplification. This requirement rules out piezoelectric and electrostrictive artificial muscles.[19,20] Artificial muscles for powered prostheses and orthoses should also be silent, which rules out the use of twisted string actuators,[18] which are essentially a type of transmission for electric motors, and not a true artificial muscle. DETs meet all three of these requirements (efficiency, strain, silence), so they are a viable choice for powering prostheses and orthoses. Further, DETs have strain rate and stress performance similar to artificial muscle, they are simple to control with a voltage input, and they can be fabricated from inexpensive, readily available materials. They have two shortcomings however. DETs typically require input voltages on the order of kilovolts, and they have short cycle life (thousands to millions of cycles). One other type of artificial muscle is viable for powered prostheses and orthoses: HASEL (Hydraulically-Amplified Self-Healing ELectrostatic) actuators.[24,25] These actuators also meet the requirements for powering prostheses and orthoses, and share the strengths of DETs mentioned here, and their need for kilovolt driving voltages. They are less prone to failure by dielectric breakdown than DETs, so they may be a better choice for powering prostheses and orthoses. However, they were not reported until 2018, when this work was already well underway.

Though DETs have been used for many robotic designs,[26] only a few works have addressed aspects of using DETs in prostheses and orthoses. The only DET-powered orthosis reported to date was designed for finger rehabilitation.[27] It featured folded, contracting-stack DETs that modulated the force applied to resist finger motion. The first prototype

demonstrated the feasibility of DETs for this role, and a later work investigated the use of a stack of planar-elongating DETs for improved performance.[28] Contractile DETs were also used to actuate a mock-up of a human forearm as part of the development of an arm exoskeleton.[29] A control method was developed to use DETs for forearm tremor suppression, though no prototype was reported.[30] The safety of using DETs close to the human body was analyzed, and safety criteria were developed.[31]

Despite the extensive research on design, modeling,[32] and control[33] of DETs, there is little generalizable design guidance for designing devices that incorporate DETs. Prior DET design research has been almost entirely focused on the design of the DETs themselves, covering the selection of materials for the elastomer[34,35] and electrodes,[36] and the design of a variety of DET configurations.[37] Only one work specifically presents design implications that pertain to incorporating DETs into actuation systems.[38] This work suggests that DETs are best suited for three application types: low extensions, alternating motion, or binary actuation. This recommendation is based on an analysis of DET performance metrics as functions of strain and strain rate. A few other principles for devices that incorporate DETs can be gleaned from works that primarily address the design of DETs themselves. These principles include minimizing bias stiffness to maximize DET displacement,[39–41] the use of antagonistic pairs of DETs to actuate a robot joint,[42] and the importance of matching the impedance of a DET with that of its load.[43]

1.3 Overview

This work gives principles and examples for designing an actuation system that uses DETs. The design principles are derived from the fundamental nature of DETs in Chapter 2. Then, two examples are given in Chapters 3 and 4 that apply the design principles to solve challenges related to powered prostheses and orthoses. Chapter 3 describes a design for a VSA, a type of actuator that is being studied for use in powered prostheses and orthoses.[9,44–47] Chapter 4 describes the design of an ankle-foot orthosis (AFO) for foot drop.

CHAPTER 2

DESIGN PRINCIPLES

One of the challenges of using dielectric elastomer transducers (DETs) in powered prostheses and orthoses is the lack of guidance for designing DET-powered devices. Though there is extensive knowledge on the design, modeling, and control of DETs themselves, there is little guidance available for designing an actuation system that incorporates DETs. This chapter explains four principles about DETs that can guide the design of DET-powered devices. To do so, it will first review the fundamentals of DET operation that lead to the intuitive understanding of DETs as variable-stiffness springs (§ 2.1). Then, it will use this understanding to derive and explain the design principles (§ 2.2).

2.1 How dielectric elastomer transducers work

Many prior works have explained how DETs work, but their explanations do not adequately explain the connection between a DET's voltage-induced stiffness change and its voltage-induced displacement. This connection and the understanding of how these two effects result from the fundamental DET transduction mechanism are crucial for incorporating DETs into practical actuation systems. Accordingly, this section reviews the fundamentals of DET operation highlighting these crucial concepts that lead to the intuitive understanding of DETs as variable-stiffness springs. An overview of the key concepts is given first (§ 2.1.1), and the derivation of these concepts with mathematics follows (§ 2.1.2). The DET model used in this section is essentially the same as in other works,[32,48,49] but its explanation here highlights the transduction between electrical and mechanical energy and the connection between a DET's voltage-induced stiffness change and voltage-induced displacement.

2.1.1 Overview

Briefly, a DET behaves like a variable-stiffness spring, as this section explains. A variable-stiffness spring exerts force F that is the product of the spring's stiffness k and the difference between its current length l and its equilibrium point l_{eq} (also called its relaxed length):

$$F = k(l - l_{\text{eq}}). \tag{2.1}$$

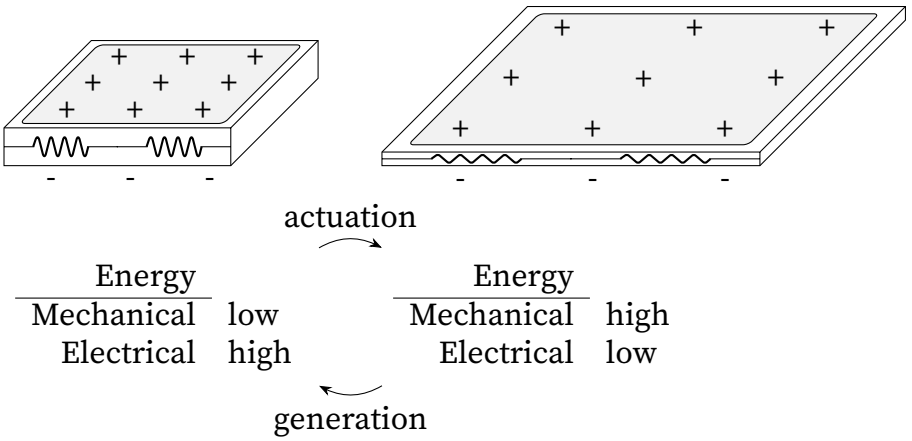

Figure 2.1: The fundamental element of a DET is an elastomer film sandwiched between a pair of stretchable electrodes. When charged, it actuates (converts electrical energy to mechanical energy) as it expands and generates (converts mechanical energy to electrical energy) as it contracts.

When a DET is charged, it experiences electrostatic forces that transduce between electrical and mechanical energy as it deforms. These electrostatic forces change the DET's stiffness and equilibrium position, and these changes can be used to create forces and displacements.

A DET transduces between electrical and mechanical energy as its area and thickness change.[48] The fundamental DET element is an elastomer film sandwiched between a pair of stretchable electrodes, which forms a stretchable capacitor (Figure 2.1). In order for the DET element to transduce electrical and mechanical energy, its electrodes must be oppositely charged. The charges exert electrostatic forces on the elastomer film that tend to compress its thickness and expand its area. The volume of an elastomer is approximately constant, so as the area increases, the thickness decreases and vice versa. When the DET element increases in area, it actuates, because the electrostatic forces convert the stored electrical energy into mechanical work (which may be stored in the stretched elastomer film) as the opposite charges move closer together, and the like charges on each electrode spread apart. When the DET element decreases in area, it generates, because mechanical work against the electrostatic forces is converted into stored electrical energy as the opposite charges are separated, and the like charges are pressed closer together. Thus, DETs can be used for both actuation and generation because they are bidirectional transducers.

A DET can be thought of as a pair of energy storage systems linked by transduction work W_t (Figure 2.2). The DET stores electrical potential energy U_e in the charges on its

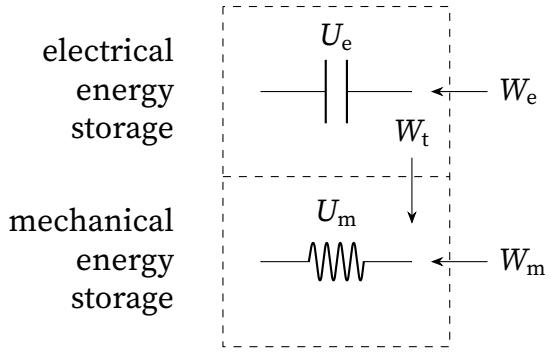

Figure 2.2: A DET has two energy storage systems (U_e and U_m) that are connected through the transduction work (W_t) done by electrostatic forces on its electrodes.

electrodes and mechanical potential energy U_m in the polymer chains in its elastomer film. External electrical work W_e and mechanical work W_m are done on the electrical and mechanical subsystems respectively. Transduction work W_t transfers energy between the electrical and mechanical subsystems when the area and thickness of the DET element change while there is charge stored on its electrodes. When the DET is used for actuation, the electrical work is considered the input, and it is used to decrease the amount of mechanical work needed to deform the DET or even cause the DET to output mechanical energy. When the DET is used for generation, the mechanical work is considered the input, and it is used to cause the DET to output electrical energy. This work focuses on actuation systems, so it will discuss the effect of electrical input on a DET's mechanical output.

The width-constrained DET configuration (Figure 2.3) provides the connection between force and displacement that will be used to explain how charging a DET affects its output force and displacement. A DET configuration is a set of force and displacement boundary conditions that represents how a DET functional element interacts with its surroundings. In the width-constrained configuration, the DET element is loaded with force F along its length l_1, its width l_2 is held constant, its thickness l_3 is constrained by the elastomer film's constant volume, and charge Q is stored on the electrodes corresponding to voltage V across the electrodes. When no force or voltage are applied to the DET, its length returns to its rest length l_r. The width-constrained configuration models the loading conditions experienced by the DETs used in the variable-stiffness actuator (VSA) of Chapter 3 and in the ankle-foot orthosis (AFO) of Chapter 4. I have not proven the applicability of the following concepts to other DET configurations, but I expect that the concepts will be applicable because all DETs share the same fundamental element regardless of their configuration.

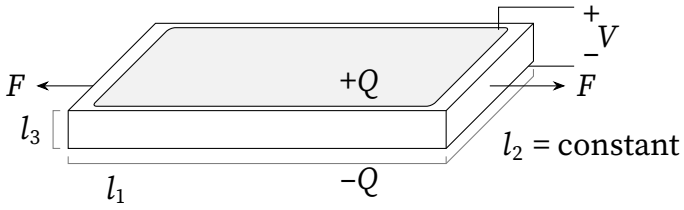

Figure 2.3: In the width-constrained configuration, a DET element is loaded with force F along its length l_1, its width l_2 is held constant, its thickness l_3 is constrained by the elastomer film's constant volume, and charge Q is stored on the electrodes corresponding to voltage V across the electrodes.

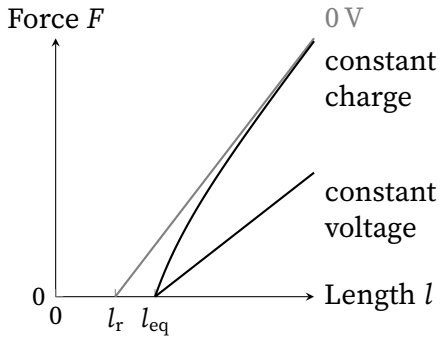

Figure 2.4: The spring curve for a width-constrained DET shifts down and to the right when the DET is charged. It stiffens (steeper slope) when the DET has a constant charge, but it softens (shallower slope) when the DET has a constant voltage. These curves are based on a width-constrained DET with linear elasticity.

A width-constrained DET behaves like a variable stiffness spring. When subjected to an external force, it lengthens from its rest length l_r until its internal elastic force balances the external force. A plot of this behavior is called a spring curve in this work. Applying a charge to the width-constrained DET alters its spring curve, shifting it down and right (Figure 2.4). The shape of the altered curve varies depending on whether the electrical input to the DET is a constant charge, constant voltage, or other condition.

The width-constrained DET's spring curve change is the net result of the width-constrained DET's stiffness and equilibrium position changes. The equilibrium position l_{eq} is the position that the width-constrained DET rests at when no external force is applied. When the DET is discharged (at 0 V), the equilibrium position is equal to the rest length l_r. When the DET is charged, the electrostatic forces on the electrodes deform the elastomer film until they are balanced by its elastic forces. This effect causes the zero-force point of the DET's spring curve (l_{eq}) to shift to the right (Figure 2.4). Charging the DET also changes its stiffness because the electrostatic forces that tend to lengthen

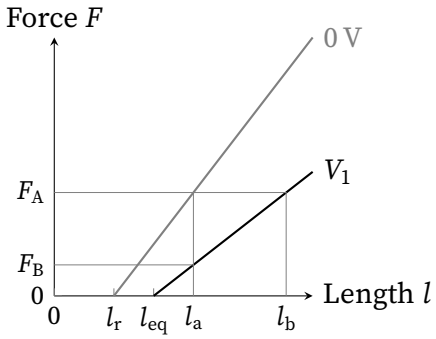

Figure 2.5: If a DET is loaded with a constant force F_A, then applying a voltage will cause the length change $l_b - l_a$. If the DET is held at a constant displacement l_a, then applying a voltage will cause the force change $F_A - F_B$.

the DET change as the DET deforms (except in special cases). If the charge on the DET is constant, then the DET will be stiffer[48] because the charges spread out as the DET lengthens, which weakens the electrostatic force making deformation more difficult. If instead, the voltage on the DET is constant, then the DET will be softer[48,49] because more charge flows onto the DET as it lengthens, which strengthens the electrostatic force assisting the deformation. The change of stiffness causes the slope of the spring curve to change: a constant charge increases the slope, and a constant voltage decreases the slope (Figure 2.4). The constant voltage condition is more commonly used to control DETs, likely because it is easier to implement, and because it is better suited to producing large amounts of work,[50] so this discussion will focus on the constant voltage condition. Note that the DET's stiffness change is solely due to energy transduction and is not a change in a material property of the elastomer film.

Under quasi-static conditions, charging induces force and displacement change for a DET in the following manner. If the DET is loaded with a constant force F_A, then it deforms from its equilibrium position until its force balances the load at length l_a (Figure 2.5). Then, if the DET is charged, it will lengthen further until its force again balances the load at length l_b. Removing the charge from the DET will cause it to contract to the previous balance point (l_a). Thus, the voltage-induced displacement for these conditions is $l_b - l_a$. If the DET is held at a constant length l_a, then it will exert a force F_A. Then, if the DET is charged, the force it exerts will drop to F_B. Removing the charge from the DET will cause it to exert the previous force (F_A) again. Thus, the voltage-induced force change (which is also known as the blocked force[51]) is $F_B - F_A$.

The schematic symbol for a DET introduced in this work (Figure 2.6) summarizes the behavior of a DET. This symbol consists of a spring coil that is placed in between the

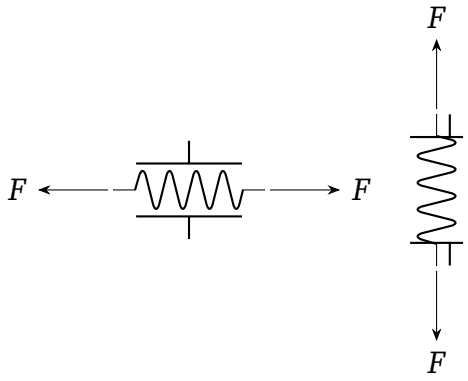

in-plane direction | thickness direction

Figure 2.6: These schematic symbols, consisting of a spring that is compressed by capacitor plates, represent DETs with voltage-induced displacements of interest in the plane of the elastomer (spring axis parallel to plates) and through the thickness of the elastomer (spring axis perpendicular to plates).

plates of a capacitor. The capacitor plates show that the DET behaves like capacitor electrically; it stores charge, and its voltage is proportional to its capacitance and the charge it stores. The spring coil shows that the DET behaves like a spring mechanically; it deforms elastically when subjected to an external force. When the spring coil is oriented parallel to the capacitor plates, the DET schematic symbol represents a DET configuration that has voltage-induced displacement of interest in the plane of the elastomer membrane because when the capacitor plates squeeze the sides of the spring coil, the spring stretches out parallel to the capacitor plates. When the spring coil is oriented perpendicular to the capacitor plates, the DET schematic symbol represents a DET configuration that has voltage-induced displacement of interest in the direction of the elastomer membrane's thickness because when the capacitor plates squeeze the ends of the spring coil, the spring compresses perpendicular to the capacitor plates.

2.1.2 Derivation

The concepts discussed in the previous section arise mathematically from consideration of the work and energy relationship for a DET element. To show this, this section first explains the work and energy relationship for a DET element. Then, it will show that this relationship causes the DET to transduce between electrical and mechanical energy as it

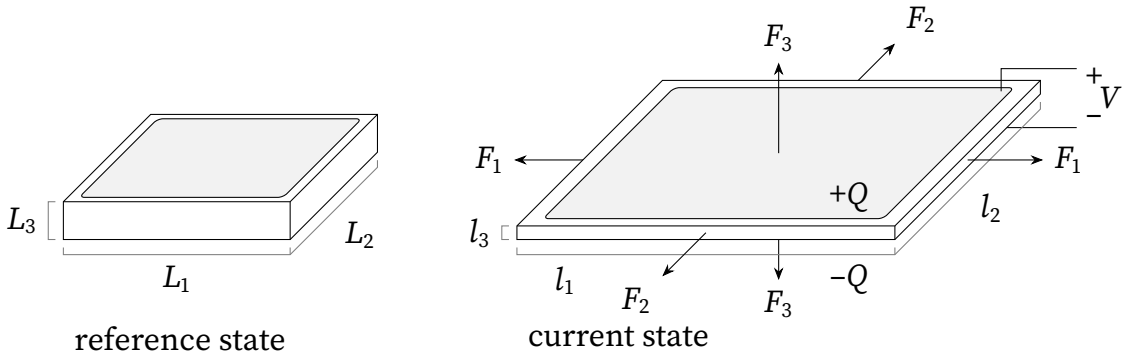

Figure 2.7: In the reference state, the DET element is undeformed and discharged. In a current state, it is deformed and may have charge stored on its electrodes.

deforms, and explain why a DET can be thought of as a pair of energy storage systems linked by transduction work. Finally, it will derive the force and displacement relationship for a width-constrained DET and use it to explain how charging a DET affects its output force and displacement.

The change of potential energy stored in a DET element is equal to the work done by the forces and voltage acting on that element, assuming either equilibrium conditions or an ideal DET with no dissipative elements (such as viscoelasticity or electrical resistance). When the DET element has no charge on its electrodes, and no external forces applied, it is in the reference state (Figure 2.7). In the reference state, it has dimensions L_1, L_2, and L_3, with L_3 (the film's thickness) being much smaller than L_1 and L_2 (the film's length and width). In a current state, the DET element's dimensions are l_1, l_2, and l_3, forces F_1, F_2, and F_3 are applied on the element's faces, and charge Q is stored on the electrodes corresponding to voltage V across the electrodes. The DET element's capacitance C is approximately that of a pair of parallel flat plates,

$$C = \frac{\epsilon l_1 l_2}{l_3}, \tag{2.2}$$

where ϵ is the permittivity of the elastomer (assumed constant here), and the charge is related to the voltage by

$$Q = CV. \tag{2.3}$$

Mechanical work is the product of force and displacement, and electrical work is the product of voltage and change of charge. The change in the DET element's stored potential energy U is the sum of the work done on it by the forces and the voltage,[32]

$$\mathrm{d}U = F_1\,\mathrm{d}l_1 + F_2\,\mathrm{d}l_2 + F_3\,\mathrm{d}l_3 + V\,\mathrm{d}Q, \tag{2.4}$$

where a positive $\mathrm{d}U$ means an increase in stored energy.

The potential energy U can be split into mechanical and electrical components as seen by integrating its total differential $\mathrm{d}U$. Holding l_1, l_2, and l_3 constant and integrating $\mathrm{d}U$ yields:

$$\begin{aligned}\int \mathrm{d}U &= \int V\,\mathrm{d}Q \\ &= \int \frac{Q}{C}\,\mathrm{d}Q \\ &= \frac{1}{2}\frac{Q^2}{C} + U_\mathrm{m}(l_1, l_2, l_3) \\ U(Q, l_1, l_2, l_3) &= U_\mathrm{e}(Q, l_1, l_2, l_3) + U_\mathrm{m}(l_1, l_2, l_3),\end{aligned} \tag{2.5}$$

where U_e and the constant of integration U_m are the electrical and mechanical potential energy stored in the DET element respectively.

A DET transduces between electrical and mechanical energy as its area and thickness change as seen from the form of transduction work. The transduction work W_t is the quantity of energy converted from electrical to mechanical form, and its form can be obtained by expanding $\mathrm{d}U_\mathrm{e}$, the total differential of U_e, and simplifying:

$$\begin{aligned}\mathrm{d}U_\mathrm{e} &= \mathrm{d}\left(\frac{1}{2}\frac{Q^2}{C}\right) \\ &= \mathrm{d}\left(\frac{Q^2}{2}\frac{l_3}{\epsilon l_1 l_2}\right) \\ &= \frac{\partial U_\mathrm{e}}{\partial Q}\,\mathrm{d}Q + \frac{\partial U_\mathrm{e}}{\partial l_1}\,\mathrm{d}l_1 + \frac{\partial U_\mathrm{e}}{\partial l_2}\,\mathrm{d}l_2 + \frac{\partial U_\mathrm{e}}{\partial l_3}\,\mathrm{d}l_3 \\ &= \frac{Q}{C}\,\mathrm{d}Q + \frac{-Q^2 l_3}{2\epsilon l_1^2 l_2}\,\mathrm{d}l_1 + \frac{-Q^2 l_3}{2\epsilon l_1 l_2^2}\,\mathrm{d}l_2 + \frac{Q^2}{2\epsilon l_1 l_2}\,\mathrm{d}l_3 \\ &= \frac{Q}{C}\,\mathrm{d}Q - \frac{1}{2}\frac{Q^2}{C}\left(\frac{\mathrm{d}l_1}{l_1} + \frac{\mathrm{d}l_2}{l_2} - \frac{\mathrm{d}l_3}{l_3}\right) \\ &= \mathrm{d}W_\mathrm{e} - \mathrm{d}W_\mathrm{t}\,.\end{aligned} \tag{2.6}$$

$$\therefore\ \mathrm{d}W_\mathrm{t} = \frac{1}{2}\frac{Q^2}{C}\left(\frac{\mathrm{d}l_1}{l_1} + \frac{\mathrm{d}l_2}{l_2} - \frac{\mathrm{d}l_3}{l_3}\right). \tag{2.7}$$

Equation (2.7) indicates that when the DET element's area increases ($\mathrm{d}l_1 > 0$, $\mathrm{d}l_2 > 0$, $\mathrm{d}l_3 < 0$), energy is converted from electrical to mechanical form, which is actuation. Also, when the DET element's area decreases ($\mathrm{d}l_1 < 0$, $\mathrm{d}l_2 < 0$, $\mathrm{d}l_3 > 0$), energy is converted from mechanical to electrical form, which is generation. These effects are summarized in Figure 2.1.

The connection between mechanical work W_m done on the DET element and transduction work can be obtained as follows. First, the partial derivatives of U_m are obtained from the partial derivatives of U:

$$\frac{\partial U}{\partial l_1} = \frac{-Q^2 l_3}{2\epsilon l_1^2 l_2} + \frac{\partial U_\mathrm{m}}{\partial l_1} = F_1, \qquad \therefore \frac{\partial U_\mathrm{m}}{\partial l_1} = F_1 + \frac{Q^2 l_3}{2\epsilon l_1^2 l_2} \tag{2.8}$$

$$\frac{\partial U}{\partial l_2} = \frac{-Q^2 l_3}{2\epsilon l_1 l_2^2} + \frac{\partial U_\mathrm{m}}{\partial l_2} = F_2, \qquad \therefore \frac{\partial U_\mathrm{m}}{\partial l_2} = F_2 + \frac{Q^2 l_3}{2\epsilon l_1 l_2^2} \tag{2.9}$$

$$\frac{\partial U}{\partial l_3} = \frac{Q^2}{2\epsilon l_1 l_2} + \frac{\partial U_\mathrm{m}}{\partial l_3} = F_3, \qquad \therefore \frac{\partial U_\mathrm{m}}{\partial l_3} = F_3 - \frac{Q^2}{2\epsilon l_1 l_2} \tag{2.10}$$

Then $\mathrm{d}U_\mathrm{m}$, the total differential of U_m, is written out and simplified:

$$\begin{aligned}
\mathrm{d}U_\mathrm{m} &= \frac{\partial U_\mathrm{m}}{\partial l_1}\,\mathrm{d}l_1 + \frac{\partial U_\mathrm{m}}{\partial l_2}\,\mathrm{d}l_2 + \frac{\partial U_\mathrm{m}}{\partial l_3}\,\mathrm{d}l_3 \\
&= \left(F_1 + \frac{Q^2 l_3}{2\epsilon l_1^2 l_2}\right)\mathrm{d}l_1 + \left(F_2 + \frac{Q^2 l_3}{2\epsilon l_1 l_2^2}\right)\mathrm{d}l_2 + \left(F_3 - \frac{Q^2}{2\epsilon l_1 l_2}\right)\mathrm{d}l_3 \\
&= F_1\,\mathrm{d}l_1 + F_2\,\mathrm{d}l_2 + F_3\,\mathrm{d}l_3 + \frac{1}{2}\frac{Q^2}{C}\left(\frac{\mathrm{d}l_1}{l_1} + \frac{\mathrm{d}l_2}{l_2} - \frac{\mathrm{d}l_3}{l_3}\right) \\
&= \mathrm{d}W_\mathrm{m} + \mathrm{d}W_\mathrm{t}\,. \qquad (2.11)
\end{aligned}$$

$$\therefore \mathrm{d}W_\mathrm{m} = \mathrm{d}U_\mathrm{m} - \mathrm{d}W_\mathrm{t}\,. \tag{2.12}$$

Equation (2.12) means that during actuation, when $\mathrm{d}W_\mathrm{t}$ is positive, the transduction work reduces the work necessary to deform the DET element.

A DET can be thought of as a pair of energy storage systems linked by transduction work. The potential energy stored in the DET can be split into electrical and mechanical components as seen from Equation (2.5). Both the electrical and mechanical components are affected by the transduction work as seen from Equations (2.6) and (2.11). Adding Equations (2.6) and (2.11) confirms that the transduction work is internal to the DET system and does not affect the total energy it stores:

$$\mathrm{d}U_\mathrm{e} + \mathrm{d}U_\mathrm{m} = \mathrm{d}W_\mathrm{e} - \mathrm{d}W_\mathrm{t} + \mathrm{d}W_\mathrm{m} + \mathrm{d}W_\mathrm{t} \tag{2.13}$$

$$\mathrm{d}U = \mathrm{d}W_\mathrm{e} + \mathrm{d}W_\mathrm{m}\,. \tag{2.14}$$

These observations verify the model depicted in Figure 2.2.

The force and displacement relationship for a width-constrained DET can be obtained as follows. First, the elastomer film is assumed to be isotropic and have constant volume. These assumptions allow the film to be modeled with hyperelasticity, which is

an approach to modeling the behavior of elastomers for large stretches[52–54] often used for modeling DETs.[32] The hyperelastic energy density function ψ_h expresses the energy stored in the elastomer chains per unit volume as a function of the elastomer's stretches, which are defined as:

$$\lambda_1 = \frac{l_1}{L_1}, \quad \lambda_2 = \frac{l_2}{L_2}, \quad \lambda_3 = \frac{l_3}{L_3} \tag{2.15}$$

Expanding Equation (2.12) yields:

$$\mathrm{d}W_m = \mathrm{d}U_m - \mathrm{d}W_t \tag{2.16}$$

$$F_1\,\mathrm{d}l_1 + F_2\,\mathrm{d}l_2 + F_3\,\mathrm{d}l_3 = L_1L_2L_3\,\mathrm{d}\psi_h - \frac{Q^2}{2C}\left(\frac{\mathrm{d}l_1}{l_1} + \frac{\mathrm{d}l_2}{l_2} - \frac{\mathrm{d}l_3}{l_3}\right) \tag{2.17}$$

$$= L_1L_2L_3\left(\frac{\partial\psi_h}{\partial l_1}\,\mathrm{d}l_1 + \frac{\partial\psi_h}{\partial l_2}\,\mathrm{d}l_2 + \frac{\partial\psi_h}{\partial l_3}\,\mathrm{d}l_3\right) - \frac{Q^2}{2C}\left(\frac{\mathrm{d}l_1}{l_1} + \frac{\mathrm{d}l_2}{l_2} - \frac{\mathrm{d}l_3}{l_3}\right) \tag{2.18}$$

In the width-constrained configuration (Figure 2.3), the DET's width l_2 is constrained to be a constant value, resulting in $\mathrm{d}l_2 = 0$, and F_3 is zero, so the force and displacement of interest are those in the length direction: F_1 and l_1. Simplifying then yields:

$$F_1\,\mathrm{d}l_1 = L_1L_2L_3\left(\frac{\partial\psi_h}{\partial l_1}\,\mathrm{d}l_1 + \frac{\partial\psi_h}{\partial l_3}\,\mathrm{d}l_3\right) - \frac{Q^2}{2C}\left(\frac{\mathrm{d}l_1}{l_1} - \frac{\mathrm{d}l_3}{l_3}\right) \tag{2.19}$$

The constant volume assumption allows further simplification. This assumption can be expressed as

$$\begin{aligned} l_1l_2l_3 &= L_1L_2L_3 \\ \lambda_1\lambda_2\lambda_3 &= 1 \\ \lambda_3 &= (\lambda_1\lambda_2)^{-1}. \end{aligned} \tag{2.20}$$

This means that ψ_h can be expressed as a function of only λ_1 and λ_2, so $\frac{\partial\psi_h}{\partial l_3} = 0$. Further, the constant volume assumption means that

$$\begin{aligned} \mathrm{d}(l_1l_2l_3) &= 0 \\ l_2l_3\,\mathrm{d}l_1 + l_1l_3\,\mathrm{d}l_2 + l_1l_2\,\mathrm{d}l_3 &= 0 \\ \frac{\mathrm{d}l_1}{l_1} + \frac{\mathrm{d}l_2}{l_2} + \frac{\mathrm{d}l_3}{l_3} &= 0 \\ \frac{\mathrm{d}l_1}{l_1} + \frac{\mathrm{d}l_2}{l_2} &= -\frac{\mathrm{d}l_3}{l_3}. \end{aligned} \tag{2.21}$$

And because $\mathrm{d}l_2 = 0$ for the width-constrained configuration,

$$\frac{\mathrm{d}l_1}{l_1} = -\frac{\mathrm{d}l_3}{l_3}. \tag{2.22}$$

Accordingly, Equation (2.19) can be further simplified to yield the relationship between force and displacement for a width-constrained DET.

$$\begin{aligned} F_1\,\mathrm{d}l_1 &= L_1L_2L_3\frac{\partial\psi_\mathrm{h}}{\partial l_1}\,\mathrm{d}l_1 - \frac{Q^2}{2C}\frac{2\,\mathrm{d}l_1}{l_1} \\ F_1 &= L_1L_2L_3\frac{\partial\psi_\mathrm{h}}{\partial l_1} - \frac{Q^2}{C}\frac{1}{l_1} \\ &= L_1L_2L_3\frac{\partial\psi_\mathrm{h}}{\partial\lambda_1}\frac{\mathrm{d}\lambda_1}{\mathrm{d}l_1} - \frac{Q^2}{\epsilon l_1}\frac{1}{l_1} \\ &= L_2L_3\frac{\partial\psi_\mathrm{h}}{\partial\lambda_1} - \frac{Q^2}{C}\frac{1}{l_1} \\ &= g(l_1) - \frac{Q^2}{C}\frac{1}{l_1} \end{aligned} \tag{2.23}$$

where $g(l_1)$ is used to express the dependence of that term on l_1 (because ψ_h is a function of λ_1, which is a function of l_1). In general, $g(l_1)$ is nonlinear, monotonic, and differentiable.

Charging a width-constrained DET always changes its equilibrium position, but the effect of charging on the DET's stiffness depends on how the charge is supplied to the DET. If the charge on the DET stays constant as l_1 changes, Equation (2.23) becomes

$$\begin{aligned} F_1 &= g(l_1) - \frac{Q^2}{\epsilon l_1 l_2}l_3\frac{1}{l_1} \\ &= g(l_1) - \frac{Q^2}{\epsilon l_1 l_2}\frac{L_1L_2L_3}{l_1l_2}\frac{1}{l_1} \\ &= g(l_1) - \frac{Q^2}{a l_1^3}, \quad \text{where} \quad a = \frac{\epsilon l_2^2}{L_1L_2L_3} \quad \text{is constant.} \end{aligned} \tag{2.24}$$

$$\text{Then,} \quad \frac{\mathrm{d}F_1}{\mathrm{d}l_1} = \frac{\mathrm{d}\,g(l_1)}{\mathrm{d}l_1} + \frac{3Q^2}{a l_1^4}. \tag{2.25}$$

If instead, the voltage on the DET stays constant as l_1 changes, Equation (2.23) becomes

$$\begin{aligned} F_1 &= g(l_1) - \frac{(CV)^2}{C}\frac{1}{l_1} \\ &= g(l_1) - \epsilon l_1 l_2\frac{l_1l_2}{L_1L_2L_3}V^2\frac{1}{l_1} \end{aligned}$$

$$= g(l_1) - aV^2 l_1. \tag{2.26}$$

$$\text{Then,} \quad \frac{\mathrm{d}F_1}{\mathrm{d}l_1} = \frac{\mathrm{d}\,g(l_1)}{\mathrm{d}l_1} - aV^2. \tag{2.27}$$

Equations (2.24) and (2.26) show that when the DET is charged, the force needed to hold it at a specific length reduces. This effect lowers the entire spring curve so that its equilibrium point (l_r) moves to the right. Equations (2.25) and (2.27) show that the charge on the DET affects its stiffness. A constant charge increases stiffness,[48] and a constant voltage decreases stiffness[48,49] as explained in § 2.1.1.

Using a linear expression for $g(l_1)$ simplifies the presentation of the concepts expressed here. In reality, g is a nonlinear function of l_1. However, it is difficult to visually compare the slope of nonlinear functions in order to see the stiffness change caused by charging a DET. Accordingly, this work uses

$$g = k(l_1 - l_\mathrm{r}) \tag{2.28}$$

so that the change of stiffness can be distinguished visually in plots like that in Figure 2.4. The spring curves plotted in Figure 2.4 are Equations (2.24) and (2.26) using g from Equation (2.28). This choice also greatly simplifies the derivation of design principle 1.

2.2 Derivation and statement of design principles

Having established the basics of how DETs work, we will now derive and discuss principles for how we can best design based on their fundamental nature. These principles do not address the design of a DET. Rather, they address the design of the actuation system and mechanism that surround and interact with the DET. These principles are not a complete design process, but rather a set of useful observations hitherto not expounded clearly in the literature.

These principles are applicable to DETs used in actuation systems, which are combinations of actuators and the components that connect them to the load, including transmission and compliant elements. These systems are used for force or motion control. This analysis is limited to quasi-static conditions, so it does not account for dynamic effects, but it is an instructive analysis nevertheless.

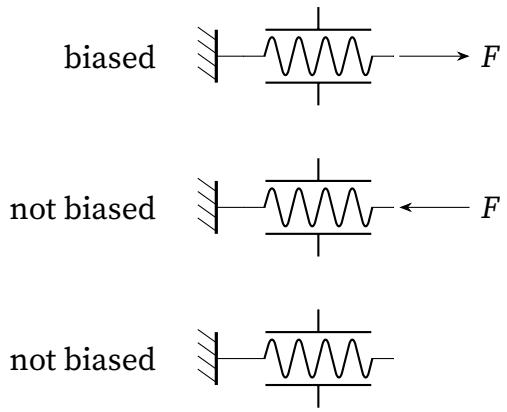

Figure 2.8: A DET is biased when it is loaded in the direction of its voltage-induced displacement (to the right in this illustration).

2.2.1 Biasing

It is often desirable for an actuation system to maximize the voltage-induced displacement of a DET. Design principle 1 describes a means to enhance the voltage-induced displacement of a DET that is commonly applied in the DET field, but not always understood properly.

Design Principle 1. Biasing a DET can increase its voltage-induced displacement.

Biasing is loading a DET in the direction of its voltage-induced displacement. The top DET in Figure 2.8 is biased because voltage on the DET would cause it to displace to the right, and the force also acts to the right. The middle DET is not biased because the force is opposing the voltage-induced displacement. The bottom DET is also not biased because no external forces are acting on it.

Biasing a DET increases its voltage-induced displacement because biasing couples the DET's stiffness change and voltage-induced displacement. When a DET is charged, the electrostatic force causes it to displace as described in § 2.1.1. If the DET is unloaded, the displacement will be equal to the equilibrium position shift, $l_{\mathrm{eq}} - l_{\mathrm{r}}$ (Figure 2.9). If the DET is biased, for example with constant force F_{A}, then the displacement, $l_{\mathrm{b}} - l_{\mathrm{a}}$, will be the sum of the equilibrium position shift and an additional contribution due to the stiffness change of the DET. If the DET is charged with a constant voltage, then charging will soften it, and the contribution of the stiffness change to the voltage-induced displacement will increase the displacement, and may even be larger than the equilibrium shift.

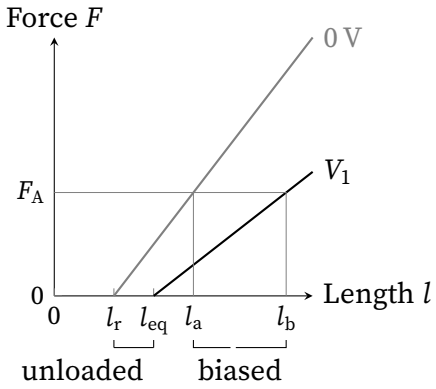

Figure 2.9: Biasing uses a DET's stiffness change to enhance its voltage-induced displacement. The biased displacement is equal to the unloaded displacement (left of the gap) plus a contribution due to stiffness change (right of the gap)

The effect of biasing on a DET's voltage-induced displacement can be derived mathematically. Substituting Equation (2.28) into Equation (2.24) gives a first-order approximation of a width-constrained DET's spring curve:

$$F = k(l_1 - l_r) - aV^2 l_1. \tag{2.29}$$

Solving for l_1 yields:

$$l_1 = \frac{F + kl_r}{k - aV^2.} \tag{2.30}$$

Then, the voltage-induced displacement $\Delta_V l_1$ is

$$\Delta_V l_1 = l_1(V) - l_1(V = 0) = \frac{aV^2(F + kl_r)}{k(k - aV^2)}. \tag{2.31}$$

When there is no force on the DET, its length is its equilibrium position, and Equation (2.31) represents the DET's equilibrium position shift, $l_{eq} - l_r$. When force is greater than zero, the voltage-induced displacement increases according to Equation (2.31). This increase occurs because the constant-voltage input to the DET softens it, allowing the force to deform the DET more than it did before the DET was charged.

Though biasing has been used extensively to enhance the voltage-induced displacement of DETs, this is the first time that its enhancement has been clearly explained as the result of stiffness change. A similar principle has been suggested previously,[55] but it was not explained in detail. This understanding of why biasing enhances a DET's voltage-induced displacement is valuable because it leads to two limitations on when biasing can be used that have not been explained previously. Though most DET designs probably will

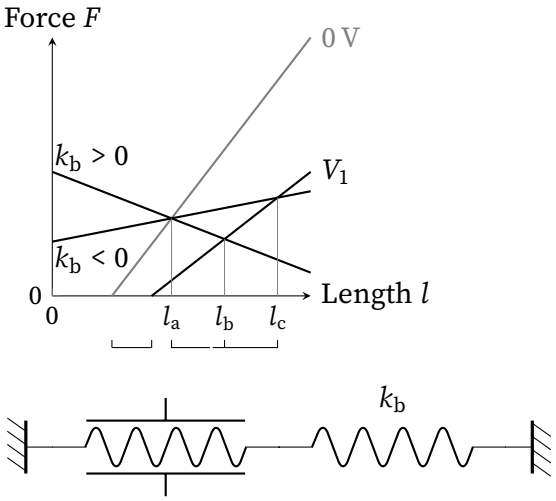

Figure 2.10: A DET can have an elastic bias with stiffness k_b. In this diagram, both the DET and the elastic bias are in tension.

not be restricted by these limitations, it is valuable to establish the limits of biasing's effectiveness.

To see these limitations, assume that the DET is loaded with an elastic bias (Figure 2.10) that has stiffness k_b and is at rest when the DET's length l_1 is equal to l_{rb}, so its force F_b is

$$F_b = k_b(l_1 - l_{rb}), \tag{2.32}$$

where $l_{rb} > l_r$. Assume further that l_{rb} is chosen according to

$$l_{rb} = \frac{k}{k_b}(l_a - l_r) + l_r \tag{2.33}$$

so that the DET and the elastic bias equilibrate when $l_1 = l_a$ for any non-zero value of k_b. Then, the voltage-induced displacement of the DET with an elastic bias can be seen visually by plotting $-F_b$ along with F for 0 V and V_1 (Figure 2.10).

The first limitation of biasing is: biasing only enhances a DET's voltage-induced displacement if the bias force stiffness is neither too greatly positive or too greatly negative (Figure 2.11). If the bias force stiffness is too greatly positive, then it can cause the voltage-induced displacement to be equal to or less than the equilibrium shift. If the bias force stiffness is too greatly negative, it will overwhelm the elastic force of the DET and cause it to overextend and break. To see these limitations mathematically, obtain an expression for the voltage-induced displacement by first setting

$$-F_b = F \tag{2.34}$$

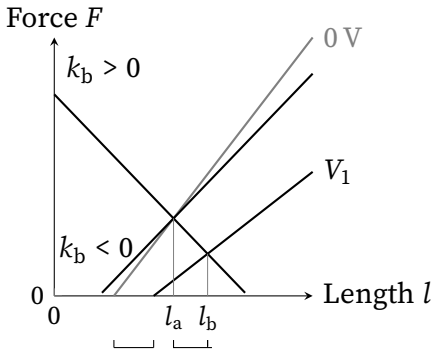

Figure 2.11: One limitation of biasing is that in order to achieve a bounded enhancement of voltage-induced displacement, the bias stiffness must not be either too greatly positive or too greatly negative.

and using Equations (2.32) and (2.33) to get

$$l_1 = \frac{k + k_b}{k + k_b - aV^2} l_a, \tag{2.35}$$

and then using Equation (2.35) to calculate the voltage-induced displacement yielding

$$l_1(V) - l_1(V = 0) = \frac{aV^2}{k + k_b - aV^2} l_a. \tag{2.36}$$

Comparing Equation (2.36) with the DET's equilibrium point shift (obtained from Equation (2.31) with $F = 0$) yields the upper limit on bias stiffness:

$$k_b < \frac{(k - aV^2)(l_a - l_r)}{l_r}. \tag{2.37}$$

To avoid an unbounded voltage-induced displacement, the denominator of Equation (2.36) must be greater than zero, so the lower limit on bias stiffness is

$$k_b > aV^2 - k. \tag{2.38}$$

The second limitation of biasing is: biasing with positive stiffness or constant force enhances a DET's voltage-induced displacement only if the DET is controlled with a constant voltage, or another softening control method (Figure 2.12). Positive stiffness and constant force biases rely on the softening of a DET to enhance its stiffness. If a DET is controlled with a constant charge, then it will be stiffer compared to its uncharged stiffness. In this case, the stiffness change will detract from the voltage-induced induced stiffness because stiffening while loaded causes the DET to be less sensitive to the load. However, it is still possible for a finely-tuned negative stiffness bias to enhance the voltage-induced displacement in this case.

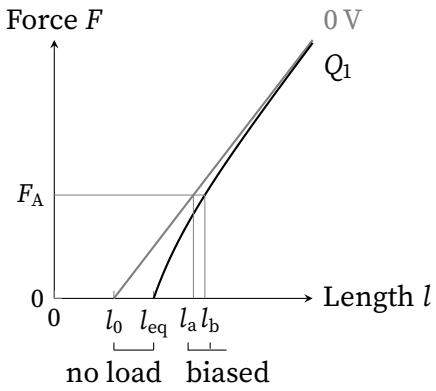

Figure 2.12: Another limitation of biasing is that positive stiffness and constant force biases will not enhance voltage-induced displacement if a stiffening control method such as constant charge is used.

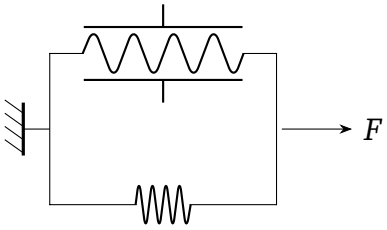

Figure 2.13: DETs are often built with bias mechanisms, such as the spring depicted here. The spring is compressed and then connected to the DET, so it holds the DET in tension providing a bias to enhance its voltage-induced displacement. This arrangement is implemented in spring roll actuators.[56]

2.2.2 Load biasing

Because of design principle 1, DETs are often built with bias mechanisms, which are dedicated loading mechanisms built into a DET (Figure 2.13). A bias mechanism ensures that a DET is always biased and its voltage-induced displacement is always greater than its equilibrium position shift. Bias mechanisms are often simple positive-stiffness springs or hanging masses. Negative stiffness mechanisms are also used because they can produce greater motions than positive stiffness springs.[40] It is also possible to bias a DET with another DET, resulting in an antagonistic configuration.

Design Principle 2. Bias mechanisms may be unnecessary and detrimental when a DET is biased by its load.

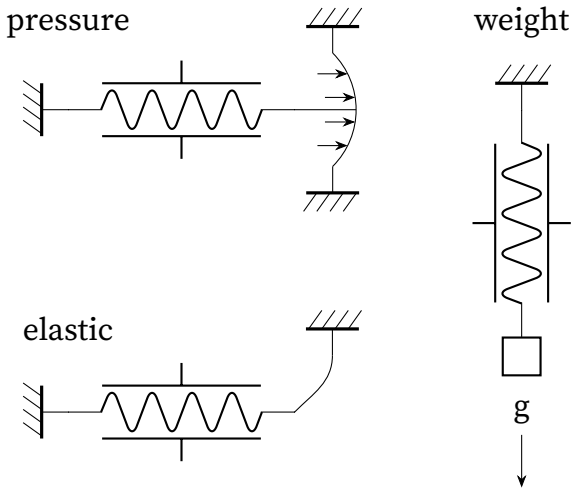

Figure 2.14: Pressure, weight, and elastic loads can bias a DET if they are oriented correctly.

A DET is biased by its load when the load tends to deform the DET in the direction of the DET's voltage-induced displacement (Figure 2.14). Such loads could be weights, pressures, or elastic loads (springs) as long as they act in the correct direction.

When a DET is biased by its load, additional biasing with a bias mechanism may be unnecessary and detrimental. It may be unnecessary because the load provides the biasing function that a bias mechanism normally provides. It may be detrimental because a bias mechanism adds unnecessary weight and mass to the system (Figure 2.15). This weight and mass includes that of the bias mechanism itself, and that of the extra DET material needed to counteract the force exerted by the bias mechanism. Therefore, in applications where the mass and volume of the actuation system are constrained, configuring the actuation system so that the load biases the DET can be beneficial.

Though this principle may seem obvious, it has not been clearly stated before (though it has been briefly mentioned[42]), and some works in the literature do use bias mechanisms in configurations where the load already provides a bias for the DET.[41,57] However, it may be possible that the applications described in these works are not suitable for load biasing due to one or more of the caveats described below.

Certain types of loads do not provide (enough) force in the direction of the voltage-induced displacement to bias a DET effectively (Figure 2.16). Damping and friction loads oppose motion, so they will always be directed opposite to a DET's motion and hinder that motion instead of enhancing it. Inertial loads do not exert any force except when being accelerated, and in that case, they exert a force opposing the desired acceleration, so they

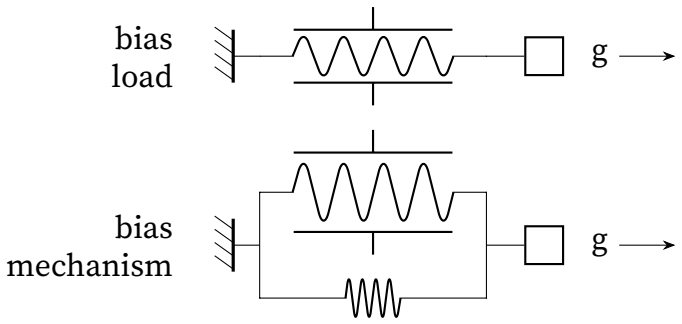

Figure 2.15: For a given load and displacement range, a DET with a bias load can be smaller than a DET with a bias mechanism because the former does not include the mass and volume of the bias mechanism or that of the extra DET material needed to counteract the bias mechanism's force.

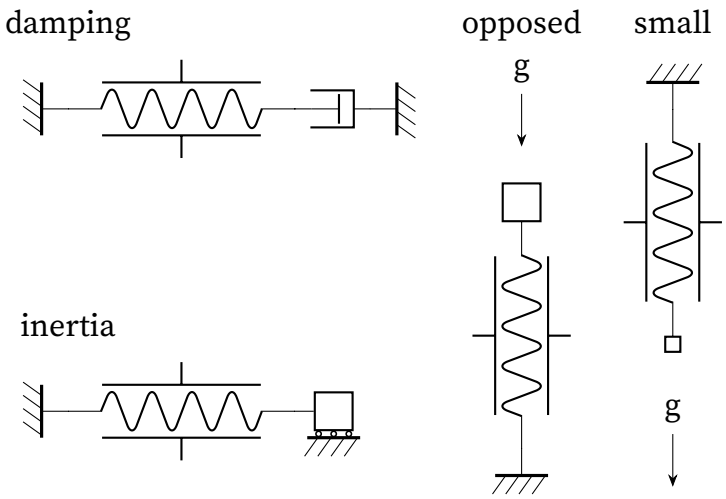

Figure 2.16: Loads like these cannot bias a DET. Damping opposes DET motion, and inertial loads do not load the DET. Load types that could bias a DET (such as the weights shown here) do not do so if they are oriented opposed to DET motion or are too small.

are also not suitable for biasing DETs. In some cases, loads of types that could bias a DET (weights, pressures, springs) are not suitable for biasing because they are either oriented opposite to the voltage-induced displacement or too small to produce the desired range of motion. Note that load biasing is still effective in the presence of non-biasing loads as long as the bias load is the dominant load.

Applications that require their range of motion to be independent of the load are not suited for using load biasing. Load biasing makes the voltage-induced displacement of a DET dependent on the load. If the load becomes zero, such as when a payload is unloaded,

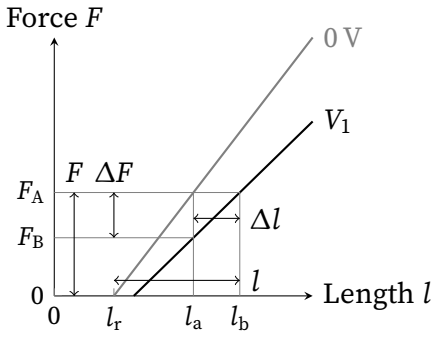

Figure 2.17: A DET can bear more force (F) than voltage can induce on it (ΔF), and can displace farther ($l_b - l_r$) than its voltage-induced displacement (Δl).

then only the DET's equilibrium shift will generate motion, and the generated amount may be very small.

2.2.3 DETs with large forces and displacements

For some applications, it may be desirable to use DETs in high-force and large-displacement actuation systems to benefit from their mechanically-simple variable compliance. However, voltage can only induce a limited amount of force and displacement change on a DET. Scaling up the size of DETs will increase their voltage-induced force and displacement, but it is important to understand another principle that can also help with this need.

Design Principle 3. A DET can bear more force and displacement than voltage can induce on it.

As explained in § 2.1.1, the force and displacement that a voltage induces on a DET can be seen from the differences between the DET's charged and uncharged spring curves. A DET's voltage-induced force change is the difference between its charged and uncharged spring curves at a given displacement. A DET's voltage-induced displacement change is the horizontal coordinate change between the charged and uncharged spring curves along a given load path.

These induced values are only a small portion of the underlying elastomer's maximum force and displacement capability (Figure 2.17). A DET can bear the force difference between its spring curve and the horizontal axis (F), which is larger than the voltage-induced force change (ΔF). A DET can displace from its unstretched length to its maximum elongation (l), which is larger than the voltage-induced displacement (Δl).

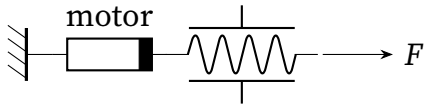

Figure 2.18: Because of design principle 3, a DET could be used as a variable-stiffness element that transmits large forces from a motor to a load.

This behavior is significantly different from that of electric motors, hydraulic actuators, and pneumatic actuators. These actuators have to be able to generate a force in order to transmit it to a load (unless they are positioned at an end stop or are not backdrivable).

Because of this principle, the stiffness modulation and compliance of DETs can be used in actuation systems with larger forces and displacements than a voltage can induce for the DETs. These large forces could be generated by another actuator, such as an electric motor (Figure 2.18). Then, the DET could serve as a compliant element with variable compliance. In such a configuration, the electric motor could also generate large strokes which would move the DET, so the DET would not have to generate the large strokes itself.

2.2.4 Antagonistic configurations

Many DET configurations can only bear tension or compression loads. In particular, a width-constrained DET can only bear a tension load. If it is compressed, it will buckle.

Because of the fundamental operation of a DET explained in § 2.1.1, a voltage that changes the DET's stiffness will also alter the DET's equilibrium position. This behavior may be undesirable in applications that use DETs primarily as variable stiffness elements because it complicates the control of the overall actuation system. When the DET is stiffened or softened, the prime mover must also change position in order to maintain a constant output position. This control difficulty could be eliminated if the DET changed only stiffness and not equilibrium position when charged.

Design Principle 4. Antagonistic DET configurations have no equilibrium position shift and can bear tension and compression loads.

An antagonistic configuration is one where the voltage-induced displacements of two (or more) DETs oppose each other (Figure 2.19). An antagonistic configuration can be formed by connecting two discrete DETs together. One can also be formed through "internal antagonism," where the voltage-induced displacements of internal DET elements oppose each other, as in the cone diaphragm[58] and multi-phase framed in-plane[59] configurations.

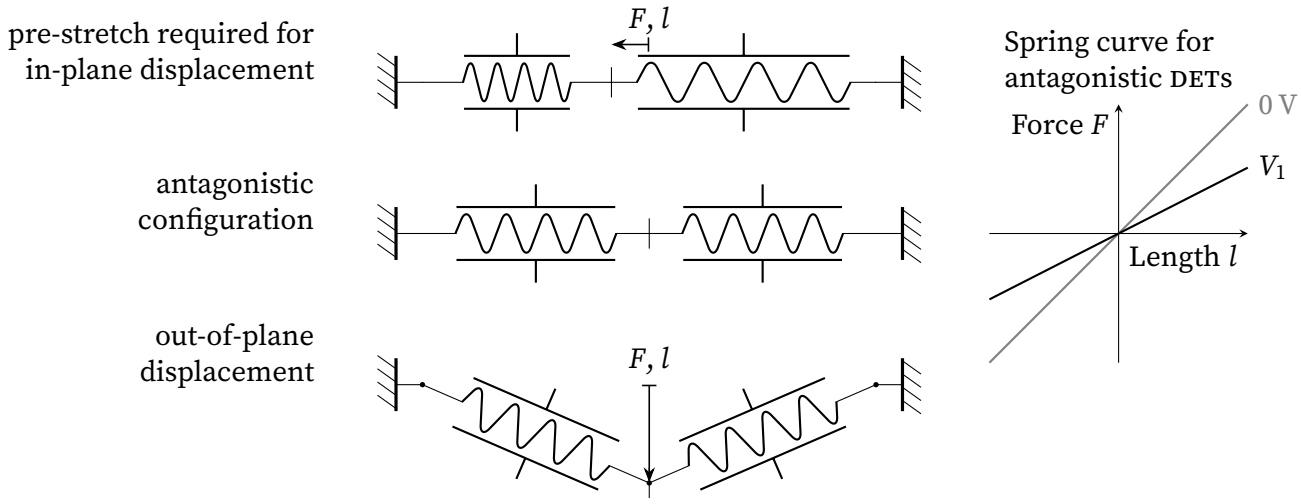

Figure 2.19: Antagonistic configurations have no equilibrium position shift because the voltage-induced displacements of their constituent DETs cancel, and they can bear tension and compression loads if the DETs have pre-stretch or out-of-plane displacement.

An antagonistic configuration has no equilibrium position shift because the equilibrium position shifts of its constituent DETs cancel each other out. When equal voltages are applied to both DETs, their equilibrium position shifts are equal in magnitude and opposite in direction, so they cancel.[49] In DETs with internal antagonism, the equilibrium position shifts of their internal elements cancel, so the equilibrium position of the DET as a whole does not change when voltage is applied.

There are two methods an antagonistic configuration can use to bear tension and compression loads: pre-stretch and out-of-plane displacement (Figure 2.19). If an antagonistic configuration holds its constituent DETs in a pre-stretched state that tensions them, then as long as the displacement is small enough that it does not cancel out the pre-stretch, the DETs will remain in tension during in-plane displacement for both tension and compression loads. Alternatively, if the load of the antagonistic configuration acts perpendicularly to the resting plane of its constituent DETs, then motion in either the tension or compression direction will tension the DETs. A configuration with internal antagonism can also use pre-stretch and out-of-plane displacement to achieve the same results.

There are also two ways to bear tension and compression loads without using an antagonistic configuration. First, if the individual layers of a DET through-plane stack are adhered together, then it can bear tension and compression loads.[60] Second, a bias mechanism pre-stretches its DET, so it can maintain tension on a film for tension and com-

pression loads as long as the compression loads are not large enough to cancel out the pre-stretch.

CHAPTER 3

VARIABLE-STIFFNESS ACTUATOR

Legged and gait-assistance robots can walk more efficiently if their actuators are compliant. The adjustable compliance of variable-stiffness actuators (VSAs) can enhance this benefit. However, this functionality requires additional mechanical components making VSAs impractical for some uses due to increased weight, volume, and cost. VSAs would be more practical if they could modulate the stiffness of their springs without additional components, which usually include moving parts and an additional motor. Therefore, we designed a VSA that uses dielectric elastomer transducers (DETs) for springs. It does not need mechanical stiffness-adjusting components because DETs soften due to electrostatic forces. This paper presents details and performance of our design. Our DET VSA demonstrated independent modulation of its equilibrium position and stiffness. Our design approach could make it practical to obtain the benefits of variable-stiffness actuation with less weight, volume, and cost than normally accompanies them, once weaknesses of DET technology are addressed.

3.1 Introduction

Compliant actuation can benefit many robots, especially if the compliance is adjustable. In particular, legged and gait-assistance robots can walk more efficiently with compliant actuators.[3,61,62] Adjusting their actuator compliance[63] could help them adapt to variations in gait speed and type.[64] However, the additional mechanical components that a variable-stiffness mechanism adds to an actuator makes VSAs impractical for some uses.[3] These components increase the VSA's weight, volume, and cost compared to rigid actuators and fixed-stiffness series elastic actuators.[3] In this work, we show how to accomplish VSA functionality without the mechanical complexity that VSAs normally entail by using DETs as the core of a VSA's variable-stiffness mechanism.

Two recent VSAs are examples of the mechanical complexity of state-of-the-art VSA design. First, the ARES-XL[44] is designed for use in a gait-assistance exoskeleton for rehabilitation. Its variable-stiffness mechanism has four major component motions when it

---

The material in this chapter is adapted from a previous publication:
Allen, D.P.; Bolívar, E.; Farmer, S.; Voit, W.; Gregg, R.D. Mechanical Simplification of Variable-Stiffness Actuators Using Dielectric Elastomer Transducers. *Actuators* **2019**, *8*, 44.

is deflected: two rotations and two sliding contacts. Second, a recent version of the MACCEPA has been used in a gait rehabilitation exoskeleton.[65] This actuator also has four major component motions in its variable-stiffness mechanism: two rotations, a chain bending, and a sliding contact. The stiffness-adjusting motors and other moving components of these two VSAs add considerably to their size and weight. Though other VSAs use a variety of variable-stiffness mechanisms,[66,67] similar observations could be made about their mechanical complexity.

Low power stiffness modulation was achieved without the complexity of VSAs by a positive-negative-stiffness actuator[68] and an electroadhesive clutch and spring mechanism,[69] but they did not have all the functionality of a VSA. The positive-negative-stiffness actuator needed only one motor to control its position and inherent stiffness, making it simpler than state-of-the-art VSAs. In experiments, it consumed 3 W while modulating its stiffness under load. However, this actuator relied on the bifurcation of its mechanism's behavior to switch between stiffness and position control, so it could not control its equilibrium position and stiffness independently. The electroadhesive clutch and spring mechanism[69] increased its stiffness by a factor of 36 and consumed an average of 0.6 mW during operation in an ankle exoskeleton. However, the nature of this device limits it to a set of discrete stiffness values rather than the continuous range of values exhibited by state-of-the-art VSAs, and it cannot modulate its equilibrium position without an external load. Both devices could be useful in robotic applications, but they cannot substitute generally for a full-featured VSA.

DETs are softening polymer devices that have been used to make compliant actuators, but not a fully functioning VSA before this work. Prior DET compliant actuators can control their equilibrium position (the output position when no load is applied) and inherent stiffness, but not independently and simultaneously. DET diaphragm modules, developed for variable-stiffness suspensions, can vary their stiffness but not their equilibrium position.[58,70,71] Coupling one or more diaphragm modules with a biasing mechanism[40] results in a dielectric elastomer actuator that has one degree of freedom. Such an actuator changes both its stiffness and equilibrium position, but these two changes are coupled. Using a second DET diaphragm module as the biasing mechanism[72,73] adds a second degree of freedom, but only partially decouples the control of stiffness and equilibrium position. A DET orthosis[28] can vary its stiffness and equilibrium independently, but it does so by using closed-loop control rather than modulating its inherent stiffness. A prior DET VSA design by some of the authors[45] sought independent control of stiffness and equilibrium

position, but it never achieved stiffness modulation because its DETs were impractical to manufacture reliably.

Our new DET VSA can control its equilibrium position and inherent stiffness independently and simultaneously without the mechanical complexity of state-of-the-art VSAs. As explained in § 3.2, our use of cone-diaphragm DETs in a VSA addresses two design challenges: 1) the shift of VSA equilibrium position when the DETs change stiffness, and 2) the need to maintain tension in the DETs' elastomer films. Our design approach also presents a means to use DETs with greater forces and displacements than they can generate themselves. The mechanical model reviewed in § 3.3 is used to derive analytical formulas that can be used to determine how the dimensions of a DET module affect its uncharged stiffness, voltage-induced stiffness change, and maximum displacement. The electrical model also reviewed in that section explains the sources of electrical energy losses in DETs. Experimental results discussed in § 3.4 confirm the feasibility of our design approach, which uses DETs with larger forces than typically present in prior works. Specifically, the results cover our actuator's stiffness change magnitude and speed, viscoelasticity at varying speeds, and electrical power requirements for stiffness change. The experimental methods used to investigate our DET VSA's functionality are given in appendix 3.A.

3.2 Design

The design of our DET VSA achieves variable-stiffness actuation without the mechanical complexity of state-of-the-art VSAs because it does not need auxiliary mechanical components to modulate the inherent stiffness of its elastic components. As this section explains, such stiffness modulation is possible because DETs soften due to electrostatic forces. To implement DET stiffness modulation, the design must account for the equilibrium point shift of DETs and the inability of elastomer films to support tension. It does so by using cone-diaphragm DET modules, which do not change equilibrium point, and which keep their elastomer films tensioned regardless of the load direction. The design achieves independent control of stiffness and equilibrium position because it uses an electric motor to control the VSA's equilibrium position and DETs to control the VSA's stiffness. This arrangement results in a variable-stiffness mechanism that has only one component motion, no rolling or sliding components, and no stiffness-adjusting motor.

DETs soften due to electrostatic forces. Essentially, a DET is a thin film of dielectric elastomer coated on its top and bottom faces with stretchable electrodes[48,74] (Figure 3.1).

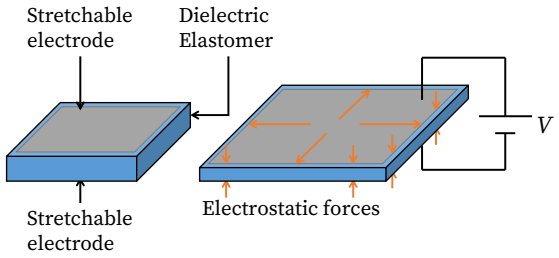

Figure 3.1: Working principle of a dielectric elastomer transducer (DET). A DET, consisting of a thin film of dielectric elastomer coated with stretchable electrodes, softens when a constant voltage V is applied across its electrodes due to electrostatic forces that tend to expand it in area and compress it in thickness.

A constant voltage V applied across the electrodes decreases the stiffness of the DET in proportion to the square of the voltage.[48,49] This softening occurs because the voltage causes the DET to store charges like a parallel-plate capacitor, and these charges exert electrostatic forces on the elastomer film that tend to expand it in area and compress it in thickness. As the DET expands and thins, its capacitance increases. If it is also subject to a constant voltage during expansion, more charge flows onto its electrodes strengthening the electrostatic forces. Thus, the constant-voltage electrostatic forces act as a negative-stiffness mechanism that counteracts the elastomer's elastic restoring forces, making the DET softer. When no voltage is applied, the DET defaults to a (relatively) stiff state.

The nature of DETs poses two challenges for the design of a DET variable-stiffness mechanism. First, the electrostatic forces that soften DETs cause some types of DETs to expand when charged. This expansion could cause the equilibrium position of a variable-stiffness mechanism to change when its stiffness changes, which is typically undesirable. Second, an elastomer film typically cannot support compression in its planar directions. This characteristic complicates the design of variable-stiffness mechanisms that must support compression and tension.

The cone-diaphragm DET configuration used in our VSA design (and some previous variable-stiffness devices[58,70,71]) addresses these challenges. In this configuration, a pre-stretched, adhesive elastomer (VHB 4910) connects center disks to an outer frame (Figure 3.2). The elastomer is coated on its top and bottom faces with conductive graphite powder, which forms the electrodes of the DET. Polyimide film reinforces the elastomer against the electric field and mechanical stress concentrations that occur at the edges of the electrodes. During operation, the center disks displace out of plane, like the motion

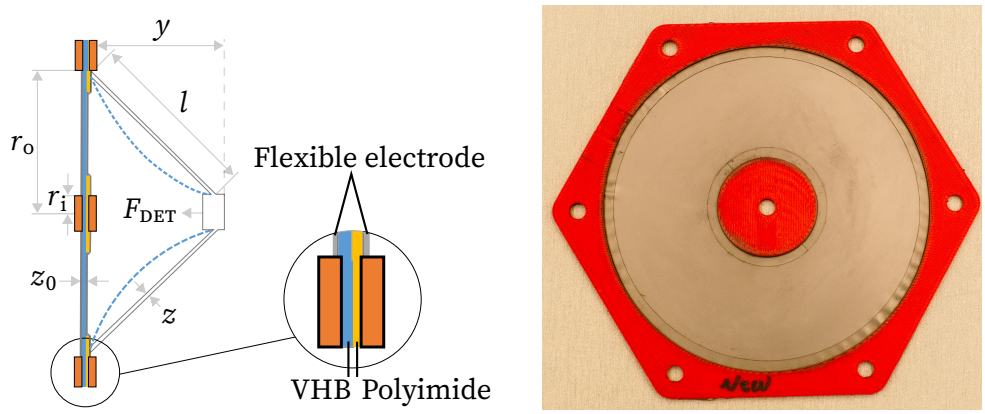

Figure 3.2: Cone diaphragm DET configuration. The DETs used in this work were cone diaphragm modules as depicted in photograph on the right. When a module's center disk is displaced, the elastomer film deforms into the curved cone shape depicted by the dashed lines in the left diagram. For modeling purposes, the deformed shape is approximated as a straight sided cone depicted by the solid outline in the left diagram.

of the center of a speaker cone, stretching the elastomer. The out-of-plane motion decouples the DET's equilibrium position from its stiffness. Additionally, it enables the DET to support bidirectional loads because a displacement in either direction tensions the elastomer film. Pairing other DET configurations together in an antagonistic pair as in our previous work[45] and other works[59] is another solution to these challenges. However, this solution requires additional design work to ensure that the antagonistic DETs remain in tension throughout the mechanism's range of motion.

Our DET VSA (Figure 3.3) achieves independent and simultaneous control of stiffness and equilibrium position, like other VSAs, and is a linear actuator to fit the linear motion of DETs. A direct drive ball screw converts the rotation of the motor (Maxon EC45 flat, 70 W) into linear motion and connects the motor to the variable-stiffness mechanism. In this arrangement, the motor sets the equilibrium position of the VSA and supplies the force to maintain that position. The variable-stiffness mechanism controls the actuator's stiffness and transmits the force to the load. The variable-stiffness mechanism consists of a stack of 30 cone-diaphragm DET modules, capped on the ends by two insulating cone-diaphragm modules. The modules' center disks are connected to the VSA's ball screw, and the module frames are connected to the actuator's output as shown in Figure 3.3. Thus, the DET modules add their force together when stretched, so the force and stiffness of the VSA are linearly proportional to the number of modules installed in the variable-stiffness mechanism. Electrically, the DET modules are connected in parallel, so they all charge

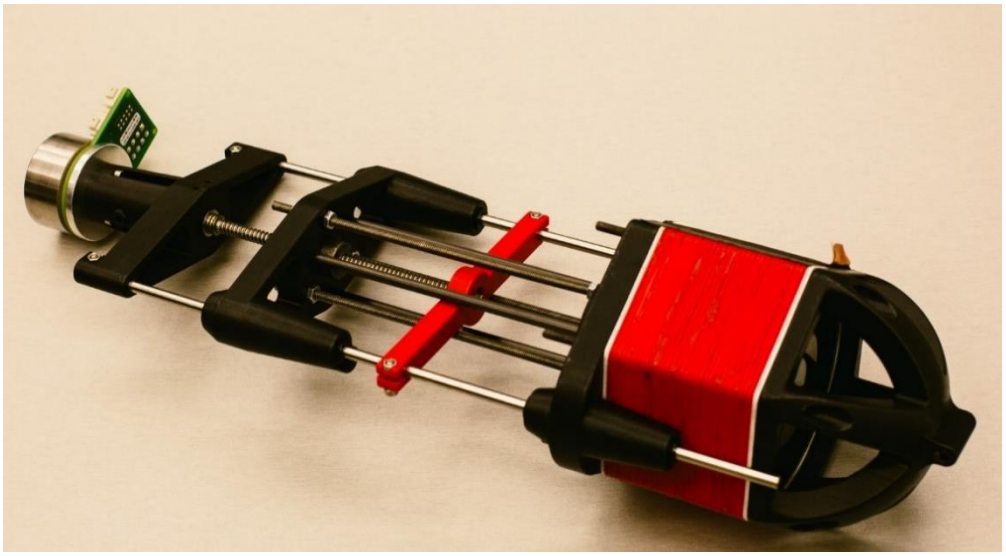

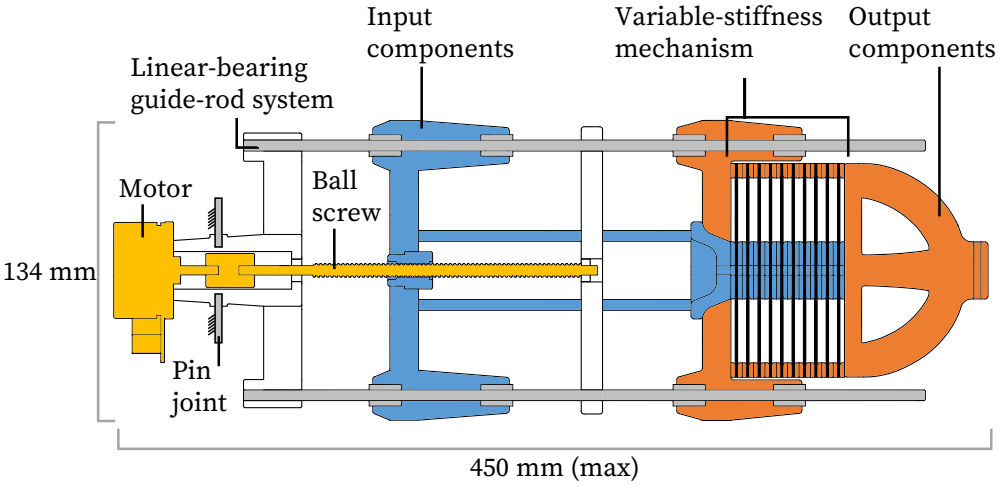

Figure 3.3: Our DET variable-stiffness actuator (VSA). This actuator has only one component motion in its variable-stiffness mechanism: the relative translation of the DET modules' center disks and outer frames. The modules' center disks are connected to the input components (blue), which are driven by the VSA's motor and ball screw (yellow). The modules' outer frames are connected to the actuator's load by the output components (orange). Both the input and output components are constrained to linear motion by the linear-bearing guide-rod system. The variable-stiffness mechanism consists of thirty-two DET modules (thirty active, and two insulating) though the diagram shows only ten for clarity. The variable-stiffness mechanism softens when the DET modules are charged with constant voltage.

Table 3.1: Dimensions of our DET VSA and its DET modules

VSA	
Max. length	450 mm
Output position travel	90 mm
Eq. position travel	42 mm
Width	134 mm
Height	108 mm
Mass	880 g
DET module	
r_o	41.3 mm
r_i	12.7 mm
y_{Max}	see § 3.4.6
z_0	63 µm

and discharge together. A linear-bearing guide-rod system serves as the backbone of the actuator maintaining its components in alignment. The dimensions of our DET VSA are given in Table 3.1.

The use of DETs makes the variable-stiffness mechanism mechanically simpler than those of other VSAs. The DET variable-stiffness mechanism has merely one major component motion: linear displacement of the center disks that stretches the DET modules. In contrast, the VSA variable-stiffness mechanisms mentioned in § 3.1[44,65] have four component motions. Rather than the variety of components in prior variable-stiffness mechanisms, our design has only one type of component: the DET modules, the number of which can be selected to fit the force and stiffness needs of the application. Because the variable-stiffness mechanism has no rolling or sliding components, it does not need any bearings or bushings, simplifying maintenance. Finally, the VSA does not need an additional motor to control its stiffness, as many others do, because its stiffness is controlled by a voltage input.

The hybrid combination of an electric motor and a DET variable-stiffness mechanism simplifies our VSA's control scheme and benefits from the strengths of each transducer. Because this approach restricts each transducer to one task: the motor to equilibrium position modulation and the DETs to stiffness modulation, it fundamentally decouples the

two functions simplifying the VSA's control scheme. In this arrangement, the two transducers complement each other. The motor readily generates large forces and motions and can be operated with simple position control methods. The DETs provide elasticity and stiffness modulation with a simple voltage input, while operating with higher forces and strokes than they could produce as prime movers themselves.

Because the DET modules soften when charged with a constant voltage, the DET VSA is stiffest by default, which could be advantageous for robotic prostheses and orthoses. Robotic prostheses and orthoses for legs should default to stiff settings when they lose power to maintain support for their wearer. They may also need to maintain stiff settings for long periods when their wearer is standing still, which could be energetically costly for a VSA that requires energy to remain stiff. VSAs that do not require power to maintain stiffness[75,76] could also be efficient in this application.

3.3 Modeling of variable-stiffness module

This section first reviews a DET electrical model and a cone-diaphragm mechanical model from other works.[33,77,78] It uses the electrical model to give insight into the causes of electrical energy storage and losses in DETs that will be used to interpret the results in § 3.4. It then uses the mechanical model to derive the effects of module dimensions on a module's uncharged stiffness, voltage-induced stiffness change, and maximum displacement. Knowledge of these effects will be useful for adapting our DET VSA's performance to specific applications.

3.3.1 Electrical

An electrical circuit consisting of a capacitance C with a series resistance R_s and parallel resistance R_p[33,77] (Figure 3.4) is a model for the electrical energy stored and dissipated in a DET. Because a DET consists of a pair of electrodes separated by a dielectric, it capacitively stores electrical energy U_c according to

$$U_c = \frac{1}{2} C V_{DET}^2, \tag{3.1}$$

where V_{DET} is the voltage on the DET capacitance. The series resistance represents the electrical resistance of the DET's electrodes, which dissipates energy through Joule heating. The energy dissipated during charging or discharging is proportional to the charge

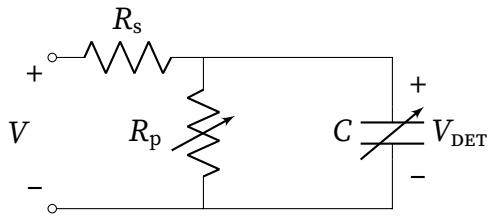

Figure 3.4: Electrical model of a DET. The electrical behavior of a DET is modeled in this work by a capacitance C that represents the charge storage of the DET that changes as the DET deforms, with a series resistance R_s that represents the resistance in the DET's electrodes, and a parallel resistance R_p that represents the current leakage path through the dielectric elastomer. Schematic redrawn and modified from reference [33].

rate and series resistance value.[79] The parallel resistance represents the pathway for leakage current through the dielectric membrane. This current dissipates power P through Joule heating in the dielectric according to

$$P = \frac{V_{DET}^2}{R_p}. \tag{3.2}$$

As the DET is displaced, its electrode area and membrane thickness change causing its capacitance and parallel resistance to change. The series resistance also changes as the DET deforms, but this change is typically negligible being much smaller than the changes in capacitance and parallel resistance.[33]

3.3.2 Mechanical

Displacement of the variable-stiffness mechanism deforms the membrane of an individual DET module into a curved-cone shape that is reasonably approximated as a straight-sided truncated cone (Figure 3.2).[70,78] In this model, when the variable-stiffness mechanism is displaced by y, the membrane takes the shape of a truncated cone with slant height l and thickness z. When undeformed, the membrane is shaped like an annulus with outer and inner radii r_o and r_i and thickness z_0, and the slant height l reduces to $l_0 = r_o - r_i$. The radial-direction stretch λ_r, obtained using the Pythagorean theorem, is

$$\lambda_r = \lambda_p \frac{l}{l_0} = \lambda_p \sqrt{1 + \left(\frac{y}{l_0}\right)^2}, \tag{3.3}$$

where λ_p is the prestretch of the membrane.[33,78] The truncated-cone model implies that the circumferential-direction stretch λ_c is equal to the constant prestretch λ_p and that the

membrane's radial stretch and thickness are homogeneous. In reality, the membrane's stretches and thickness are inhomogeneous as shown by more accurate analyses using numerical solutions of coupled nonlinear differential and algebraic equations[80] and finite element analysis.[58,71] However, we chose to use the truncated-cone model because it simplifies the derivation of the effects of module dimensions given in § 3.3.3 and predicts module behavior with a useful level of accuracy[78] without the computational burden of the more accurate methods.

The net force exerted by a DET module F_{DET} is caused by the radial-direction stress σ_r in the module's membrane. With the assumption that the membrane has constant volume, the relation between DET force and material stress is

$$F_{\text{DET}} = \sigma_r \pi (l_0 + 2r_i) l_0 z_0 \frac{y}{l_0^2 + y^2} \tag{3.4}$$

as seen from references.[33,78] The material stress is the sum of hyperelastic, electrical, and viscoelastic stresses. For a DET with constant volume, constant permittivity, and a single mechanical degree of freedom oriented perpendicular to the electric field, material stress in the actuation direction is given by

$$\sigma_r = \underbrace{\lambda_r \frac{\partial \psi_h}{\partial \lambda_r}}_{\text{hyperelastic}} \underbrace{- \epsilon_0 \epsilon_r E^2}_{\text{electrical}} + \underbrace{\sum_{i=1}^{n} k_i (\lambda_r - 1 - \xi_i) + \eta_{n+1} \dot{\lambda}_r}_{\text{viscoelastic}}, \tag{3.5}$$

where ψ_h is a hyperelastic energy density function, ϵ_0 is the permittivity of free space, ϵ_r is the dielectric elastomer's relative permittivity, E is the electric field applied across the dielectric elastomer, η_i are damping coefficients, k_i are spring stiffnesses, and ξ_i are damper strains, with $\xi_{n+1} = \lambda_r - 1$.[33] Though a cone diaphragm displaces out of plane, this model is applicable because the cone diaphragm's material stretch is perpendicular to the electric field applied across its membrane.

3.3.3 Effect of module dimensions

This subsection discusses the effect of module dimensions (r_o and r_i) on a cone-diaphragm module's uncharged stiffness, voltage-induced stiffness change, and maximum displacement.

This work defines the stiffness of a DET module to be F_{DET}/y rather than the standard definition $\partial F_{\text{DET}}/\partial y$ because this definition captures the change in force at a given displacement caused by the adjustment of a variable-stiffness mechanism. Accordingly, in this

work, stiffness means

$$\frac{\Delta F_{\text{DET}}}{\Delta y} = \frac{F_{\text{DET}}(y) - F_{\text{DET}}(y=0)}{y-0} = \frac{F_{\text{DET}}}{y}. \tag{3.6}$$

This metric can be understood as a linear approximation of the net effect of nonlinear behavior over a finite region.

The effect of module dimensions on a cone-diaphragm's stiffness can be calculated by combining Equations (3.4) and (3.5) to get

$$\frac{F_{\text{DET}}}{y} = \frac{1}{y}\left[\left(\lambda_{\text{r}}\frac{\partial \psi_{\text{h}}}{\partial \lambda_{\text{r}}} - \epsilon_0 \epsilon_{\text{r}} E^2\right)\pi(l_0 + 2r_{\text{i}})l_0 z_0 \frac{y}{l_0^2 + y^2}\right], \tag{3.7}$$

where the effects of viscoelasticity have been neglected. Proceeding further requires a choice for the strain-energy density function ψ_{h}. Let ψ_{h} be the Neo-Hookean strain-energy density function for simplicity. Simplified for a constant volume cone-diaphragm DET, this function is

$$\psi_{\text{h}} = \frac{\mu}{2}\left(\lambda_{\text{r}}^2 + \lambda_{\text{p}}^2 + (\lambda_{\text{r}}\lambda_{\text{p}})^{-2} - 3\right). \tag{3.8}$$

Substituting Equation (3.8) into Equation (3.7) and simplifying yields the DET module's stiffness:

$$\frac{F_{\text{DET}}}{y} = \frac{\pi(l_0 + 2r_{\text{i}})z_0}{l_0}\left[\mu\left(\lambda_{\text{p}}^2 + \frac{l_0^4}{\lambda_{\text{p}}^4\left(l_0^2 + y^2\right)^2}\right) - \frac{\epsilon_0 \epsilon_{\text{r}} V_{\text{DET}}^2}{z_0^2}\right]. \tag{3.9}$$

A similar expression can be derived using the standard definition of stiffness $\partial F_{\text{DET}}/\partial y$. Accordingly, the module's uncharged stiffness (when $V_{\text{DET}} = 0$) varies with its dimensions as shown in Table 3.2.

The effect of module dimensions on a cone-diaphragm's voltage-induced stiffness change can be determined from Equation (3.9) as

$$\frac{\partial}{\partial V}\frac{F_{\text{DET}}}{y} = -\frac{2\epsilon_0 \epsilon_{\text{r}} \pi V}{z_0}\left(\frac{2r_{\text{i}}}{l_0} + 1\right), \tag{3.10}$$

where electrical dynamics are neglected by assuming $V_{\text{DET}} = V$ and viscoelasticity is neglected by setting $k_i = 0$ and $\eta_{n+1} = 0$. According to this equation, the voltage-induced stiffness change varies with r_{o} and r_{i} as reported in Table 3.2.

The effect of module dimensions on a cone diaphragm's maximum displacement can be calculated by substituting the maximum stretch for the membrane material $\lambda_{\text{r, Max}}$ into Equation (3.3) and solving for y:

$$y_{\text{Max}} = l_0\sqrt{\left(\frac{\lambda_{\text{r, Max}}}{\lambda_{\text{p}}}\right)^2 - 1}. \tag{3.11}$$

Table 3.2: How module dimensions affect the performance of cone diaphragm modules

	Constant	Increasing	Uncharged Stiffness	Voltage-Induced Stiffness Change	Maximum Displacement
Case 1	l_0	r_i	increases	increases	is constant
Case 2	r_i	r_o	undetermined	decreases	increases
Case 3	r_o	r_i	undetermined	increases	decreases

According to this equation, the maximum displacement of a cone-diaphragm module varies with r_o and r_i as reported in Table 3.2.

3.4 Results and discussion

This section reports the functionality of our DET VSA: its independent and simultaneous modulation of stiffness and equilibrium position, and the magnitude and speed of its stiffness change. Then, it reports on characteristics of the variable-stiffness mechanism relevant to determining its efficiency: its viscoelasticity and the electrical energy and power required to change its stiffness. Finally, the section discusses the maximum displacement achievable by the variable-stiffness mechanism, and potential solutions for weaknesses of DET technology. Details of the test procedures are given in appendix 3.A.

3.4.1 Modulation of stiffness and equilibrium position

A force-displacement plot of a VSA's behavior can show the coupling between a VSA's stiffness and equilibrium position. A suitable plot is generated by fixing a VSA's equilibrium position, perturbing the VSA's output point with a range of stiffness settings, and repeating these steps for additional equilibrium positions. The stiffnesses of the VSA appear in this plot as the slopes of the curves generated with the equilibrium position fixed, and the equilibrium positions appear as displacement values where force is zero. If the VSA's stiffness and equilibrium position are coupled, then the VSA cannot display a full range of stiffnesses at all equilibrium positions.

Our DET VSA can modulate its stiffness and equilibrium position independently. A force-displacement plot generated by our DET VSA (Figure 3.5) has a pair of stiffer and softer curves that originate from equilibrium position 1 at 0 mm. The stiffer curve was

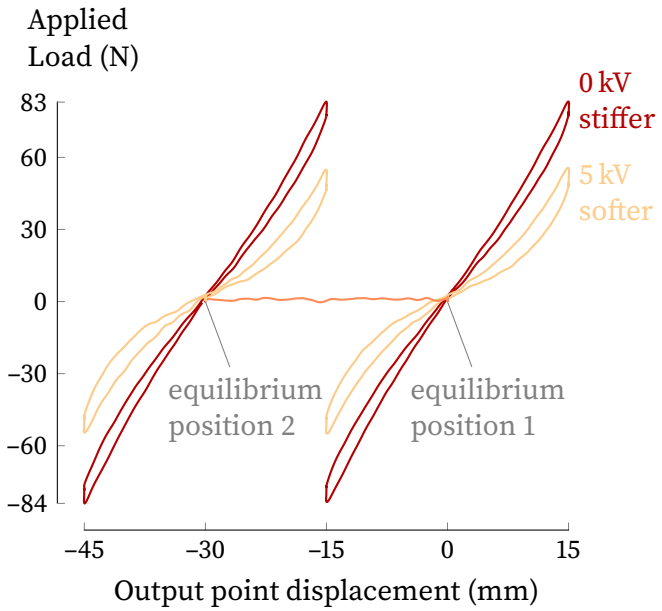

Figure 3.5: Our DET VSA can independently modulate its stiffness and equilibrium position as seen in this plot of the load applied to the DET VSA and its output point displacement. It has the same range of stiffnesses after the actuation motor shifted the equilibrium position from equilibrium position 1 to equilibrium position 2.

generated with our VSA's variable-stiffness mechanism discharged, and the softer curve with the mechanism charged to 5.0 kV. These curves show that the VSA can modulate its stiffness. The VSA can also have intermediate stiffness values, as discussed in § 3.4.2. Our VSA's force-displacement plot has a range of zero-force points between equilibrium positions 1 and 2 that was generated by using the actuation motor to shift the VSA's equilibrium position. This feature shows that the VSA can control its equilibrium position. Finally, the signature has another pair of stiff and soft force-displacement trajectories that originate from equilibrium position 2. These curves are identical to those originating from equilibrium position 1, so the plot shows that the VSA can reach its full range of stiffnesses across its range of equilibrium positions.

3.4.2 Stiffness change magnitude

We calculated the stiffness change from force-displacement data from tensile tests (Figure 3.6). In these tests, a testbed displaced the VSA's output point while the VSA's actuation motor maintained a constant equilibrium position for three compression-tension cycles. In keeping with our definition of stiffness in § 3.3.3, stiffness was calculated as F_{DET}/y for [5,

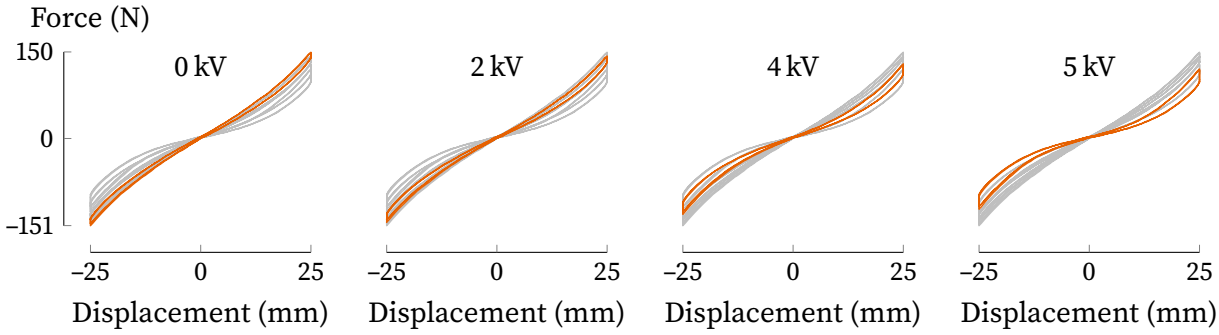

Figure 3.6: The VSA's variable-stiffness mechanism softens when charged with a constant voltage, as seen in these tensile test results with a displacement rate of 1 mm/s. The loops progress in a clockwise direction. The light gray curves are data from the other voltage levels given for context.

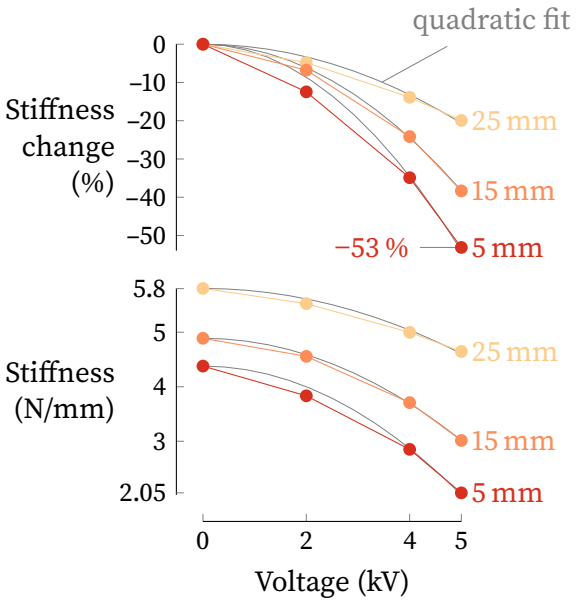

Figure 3.7: Our DET VSA softened approximately quadratically with the applied voltage up to 53 %. These values were calculated from the rising tension portion of the third cycles of the trajectories shown in Figure 3.6 by dividing the force at [5, 15, 25] mm by the corresponding displacement. Because the DET stiffness is quadratically dependent on voltage, quadratic fits using only a quadratic term and a constant term equal to the initial point are plotted for comparison with the experimental data.

15, 25] mm. The corresponding stiffness changes in Figure 3.7 were determined from the rising tension portion of the third cycle.

As the voltage on the DET modules increased, our DET VSA softened approximately quadratically up to 53 % (Figure 3.7). Quadratic fits (using only a quadratic term and a constant term equal to the initial point) are plotted for comparison with the experimental data because the DET stiffness is quadratically dependent on voltage (Equation (3.9)). Though we only report data at discrete voltage levels, the VSA can have a continuous range of stiffness levels because the stiffness change is controlled by voltage input, which can have a continuous range of values.

The 53 % stiffness reduction of our DET is not a fundamental limit of the design, and greater stiffness changes are possible. Because the stiffness change increases dramatically with the DET voltage, even a slightly higher voltage can noticeably increase the stiffness change. While the elastomer in our DET modules (VHB 4910 with a 400 % biaxial prestretch) can sustain 15 kV when the energized region is small,[81] under more relevant test conditions its breakdown voltage is about 6 kV.[82] In the development of our DET VSA, we tested many prototype DET modules at 6 kV, and these tests yielded greater stiffness reductions than those at 5 kV. DET diaphragm modules with different proportions and 385 % biaxial prestretch have displayed zero stiffness (100 % reduction) for small displacements when charged with 6.25 kV.[58]

3.4.3 Stiffness change speed

To measure how fast the VSA could change stiffness, the variable-stiffness mechanism was charged to 5 kV with displacements of [5, 15, 25] mm. The DET modules used in the variable-stiffness mechanism can charge rapidly because they are capacitors, but the high-voltage power supply used in this work could not supply enough current to charge all of them simultaneously at their maximum rate. Accordingly, when testing to see how rapidly the VSA could soften, only three DET modules were installed on the VSA. Stiffness was calculated as force divided by displacement consistent with the definition in § 3.3.3. This method is also consistent with that used to measure the speed of stiffness change in reference.[58]

The VSA's stiffness change can be rapid (within 50 ms), because it is limited primarily by charge rate, but it is also limited by a slow-decay mechanism. During testing, the VSA's stiffness dropped rapidly and then decayed slowly (Figure 3.8). The rapid drop corresponds to the period when the DETs were charging (0 ms to 40 ms), so the power supply's

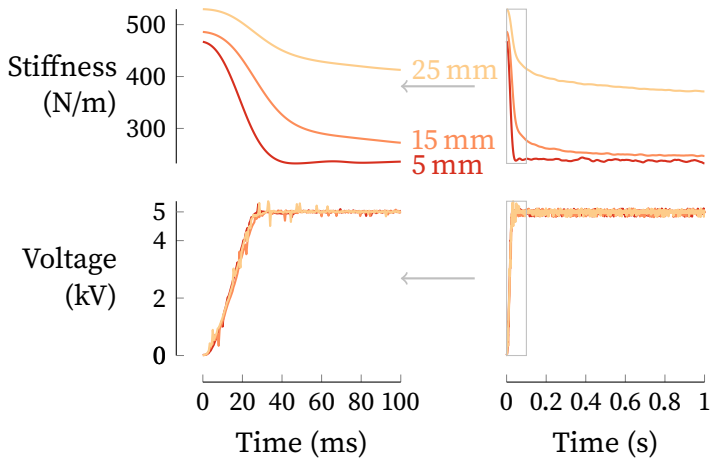

Figure 3.8: The DET VSA changed stiffness rapidly while charging to 5 kV with only three DET modules installed and the variable-stiffness mechanism's displacement fixed at [5, 15, 25] mm.

performance limits the stiffness change during this period. The slow decay was short for 5 mm displacement, so that the stiffness changed within 50 ms. In another work,[58] a smaller cone-diaphragm module softened in 12 ms when charged with a power supply with a faster voltage change rate than that of our power supply (DCH3320P1, High Voltage Power Solutions).

The slow decay that follows the rapid drop does not appear to be caused directly by electrostatic forces because the voltage is steady during the slow decay period. We suggest that the slow decay may be caused by viscoelastic relaxation within the membrane. The application of voltage to a module's electrodes may cause its elastomer membrane's deformed shape to become more curved and reduce the force exerted by the module. The deviation between the actual curved-cone shape of a displaced cone-diaphragm module and the straight-sided cone approximation increases with displacement y, so this effect should be more prominent for larger displacements. Furthermore, this voltage-induced curvature would likely be damped by the viscoelasticity of the elastomer membranes, resulting in the slow decay of stiffness seen in the stiffness-change speed tests (Figure 3.8).

3.4.4 Viscoelasticity

The viscoelastic behavior of the DET modules had a significant influence on the DET VSA's force and stiffness (Figure 3.9). Tensile tests with greater displacement rates yielded greater forces and more hysteresis. The viscoelasticity of the dielectric elastomer used in

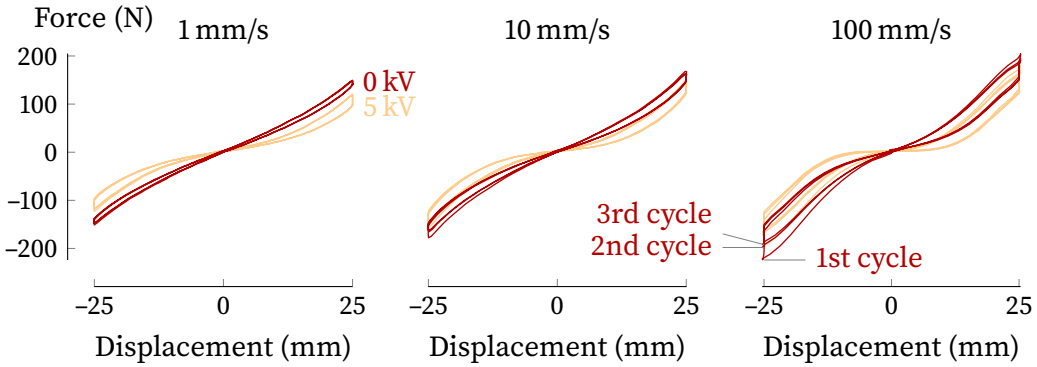

Figure 3.9: The viscoelasticity of the DET modules caused them to exert more force and have more hysteresis when the variable-stiffness mechanism was displaced more rapidly. The force-displacement trajectories settled towards a steady-state response producing peak forces of less magnitude on each subsequent cycle. The loops progress in a clockwise direction, so the hysteresis is dissipative.

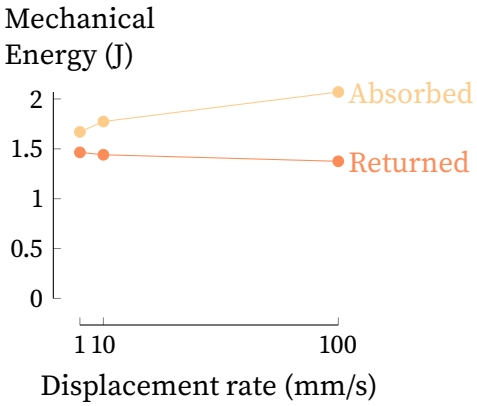

Figure 3.10: Our DET VSA absorbed more and returned less mechanical energy at faster displacement rates. Thus, it dissipated more mechanical energy at faster displacement rates. These values were calculated by integrating the third tension cycle of the 0 kV curves in Figure 3.9.

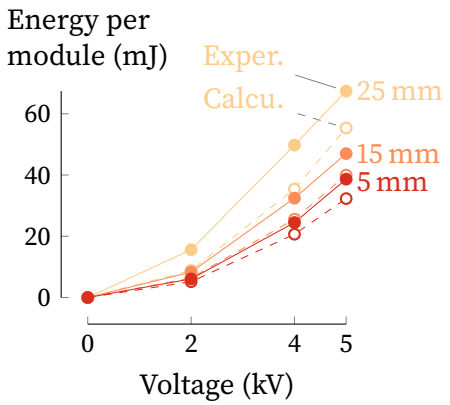

Figure 3.11: Much of the electrical energy used to charge the DET modules was stored in the modules and could be recovered to increase the efficiency of stiffness changing. These values are the energy used to change stiffness during relaxation tests. The stored energy values calculated from Equation (3.1) are marked with hollow markers connected by dashed lines, and experimental values are shown with circular markers connected by solid lines.

the DET modules explains these two effects because viscosity damps motion.[83] Viscoelasticity also caused forces to be highest on the first cycle and to be lower on subsequent cycles as the DETs settled into a steady-state response. This effect is most obvious for the 100 mm/s trials, but it occurred for all measured data. The viscoelastic hysteresis was quantified by integrating the third tension cycle of the 0 kV curves in Figure 3.9, yielding the mechanical energy absorbed and returned by the variable-stiffness mechanism (Figure 3.10). The difference between the energy absorbed and returned is the energy dissipated by viscoelasticity.

3.4.5 Electrical power requirements for stiffness change

Most of the electrical energy used to change stiffness is stored in the DET modules, and much of this stored energy could be recovered with appropriate circuitry. We measured the energy used to change stiffness by integrating the electrical power supplied to the variable-stiffness mechanism during relaxation tests, wherein the VSA was held at a constant displacement while its variable-stiffness mechanism was charged. The energy stored in the DET modules during the relaxation tests according to Equation (3.1) is only a little less than the experimentally measured energy used to change stiffness (Figure 3.11) and could potentially be recovered.

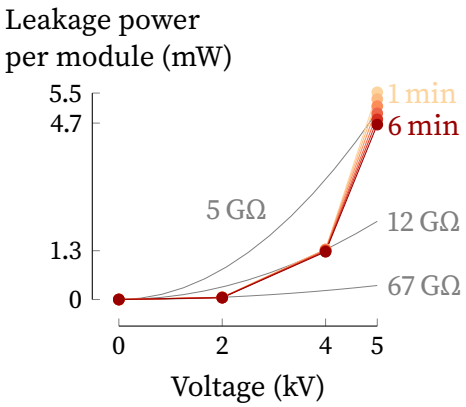

Figure 3.12: Current leakage through the dielectric causes our DET VSA to draw continuous electrical power while holding reduced stiffness as determined from measurements of the leakage current through five DET modules connected in parallel. The leakage power we measured was not consistent with the power dissipated through a constant resistance value (shown by the gray curves). The leakage power decreased over time while the DETs were held at constant voltage.

Our DET VSA requires continuous electrical power to hold a reduced stiffness due to current leakage through the dielectric. To determine the amount of power required, we measured the leakage current through five DET modules connected in parallel for 6 min and multiplied the measurement by the supply voltage (Figure 3.12). The current decreased with time, and the leakage power at 3 min was [0.06, 1.33, 5.15] mW for [2, 4, 5] kV. Using these power and voltage values in Equation (3.2) to calculate the leakage resistance yields [67, 12, 5] GΩ. The theoretical power consumption by constant resistances of these values according to Equation (3.2) are plotted in Figure 3.12 to make it clear that the leakage power of the DETs is not well represented by a constant resistance. This behavior can be explained by the decrease of VHB 4910's volume resistivity under high electric fields.[84] The change in leakage current over time can be explained by the process of dielectric absorption.[85]

3.4.6 Maximum displacement of variable-stiffness mechanism

In the experiments in this work, displacements of the variable-stiffness mechanism were limited to 25 mm to avoid failure, but previous work and our experience indicate that greater displacement is possible. The state of stress in a cone-diaphragm DET is similar to that in a "pure shear" DET.[78] Such a DET made with VHB 4905 has been actuated to a state of 700 % × 400 % stretch.[86] In a uniaxial tensile test, a strip of VHB 4910 endured

over 1200 % stretch before breaking, but in relaxation tests, strips of VHB 4910 broke while being held at 700 % stretch.[87] Therefore, it is reasonable to assume a failure stretch of 700 % for VHB 4910. Substituting $\lambda_{r,\,Max}$ = 700 % into Equation (3.11) yields a maximum displacement for the variable-stiffness mechanism y_{Max} = 41 mm. This calculation fits with our observations that 42.3 mm to 61.6 mm was the range of failure displacements for prototype cone-diaphragm modules with the same dimensions as those used in this work.

3.4.7 Discussion of solutions for DET weaknesses

Other research discussed in this section has reported potential solutions for the weaknesses of DET technology: poor reliability, viscosity, and the need for high voltages.

The biggest challenge in this work was achieving reliable operation of the DET modules. Several modules initially worked well, but later failed with less than a thousand motion cycles after being stored for about two months. Reliability can be improved through proper choice of electrode formulation, operating in a dry environment (<5 % relative humidity), or operating at low electric fields.[88] Some DETs have operated for millions of cycles.[88] Cone diaphragms in particular have achieved tens of thousands of cycles before failure.[58]

Some applications may benefit from the viscous damping of the DET modules,[89] but it hampers their ability to return stored energy, and it makes precise force control more challenging. The viscoelastic behavior in our DETs could be greatly reduced by using silicone for their dielectric elastomer[90,91] because silicones typically have much less viscosity than the acrylic elastomer used in this work. Because of their reduced viscosity, silicones have a greater response bandwidth than acrylics,[90,91] so they could yield faster stiffness changes than demonstrated here, especially for larger elongations. Silicones typically have a smaller stretch capacity than VHB 4910, but the actuation stretch (λ_r/λ_p) of cone diaphragms (33 % in this work) is achievable for silicones because they need less prestretch than VHB 4910 (merely 20 % prestretch was used in reference[78]).

Our DET VSA's stiffness change is smaller than that of state-of-the-art VSAs,[76] but it could be increased by changing the elastomer used in its DET modules. An elastomer with greater relative permittivity could generate a larger stiffness reduction as seen from Equation (3.9). This possibility and others have been extensively researched.[34]

The high voltages that DET modules require can be difficult to supply in mobile applications. However, small (<2 cm^3) DC-DC power converters are commercially available,[92]

and researchers are developing power supplies optimized for DETs.[73,93] The stiffness variation of a DET is governed by the electric field across it, so DETs with thinner dielectric elastomers can operate at lower voltages. The acrylic material used in this work is also available in half of the thickness that we used (VHB 4905 from 3M), so these devices could be easily redesigned to operate at half of the voltage they use now, though twice as many of them would be required for a given stiffness. Other work has demonstrated DET operation at as low as 300 V with a thinner elastomer.[94] These advancements are paving the way to practical and higher-performance DET devices.

3.5 Conclusions

The DET VSA achieved VSA functionality by using a hybrid actuation architecture: an electric motor modulates the actuator's equilibrium position, and the DET variable-stiffness mechanism modulates the actuator's stiffness. Such decoupled modulation is common in state-of-the-art VSAs but has not been demonstrated with DETs before. This resulting actuator has merely a single component motion in its variable-stiffness mechanism, giving it a mechanical complexity similar to that of series elastic actuators. This simplicity could make it practical to obtain the benefits of variable-stiffness actuation without the weight, volume, and cost that normally accompany them, once weaknesses of DET technology are addressed.

3.A Materials and Methods

3.A.1 DET materials

Because the purpose of this project was to demonstrate an application of DET technology rather than improve it, we used DET materials that simplified manufacturing rather than those that might provide maximum performance. The dielectric elastomer was VHB 4910, an acrylic elastomer that is sold commercially by 3M as a double-sided adhesive tape. VHB 4910 is 1 mm thick, but we stretch it by hand to 400 % biaxial stretch during construction, which thins it to about 63 µm making it more responsive to lower voltages. The electrode material was graphite nanopowder (US Research Nanomaterials # US1058), and it was applied by hand with a sponge applicator. Strips of conductive fabric (Less EMF Stretch Conductive Fabric, # A321) were used to make electrical contact with the graphite electrodes. The module frames and center disks were 3D printed from Stratasys ABS-M30

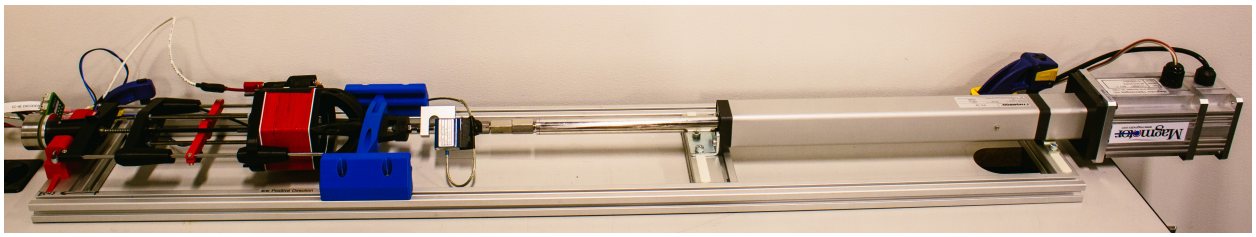

Figure 3.13: The custom universal testing machine (UTM) used for testing is depicted here with the DET VSA connected and the 200 N load cell installed.

on a Stratasys Fortus 400mc 3D printer. The reinforcement material was 76.2 µm (3 mil) thick polyimide adhesive tape, cut to shape with a laser cutter, and applied to the frames and center disks by hand. It extended 2.54 mm (0.1 in.) from the frame into the electrode region. The materials used to make a single module cost less than $5.

3.A.2 Testbed

We used a custom-built universal testing machine (UTM) (depicted in Figure 3.13) to demonstrate and quantify our VSA's capabilities. Its frame is made from aluminum T-slot tubing. This test bed has a linear actuator (Thomson PC32LX powered by Magmotor BF34-200) which we refer to as the load actuator, that is connected to the output point of our VSA through a load cell (Interface Force SM2000). During experiments, the load actuator displaced the VSA's output point, and the load cell measured the force output of the VSA.

The testbed's microcomputer (National Instruments myRIO 1900) controls the UTM and the DET VSA, and records sensor data. The myRIO communicates with two motor controllers (Maxon EPOS2 70/10) with the CAN protocol and these motor controllers control the UTM motor and the VSA motor. Using analog signals, the myRIO controls the high-voltage power supply (DCH3320P1, Dean Technology) that powers the VSA's variable-stiffness mechanism. Since the UTM was rigidly connected to the VSA's output point, the position of this point was measured with the encoder on the UTM motor. The load cell signal passed through a signal conditioner (DMA2, Interface) and was then read by the myRIO through an analog input. The myRIO recorded the analog signal for the output voltage and current of the high-voltage power supply. During the tensile and VSA signature tests, the sample frequency for all measurements was 50 Hz. During the relaxation and stiffness changing speed tests, the analog signals were sampled at 2 kHz. During post processing, all signal data was filtered with a low-pass filter with a 40 Hz cutoff. All testing was performed at ambient temperature and humidity.

3.A.3 Test procedures

The tensile tests resembled cyclic tensile tests, which are used to determine stress-strain behavior of material samples. In these tests, the UTM cyclically compressed the DET VSA 25 mm, stretched it 25 mm, and returned it to its equilibrium length three times, while the DET VSA's motor fixed the VSA's equilibrium position at zero. The motion was performed at constant speeds of [1, 10, 100] mm/s and paused at the extreme points for [20, 2, 0.2] s for the speeds, respectively.

Our DET VSA's ability to independently modulate its stiffness and equilibrium position was tested with a modified tensile test. In this test, the motion cycles traversed 15 mm of compression and tension instead of 25 mm to keep the overall motion within the VSA's travel limits. The cycles were conducted at 10 mm/s with 1.2 s of dwell time at each extreme position. The first cycle was performed with the DET modules discharged, then the motion paused while the modules were charged to 5.0 kV, and then a second cycle was performed. The modules were discharged and the VSA's motor shifted the VSA's equilibrium 30 mm from equilibrium position 1 to equilibrium position 2 while the UTM kept the variable-stiffness mechanism unstretched. Finally, another pair of motion cycles like the first were performed.

We used the relaxation tests, so called because they resemble relaxation studies for viscoelastic materials,[95] to determine the amount of energy required to soften the variable-stiffness mechanism. In these tests, the VSA's motor was commanded to maintain the equilibrium position at zero, and the UTM held the output at a fixed position. Then, the high-voltage power supply charged the DET modules causing the variable-stiffness mechanism to soften, while the output current and voltage of the high-voltage power supply were recorded. The power supply maintained the charge for 10 s, which allowed the DET modules to charge fully. The input power for the variable-stiffness mechanism was calculated as the product of the high-voltage power supply's output voltage and current. The energy required to soften the variable-stiffness mechanism was the integral of its input power from the start of the experiment until the input power dropped to its steady-state level. Trials were performed with combinations of [5, 15, 25] mm of stretch, and [2, 4, 5] kV of voltage. To keep the output current of the high-voltage power supply to less than 5 mA and not exceed its capabilities, the voltage on the DET modules was ramped for a period of 0.25 s for the [2 and 4] kV trials and 0.5 s for the 5.0 kV trials before being held steady.

Because the high-voltage power supply's current capability limited the charging speed during the relaxation tests, an additional set of relaxation tests were performed to demonstrate how fast our DET VSA could soften. In these tests, only three DET modules were installed in the variable-stiffness mechanism, without the insulating modules that would dilute the stiffness change. The 2 kN load cell was replaced with a 200 N load cell (SM200, Interface) to increase measurement sensitivity. The variable-stiffness mechanism was charged to 5.0 kV with displacements of [5, 15, 25] mm.

The power to maintain a stiffness reduction was investigated by measurements of the leakage current through a set of five DET modules connected in parallel. The leakage current through the five DET modules was measured by connecting them to a high-voltage power supply (Matsusada EQ-30P1), with a multimeter (ANENG AN8008) in ammeter mode in series between the DET modules and ground because the current measurements from the DCH3320P1 high-voltage power supply's current monitor were not precise enough. The voltage was ramped manually to 5 kV, and then current readings from the multimeter were recorded every 30 s for 6 min. The voltage was then ramped to 0 kV, and after a waiting period of a few minutes, the process was repeated with [4 and 2] kV.

CHAPTER 4

ANKLE-FOOT ORTHOSIS

4.1 Background on foot drop remedies

Foot drop is the condition of not being able to dorsiflex the ankle (raise the toes) properly due to a neuromuscular impairment.[96] People with foot drop are prone to trip and fall because their toes catch on obstacles, and their affected foot slaps onto the ground after heel contact. Foot drop can be caused by stroke or injuries that affect the peroneal nerve, so people with foot drop are often otherwise healthy and have the ability to plantarflex their affected ankles (lowering the toes).

Current treatments for chronic foot drop improve mobility, but they have drawbacks. Passive ankle-foot orthoses (AFOs) are essentially springs that lift a patient's foot so that it has sufficient toe clearance while the leg is swinging. These devices are effective, lightweight, simple, cheap, and common. However, the dorsiflexion assistance they provide comes at the cost of making plantarflexion more difficult. Functional electrical stimulation devices do not have this drawback. They provide dorsiflexion by applying neural stimulation to the patient's peroneal nerve causing the ankle dorsiflexors to contract and lift the toes.[96] They deactivate during push-off allowing the ankle to plantarflex freely. However, they only work for a limited patient population because they rely on functional muscles and nerves, and not all patients tolerate the stimulation sensation.

Powered AFOs can relieve foot drop symptoms without the drawbacks of passive AFOs and functional electrical stimulation, but the drawbacks of state-of-the-art prosthesis and orthosis actuators described in § 1.1 are quite evident in attempts to develop powered AFOs. A powered AFO driven by a series elastic actuator provided dorsiflexion assistance during swing and minimized plantar flexion impedance during push-off.[97] Study participants who used the device preferred it over passive AFOs, and one participant "remarked that the [powered AFO] made walking 'almost subconscious, like normal walking' ".[97] However, this AFO had a mass of 2.6 kg, required a tethered power supply, and was too bulky for everyday use. Another powered AFO weighed less (1.75 kg) and provided dorsi- and plantarflexion assistance,[98] but it also used a tethered power supply and was impractically bulky. A pneumatic AFO operated from a portable carbon dioxide tank worn on the user's belt and demonstrated untethered operation.[15] Still, it was bulky and heavy (1.9 kg AFO + 1.2 kg on belt), and its carbon dioxide supply was only sufficient for 1914 steps. An

AFO powered by pneumatic muscles had less bulk, a soft construction, and a mass of 950 g without its air source.[16] It powered foot inversion and eversion in addition to plantarflexion and dorsiflexion. It could operate with a portable carbon dioxide cylinder but only for "more than 320 full actuation cycles".[16] Though none of these works address the sound of these devices, they were all likely too noisy for practical everyday use.

A question thus arises: how can we obtain the benefits of powered AFOs without the noise, bulk, and inefficiency that normally accompany them? Doing so would improve the quality of life for people with foot drop, and it could also lead to improvements in other prosthesis and orthosis designs.

Clutched-spring and semi-active AFOs could be quieter, lighter, and less energy-hungry than powered AFOs, but none of the designs reported to date provide dorsiflexion assistance during swing without impeding push off. A clutched-spring AFO reduced the metabolic cost of walking without using actuators or doing net positive work.[99] This remarkable achievement inspired two other clutched-spring AFOs with mechanical improvements to the design. One of these had a slimmer form factor that could be worn under clothing.[100] The other was able to vary its stiffness by changing the number of springs engaged by its electrostatic clutches.[69] However, these AFOs only provide plantarflexion assistance, not dorsiflexion assistance. Two semi-active AFOs used variable dampers to prevent foot drop,[101,102] but these designs impede push off like passive AFOs.

Dielectric elastomer transducers (DETs) may be able to power an AFO that provides dorsiflexion assistance without impeding plantarflexion, and have been suggested for this very application.[22,23] The research question that this work seeks to answer is: how can we design a DET-powered AFO that will relieve foot drop symptoms with less mass, volume, noise, and energy consumption than electric and pneumatic powered AFOs? To answer this question, we analyzed the application requirements for a DET AFO that provides foot drop assistance and started building a proof of concept device. This chapter reports the results of our analysis (§ 4.2), describes the device (§ 4.3), and reports the methods (§ 4.4) and results (§ 4.5) of our benchtop tests.

4.2 Analysis of application requirements

Our analysis of application requirements guides the design of our DET AFO. It starts by examining how the effects of foot drop on walking gait can be counteracted. This analysis leads to the overall structure of our DET AFO. Then, the geometry of the DET AFO is analyzed to determine how to minimize the force and actuation stretch required from the

DET. Finally, the function of a charge recovery system is analyzed to help increase the AFO's battery life.

4.2.1 Counteracting foot drop

During normal-speed walking on level ground, the ankle flexes cyclically over a period of approximately 1 s[103] (Figure 4.1, Ankle angle[104]). The walking gait cycle starts at *heel strike*, the moment when the foot touches the ground, in a phase called *loading response*. During loading response, the ankle plantarflexes, lowering the toes until they also contact the ground at the moment of *toe contact*, which begins the *foot flat* phase. During foot flat, the shank pivots forward over the ankle. The moment of *heel off*, when the heel leaves the ground, starts the *push off* phase. During push off, the ankle plantarflexes rapidly. Push off ends and the swing phase begins at the moment of *toe off*, when the toes leave the ground. At the start of *swing*, the ankle dorsiflexes, raising the toes so that the foot is clear of the ground as it swings forward for the next gait cycle that begins at heel strike.

An AFO can counteract foot drop without impeding plantarflexion by mimicking the function of the ankle dorsiflexor muscles. Foot drop is an impairment of the ankle dorsiflexor muscles that allows the ankle to plantarflex too quickly during loading response, which can cause an audible foot slap, and reduces toe clearance during swing, which can cause trips and falls.[103] Passive AFOs counteract foot drop by exerting dorsiflexion torque throughout the gait cycle, which not only counteracts foot drop, but also impedes plantarflexion. Impeding plantarflexion is undesirable because it increases the effort that the ankle plantarflexor muscles exert during push off to achieve normal ankle motion. Accordingly, to counteract foot drop without impeding plantarflexion, an AFO should provide dorsiflexion torque during loading response, relax during push off, and provide dorsiflexion torque again during swing, which is nearly the same pattern as normal dorsiflexor muscle activity.[103]

The core of our DET AFO design is a DET strap that connects the foot near the toes to the shank near the knee (Figure 4.2). The DET passively holds the foot up (dorsiflexed) to the maximum angle experienced during normal walking. This arrangement leads to three benefits. First, passive dorsiflexion support means that the AFO can provide toe-lift support even when powered off, so it can still relieve foot drop like a passive AFO even if it runs out of battery power. Second, attaching the DET to the foot in front of (anterior to) the ankle makes the DET support the weight of the foot with a tensile force, so there is no concern about it buckling under load like there would be if it was loaded with a

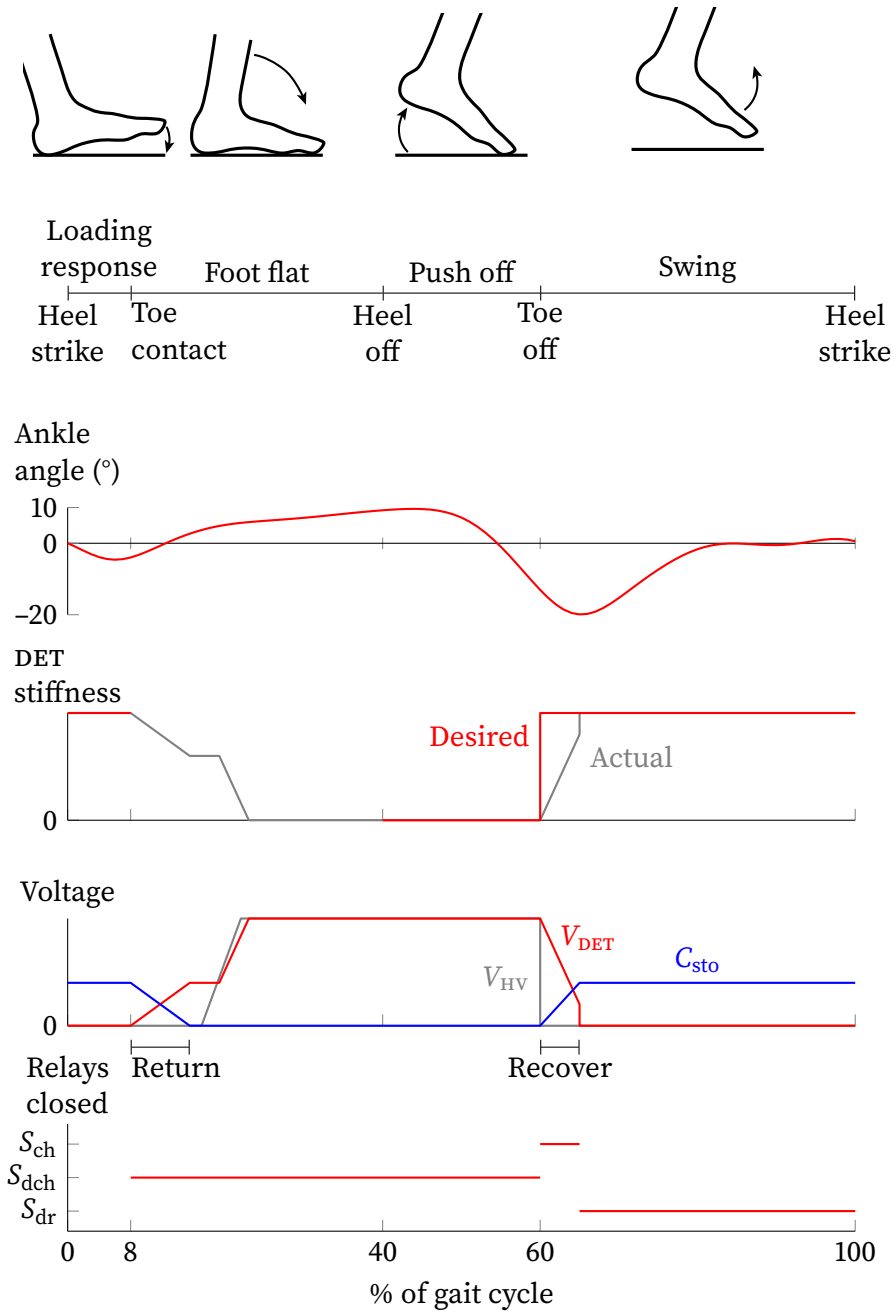

Figure 4.1: The DET AFO provides dorsiflexion support to relieve foot drop symptoms by stiffening during swing and loading response, and it avoids impeding push off by softening during push off. To increase battery life, the DET AFO's charge recovery system recovers charge from the DET at the start of swing and returns it at the start of foot flat.

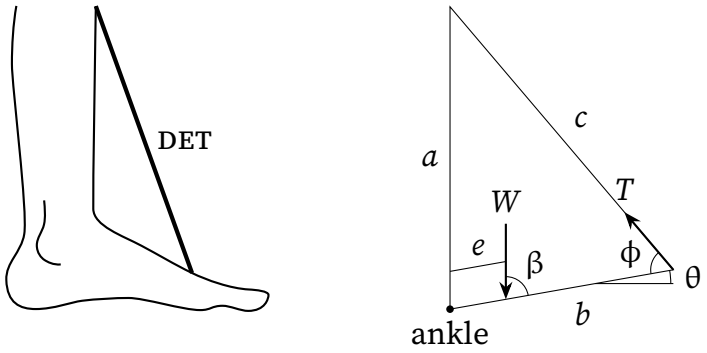

Figure 4.2: The core of our DET AFO design is a DET strap that lifts the toes. To determine actuation stretch required from the DET, the geometry of the DET AFO is modeled by a triangle with sides a and b representing the distances from the strap's attachment points to the ankle and side c representing the length of the DET. To determine the force required from the DET, the DET's loading is modeled as foot weight W and DET tension T acting on the lever arm b.

compressive force. Third, a DET that is loaded in tension and actively lengthens has a biasing load, so it does not need a bias mechanism.

Our DET AFO is controlled with merely a single sensor for detecting gait timing: a toe contact sensor. The AFO should be stiff during loading response to prevent foot slap, soft during push off to allow push off, and stiff during swing to prevent toe dragging (Figure 4.1, DET stiffness). Accordingly, the voltage on the DET should be low during loading response, high during push off, and low during swing. The stiffness during foot flat is not very important, so we use this phase to ramp up the voltage on the DET, which wastes less energy than stepping up the voltage.[79] The moments for changing voltage correspond to the moments of toe contact and toe off, and these can be detected with a toe contact sensor such as a pressure switch or force-sensing resistor.

4.2.2 Minimizing force and actuation stretch

The goals for this section are to 1) determine where to place the DET's foot and leg connections so as to minimize the force and actuation stretch required from the DET, and 2) to calculate the force and actuation stretch requirements for the DET. To do so, the geometry of the AFO is modeled and analyzed to determine the effect of connection placement on the force and actuation stretch requirements. Then, connection placements are selected based on the results of the analysis in order to achieve a compromise between the goals of minimizing actuation stretch and minimizing force. Finally, the model is used with the

selected connection placements to calculate the force and actuation stretch requirements for the DET.

We can calculate the required actuation stretch for the DET by modeling the AFO's geometry as a triangle (Figure 4.2). In this triangle, a and b are the distances from the ankle joint to the DET's shank and foot attachments respectively, and θ is the ankle angle, where $\theta = 0$ means the ankle is perpendicular to the shank. Length c represents the length of the DET, which includes active stretchable length c_{DET} and length c_{stiff} that represents the unstretchable portions of the DET such as its mounting connectors, so we have

$$c_{\text{DET}} = c - c_{\text{stiff}}. \tag{4.1}$$

The DET's actuation stretch S is the ratio of its maximum length to its minimum length, which occur at the minimum and maximum values of θ:

$$S = \frac{c_{\text{DET, max}}}{c_{\text{DET, min}}} = \frac{c_{\text{DET}}(\theta_{\text{min}})}{c_{\text{DET}}(\theta_{\text{max}})}. \tag{4.2}$$

The length c_{DET} can be calculated by using the law of cosines and simplifying with trigonometry and algebra:

$$c_{\text{DET}} = \sqrt{a^2 + b^2 - 2ab\sin(\theta)} - c_{\text{stiff}}. \tag{4.3}$$

We can calculate the force the DET must support from summing the moments about the ankle due to the DET force and the foot's weight (Figure 4.2). The foot weight W acts at angle β at the position of the foot's center of mass, which is distance e away from the ankle. The DET force T acts at angle ϕ at the DET's foot connection point, which is distance b from the ankle. The sum of moments about the ankle is:

$$\begin{aligned}
\sum M_{\text{ankle}} &= Tb\sin(\phi) - We\sin(\beta) \\
&= (Tab/c)\sin(\beta) - We\sin(\beta) \\
&= (Tab/c - We)\sin(\beta) \\
&= (Tab/c - We)\sin(\pi/2 - \theta) \\
&= (Tab/c - We)\cos(\theta) \\
&= \left(\frac{Tab}{\sqrt{a^2 + b^2 - 2ab\sin(\theta)}} - We\right)\cos(\theta) = 0
\end{aligned} \tag{4.4}$$

Table 4.1: Parameters used for calculating AFO specifications

Quantity	Symbol	Value
distance from ankle to		
leg attachment point	a	1 cm to 35 cm
foot attachment point	b	1 cm to 16 cm
foot center of mass	e	8 cm
stiff portion of DET	c_{stiff}	9.2 cm
ankle angle	θ	$-20°$ to $10°$
foot weight	W	12 N

Because $-90° < \theta < 90°$, $\cos(\theta)$ is greater than zero, so we must have

$$T = \frac{\sqrt{a^2 + b^2 - 2ab\sin(\theta)}}{ab} We. \tag{4.5}$$

We use $\theta = \theta_{\text{max}}$ for calculating design requirements to determine the force the DET must exert to hold the foot at its greatest angle.

The connection placements of $a = 35\,\text{cm}$ and $b = 5\,\text{cm}$ achieve a compromise between minimizing actuation stretch and force requirements. We analyzed the effect of connection placements on force and actuation stretch numerically using the parameters in Table 4.1 in Equations (4.2) to (4.4). Actuation stretch can be minimized by either minimizing a and maximizing b, or maximizing a and minimizing b (Figure 4.3). In contrast, force is minimized by maximizing both a and b. We chose to achieve a compromise between these goals by first setting a to its maximum value (35 cm) because maximizing a minimizes both force and actuation stretch. Then we selected $b = 5\,\text{cm}$ because it resulted in the minimum force requirement for an actuation stretch which we expected to be attainable by our DET design. Plugging $a = 35\,\text{cm}$ and $b = 5\,\text{cm}$ into Equations (4.2) to (4.4) yields the force and actuation stretch requirements for the AFO's DET:

$$S = 1.1 \text{ (unitless), and} \tag{4.6}$$

$$T = 19\,\text{N}. \tag{4.7}$$

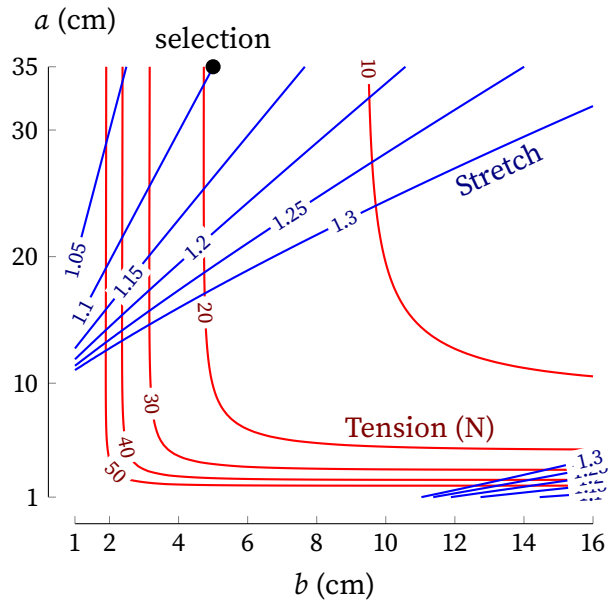

Figure 4.3: The selection of $a = 35\,\text{cm}$ and $b = 5\,\text{cm}$ for the connection placements achieves a compromise between minimizing actuation stretch and force requirements.

4.2.3 Increasing battery life with charge recovery

One of the application requirements is that the AFO run on a battery. Ideally, the battery would last long enough for a full day of walking (5000 to 10 000 steps). There are many ways to help increase the battery life of the AFO with common electrical engineering practices. Here, we concentrate on a practice that is less known, designing a charge recovery system to decrease the amount of energy needed from the high-voltage DC-DC converter. To do so, this section will first explain why a charge recovery system helps improve the energy efficient of a DET actuation system, and then it will analyze how the recovery system should be designed.

A charge recovery system can increase the AFO's battery life. If a DET is held at a constant voltage while being stretched to a larger area, half of the electrical energy that flows into the DET during the stretching (W_e, Figure 2.2) is converted to mechanical work W_m, and the other half is stored as electrical energy U_e in the DET.[48,50] Often, the stored electrical energy is subsequently drained through a resistor so that the DET will return to its uncharged shape, resulting in energy efficiency of no more than 50 %. This 50 % efficiency limit comes from the fundamental energy conversion process, and does not account for other loss mechanisms, which reduce energy efficiency further.[50] This limit can be re-

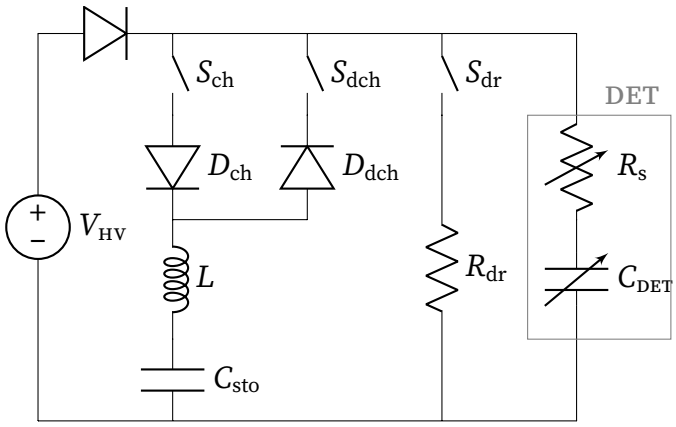

Figure 4.4: The DET AFO's high-voltage power system features a charge recovery system to reduce the amount of energy needed from the high-voltage DC-DC converter to charge the DET. The charge recovery system recovers charge from the DET by closing S_{ch}, and it returns charge to the DET by closing S_{dch}. The system can also drain the DET by closing S_{dr}.

moved by using a charge recovery system to transfer the electrical energy off the DET and store it elsewhere for later use.

Our charge recovery system (Figure 4.4) uses a high-voltage capacitor bank to recover charge from the AFO's DET. It recovers charge from the DET by closing the charge relay S_{ch} when the capacitor bank C_{sto} is at a lower voltage than the DET. It returns charge to the DET by closing the discharge relay S_{dch} when the capacitor bank is at a higher voltage than the DET. This charge recovery method avoids losses incurred in converting the DET's electrical energy to a low voltage for storage in a battery or low-voltage capacitor.[105,106]

A capacitive charge recovery system must have inductance to recover more than 25 % of the energy stored on a DET. If a charged capacitor is connected directly to an uncharged capacitor, charge will flow from the first capacitor to the second until their voltages equalize. This process will dissipate at least half of the energy originally stored on the first capacitor,[107] and no more than 25 % of the original energy will be stored in the second capacitor. Therefore, if the inductance L in our charge recovery system was zero, then no more than 25 % of the energy stored in the DET could be transferred from the DET to the capacitor bank. The energy loss occurs because the kinetic energy of the moving charges, which is the difference between the electrical potential energy in the original capacitor and that in the two-capacitor system, is dissipated (a variety of dissipation processes are possible[107]) rather than stored. An inductor placed in series between the two capacitors

will store the kinetic energy of the moving charges and then release it to the second capacitor, so the second capacitor can receive all of the energy originally stored on the first capacitor if there is no resistance.[106] Because of this principle, we have an inductor bank L in series with the capacitor bank. If the inductor bank is chosen so that the recovery circuit is underdamped, then the inductor bank will keep current flowing once the DET and capacitor bank have the same voltage, so the capacitor bank will end up with a greater voltage than the DET. The charge diode D_{ch} prevents the charge from flowing back towards the DET. The charge recovery system can later transfer charge from the capacitor bank to the DET by closing the discharge relay S_{dch}.

The charge recovery system needs to recover as much energy as possible from the DET. Accordingly, we derive energy recovery as a function of the capacitance and inductance of the capacitor and inductor banks respectively as follows. Applying Kirchoff's voltage law to the loop through C_{DET}, S_{ch}, D_{ch}, L, and C_{sto} yields the following equation:

$$\frac{Q_{\text{DET}}}{C_{\text{DET}}} = L\ddot{Q}_{\text{sto}} + R_{\text{s}}\dot{Q}_{\text{sto}} + \frac{Q_{\text{sto}}}{C_{\text{sto}}}, \tag{4.8}$$

where D_{ch} is assumed to have negligible voltage drop. If this loop is isolated from the rest of the circuit (i.e., S_{dch} and S_{dr} open, $V_{\text{HV}} = 0$, negligible current through the voltage dividers), then the total charge in the loop Q_{T} is

$$Q_{\text{T}} = Q_{\text{DET}} + Q_{\text{sto}}, \tag{4.9}$$

and Equation (4.8) simplifies as

$$\begin{aligned}
\frac{Q_{\text{T}} - Q_{\text{sto}}}{C_{\text{DET}}} &= L\ddot{Q}_{\text{sto}} + R_{\text{s}}\dot{Q}_{\text{sto}} + \frac{Q_{\text{sto}}}{C_{\text{sto}}} \\
\frac{Q_{\text{T}}}{C_{\text{DET}}} &= L\ddot{Q}_{\text{sto}} + R_{\text{s}}\dot{Q}_{\text{sto}} + \frac{Q_{\text{sto}}}{C_{\text{sto}}} + \frac{Q_{\text{sto}}}{C_{\text{DET}}} \\
&= L\ddot{Q}_{\text{sto}} + R_{\text{s}}\dot{Q}_{\text{sto}} + \frac{C_{\text{sto}} + C_{\text{DET}}}{C_{\text{sto}}C_{\text{DET}}}Q_{\text{sto}} \\
V_0 &= L\ddot{Q}_{\text{sto}} + R_{\text{s}}\dot{Q}_{\text{sto}} + \frac{Q_{\text{sto}}}{C},
\end{aligned} \tag{4.10}$$

where

$$C = \frac{C_{\text{DET}}C_{\text{sto}}}{C_{\text{DET}} + C_{\text{sto}}} \tag{4.11}$$

is the total capacitance of the loop and V_0 is the voltage that the DET is charged to at the moment that the charge switch is closed. Equation (4.10) is a second-order differential

equation with a constant forcing term. The circuit is designed to be underdamped, so we must have

$$L > \frac{R_s^2 C}{4}. \tag{4.12}$$

Solving with the method of undetermined coefficients and the initial conditions

$$Q_{sto}(t = 0) = 0, \text{ and} \tag{4.13}$$

$$\dot{Q}_{sto}(t = 0) = 0 \tag{4.14}$$

yields

$$Q_{sto} = V_0 C\left[1 - e^{-\alpha t}\left(\frac{\alpha}{\omega}\sin(\omega t) + \cos(\omega t)\right)\right], \tag{4.15}$$

where

$$\alpha = \frac{R_s}{2L}, \text{ and} \tag{4.16}$$

$$\omega = \sqrt{\frac{1}{LC} - \frac{R_s^2}{4L^2}}. \tag{4.17}$$

Q_{sto} reaches its maximum value when

$$\dot{Q}_{sto} = 0, \tag{4.18}$$

which occurs when

$$t = k\frac{\pi}{\omega}, \tag{4.19}$$

where k is a positive integer. Substituting Equation (4.19) into Equation (4.15) yields:

$$Q_{sto}\left(t = k\frac{\pi}{\omega}\right) = V_0 C\left[1 + \exp\left(-\alpha k\frac{\pi}{\omega}\right)\right]. \tag{4.20}$$

The maximum value of Q_{sto} occurs when $k = 1$ so

$$\max\left(Q_{sto}\right) = Q_{sto}\left(\frac{\pi}{\omega}\right) = V_0 C\left[1 + \exp\left(-\frac{\alpha\pi}{\omega}\right)\right]. \tag{4.21}$$

Then, the energy stored in the capacitor bank U_{sto} relative to the energy initially stored in the DET U_{DET} is

$$\begin{aligned}
\frac{U_{sto}\left(\frac{\pi}{\omega}\right)}{U_{DET}(0)} &= \frac{\frac{1}{2}C_{sto}^{-1}Q_{sto}^2\left(\frac{\pi}{\omega}\right)}{\frac{1}{2}C_{DET}^{-1}Q_{DET}^2(0)} \\
&= \frac{C_{DET}}{C_{sto}Q_{DET}^2(0)}\left(V_0 C\left[1 + \exp\left(-\frac{\alpha\pi}{\omega}\right)\right]\right)^2 \\
&= \frac{C_{DET}}{C_{sto}Q_{DET}^2(0)}\left(\frac{Q_T C_{sto}}{C_{sto} + C_{DET}}\left[1 + \exp\left(-\frac{\alpha\pi}{\omega}\right)\right]\right)^2.
\end{aligned} \tag{4.22}$$

Letting g be the ratio of the capacitances C_{sto}/C_{DET} and substituting $C_{sto} = gC_{DET}$ into Equation (4.22) and simplifying yields:

$$\begin{aligned}
\frac{U_{sto}\left(\frac{\pi}{\omega}\right)}{U_{DET}(0)} &= \frac{C_{DET}}{gC_{DET}Q_{DET}^2(0)}\left(\frac{Q_T\, gC_{DET}}{gC_{DET}+C_{DET}}\left[1+\exp\left(-\frac{\alpha\pi}{\omega}\right)\right]\right)^2 \\
&= \frac{Q_T^2}{Q_{DET}^2(0)}\frac{g}{(g+1)^2}\left[1+\exp\left(-\frac{\alpha\pi}{\omega}\right)\right]^2 \\
&= \frac{\left(Q_{DET}(0)+Q_{sto}(0)\right)^2}{Q_{DET}^2(0)}\frac{g}{(g+1)^2}\left[1+\exp\left(-\frac{\alpha\pi}{\omega}\right)\right]^2 \\
&= \frac{g}{(g+1)^2}\left[1+\exp\left(-\frac{\alpha\pi}{\omega}\right)\right]^2, \qquad (4.23)
\end{aligned}$$

which is the equation we sought.

Analysis of Equation (4.23) shows that increasing L increases energy recovery, increasing R_s decreases energy recovery, and there is a value of g that maximizes energy recovery. The effects of L and R_s on energy recovery are contained in the ratio

$$\frac{\alpha}{\omega} = \sqrt{\frac{R_s^2}{4L(1+g)\,g^{-1}C_{DET}^{-1} - R_s^2}}. \qquad (4.24)$$

Decreasing α/ω makes the circuit less damped and increases the energy recovered according to Equation (4.23). Increasing L decreases α/ω and increases energy recovery. Increasing R_s increases α/ω and decreases energy recovery. The effect of capacitance ratio g, which determines C_{sto} is more complex. Increasing g increases α/ω and decreases energy recovery. However, the term $g/(g+1)^2$ in Equation (4.23) has a maximum when $g = 1$. Numerical analysis using values applicable to our charge recovery circuit indicated that optimal charge transfer is obtained for $g \approx 0.9$.

4.3 Implementation

Our DET AFO prototype (Figure 4.5) is designed to counteract foot drop without the drawbacks of AFOs actuated by electric motors, hydraulics, and pneumatics. The DET strap connects the foot to the shank and provides passive dorsiflexion support. Its foot connector is a 3D-printed component that is laced into a shoe. Its shank connector is a commercial knee brace (MD4200, Elite Bio-Logix, McDavid). The complete design of the AFO would have a pressure-sensitive resistive sensor in the shoe and the control and power electronics worn in a waistpack. The mass of the components currently used is 1.3 kg (Table 4.2).

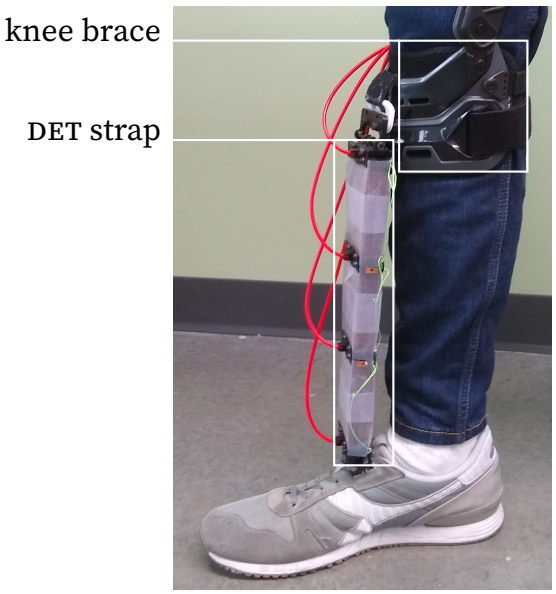

Figure 4.5: Our DET AFO prototype consists of a DET strap that connects a shoe to a knee brace. The control and power electronics (not shown here) would be worn in a waistpack.

Table 4.2: Mass of DET AFO components

Component	Mass (kg)	of total
electronics	0.49	38 %
knee brace	0.47	36 %
DET assembly	0.33	26 %
foot connector	0.01	0 %
Total	1.30	

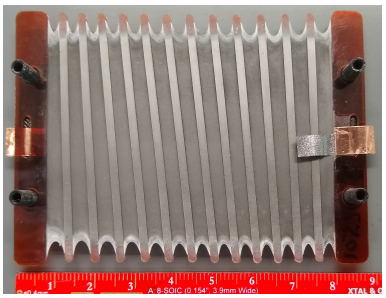

Figure 4.6: A width-constrained DET of the type used in the DET AFO has polyimide fibers that maintain a 400 % width prestretch of the VHB 4905 elastomer film. The DET is pictured on a storage frame.

The DET strap is an assembly of 81 individual DETs for ease of manufacturing. The DETs are configured in three stacks connected in series mechanically (so that their length changes sum to the total length change), and each stack has 27 DETs connected in parallel mechanically (so that their forces sum to the total force). The DETs (Figure 4.6) use parallel polyimide fibers to maintain a 400 % width prestretch of the VHB 4905 elastomer film (made by 3M). Their electrodes are graphite powder (US1058, US Research Nanomaterials), which connect to the electrical supply through leads made of "graphene sheets" (1334N1, McMaster-Carr) and copper tape. The DETs were fabricated by hand using a process designed to enhance manufacturing precision without the use of expensive manufacturing equipment and dedicated floor space.[108] The DETs are all connected in parallel electrically so that their capacitances sum to the total capacitance of the assembly. In between the DETs are pairs of sliding shields made from polyimide film of 50.8 µm (2 mil) thickness. These shields prevent shorting from one DET around the free edges of the DET below it to the DET below that and also protect the DETs from breakdown arcing of neighboring DETs in the event of an electrical breakdown. The DET assembly is wrapped with UHMW polyethylene film of 102 µm (4 mil) thickness to protect humans against electrical shocks.

The AFO's electronics (Figures 4.4 and 4.7) are designed to control the voltage on the DET strap. The electronics are designed to be driven from an 11.1 V lithium polymer battery. A high-voltage DC-DC converter (V_{HV}: FS60P12, XP Power) converts the 11.1 V input to a high voltage (up to 6 kV) for powering the DET strap. Three high-voltage normally-open relays (S_{ch}, S_{dch}, and S_{dr}: DAT71210F, Cynergy3 Components) route current between the capacitor bank C_{sto}, the drain resistor (R_{dr}), and the DET strap. The capacitor bank consists of two high-voltage capacitors (C4BSYBX3220ZAFJ, Kemet) connected in series to give a total capacitance of 110 nF. Its purpose is to store the energy that is removed from the

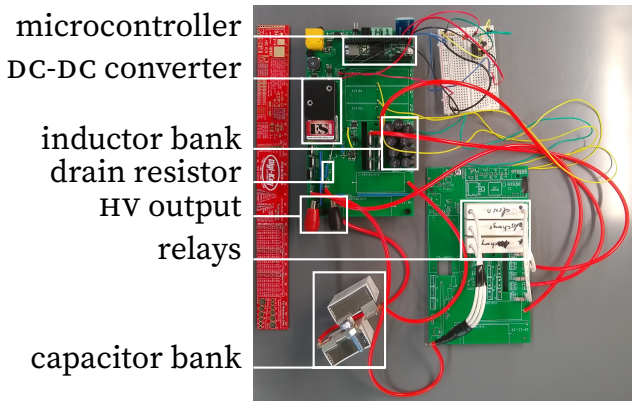

Figure 4.7: The AFO's power and control electronics.

DET strap to make the strap contract until the energy is transferred back to the strap in the next gait cycle. The inductor bank consists of 9 inductors (LHL10TB154J, Taiyo Yuden) connected in series to give a total inductance of 1.35 H. Its purpose is to reduce the energy lost during transfers to and from the capacitor bank. The drain resistor (SM102032004FE-ND, Ohmite) has 2 MΩ of resistance and is used to drain the energy from the DET strap and the capacitor bank. A microcontroller (Teensy 3.6, PJRC) processes sensor inputs and controls the high-voltage DC-DC converter and relays to operate the AFO.

4.4 Experimental methods

As a stepping stone before human subject trials, we conducted benchtop tests for preliminary proof of concept. These tests were used to answer several questions:

1. Could the DET AFO dorsiflex an ankle?
2. Would plantarflexion be easier with the DET strap charged than with it discharged?
3. How long could the AFO run on a battery?
4. Could charge recovery help it run longer on a battery?

For these benchtop tests, the DET strap was mounted on a testbed (Figure 4.8) designed to implement the geometry analyzed in § 4.2 (Figure 4.2). The testbed's upright tube is fixed in place, and its lever arm can rotate about the pin joint that represents the ankle. A pair of hard stops limits the lever arm's range of motion to approximately −20° to 10° (matching the ankle's range of motion during normal walking). A weight of 7.8 N was

suspended from the lever arm at a distance of 6 cm from the ankle joint. This loading represents approximately 49 % of the ankle torque caused by the foot weight of a person with 800 N body weight, which would be useful assistance to a foot drop patient with partial dorsiflexor function. The DET strap is connected to the testbed with two pin joints. The joint on the upright tube is 35 cm from the ankle joint, and the joint on the lever arm is 5 cm from the ankle joint, matching the values of a and b given near the end of § 4.2.2. Once the DET strap was mounted on the testbed, the strap held the lever arm against the upper hard stop. To reduce the effect of viscoelastic stress relaxation on the repeatability of the experiments, the strap was left in this position for about 30 min before the sequence of experiments began. All tests started with the arm resting at the upper hard stop. During the tests, the AFO's microcontroller recorded the voltages on the DET, capacitor bank, and power input, and the current from the power input at 50 Hz. A video camera recorded the motion of the test bed at 30 Hz, and the arm angle was extracted from these recordings using Tracker video analysis software (`physlets.org/tracker/`) and MATLAB. For the benchtop tests, the AFO's electronics were powered from a benchtop power supply providing 11.1 V in place of a battery.

To determine whether the AFO could dorsiflex an ankle, the lever arm was displaced to the bottom hard stop by hand and then released to see whether it would return to the upper hard stop. In the first test, the arm was released immediately after it reached the bottom hard stop. This test minimized the effect of viscoelastic relaxation on the DET strap's ability to raise the arm because the DET strap was fully stretched for only a short time. A second test was run to check whether viscoelastic relaxation would affect the DET strap's ability to return to the top hard stop. In the second test, the arm was held at the bottom hard stop for 120 s and then released. The longer delay at the bottom hard stop gave more time for viscoelastic relaxation. After being released, the arm was allowed to rise on its own for 90 s, and then it was raised to the upper hard stop by hand and released. The arm was raised by hand and released to check whether friction was a significant factor in preventing the arm from rising fully.

The AFO's ability to ease plantarflexion was tested by charging the DET strap to 2.8 kV so that it lowered due to the weight of the suspended mass. After the arm reached the bottom hard stop, the DET was discharged and raised the arm.

To determine how long the AFO might last on a battery and whether charge recovery could improve the AFO's battery life, the AFO was tested with gait cycle tests that simulated walking with and without charge recovery. In these tests, the AFO's microcontroller operated the DC-DC converter and the relays according to the pattern that would be used

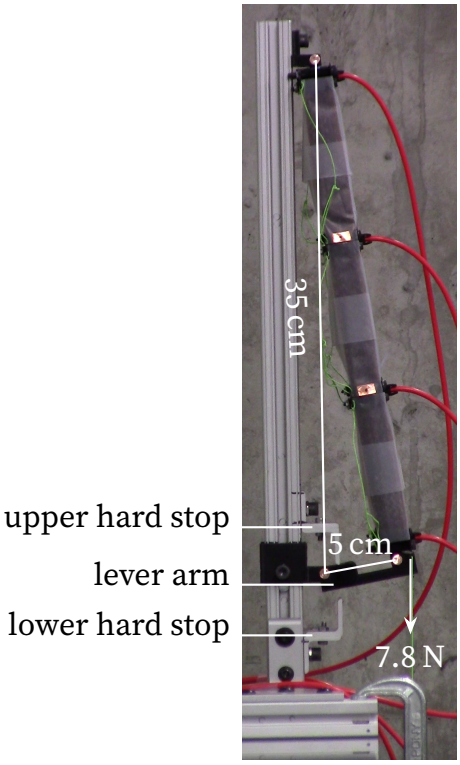

Figure 4.8: The DET AFO's testbed connected to the DET with pin joints [5 and 35] cm from the ankle joint to use the geometry selected during analysis. The motion of the lever arm was constrained by hard stops to approximately −20° to 10°. The DET was loaded by a 7.8 N weight connected to the lever arm 6 cm from the ankle joint.

during normal walking (Figure 4.1: Voltage, Relays closed) and the DET strap cyclically raised and lowered the lever arm. A cycle with charge recovery starts at heel strike with the voltage off and none of the relays closed. Then, at toe contact, the discharge relay is closed to transfer energy from the capacitor bank to the DET. After a delay to allow the energy to transfer, the voltage is raised to 2.8 kV to charge the DET so that the lever arm will lower as much as possible. At toe off, the voltage is switched off, the discharge relay is opened, and the charge relay is closed in order to transfer the energy stored on the DET to the capacitor bank and raise the lever arm. After a delay to allow the energy to transfer, the charge relay is opened, and the drain relay is closed to drain the remaining energy from the DET so that the lever arm raises as much as possible. A cycle without charge recovery uses the same voltage commands, but the charge and discharge relays are always open, and the drain relay is closed at toe off instead of later. A single test consisted of 11 continuous cycles, in order to give the system time to reach steady-state operation. The cycles were run on timers instead of being triggered by the toe sensor. Each cycle type

was run with two gait periods: 1 s periods to match the pace of normal walking, and 5 s periods to allow more time for charging, discharging, and arm motion.

We used the input power measured by the AFO's onboard sensors to estimate how long the AFO would be able to run on a battery. The input power is the product of the input current and input voltage measurements. The total energy consumed during each cycle in the gait cycle tests was calculated by integrating the input power measurement over the gait cycle. To gain more insight into the AFO's power consumption, we measured the power consumed by the electronics with the converter off and all relays open to obtain the power draw of the electronics other than the relays and the converter. This power was multiplied by the gait period to obtain the amount of energy consumed by "other" electronics during each cycle. The power consumed by a single relay was obtained by subtracting the power drawn by other electronics from the power measured when one relay was closed. The relay power consumption was multiplied by the gait period and the relay duty cycle (portion of the gait period that a relay was active, 20 % with charge recovery inactive, 92 % with charge recovery active) to obtain the energy consumed by relays during each cycle. The energy consumed by the DC-DC converter during each cycle was calculated by subtracting the energy consumed by relays and other electronics from the total energy. The battery life was calculated assuming a 10 W h battery capacity. Such a battery could be an 11.1 V lithium-polymer battery with 900 mA h capacity, which would not be a great burden due to its mass of about 100 g.

We calculated the energy stored on the DET to assess the performance of the charge recovery system. The energy stored on the DET U_e can be calculated from the DET's voltage V_DET:

$$U_\mathrm{e} = \frac{1}{2} C_\mathrm{DET} V_\mathrm{DET}^2. \tag{4.25}$$

The total energy stored in the DET during each cycle was calculated from the peak DET voltage that the converter supplied, and the energy contributed by the charge recovery system during each cycle was calculated from the voltage that the capacitor bank charged the DET to. The capacitance of the DET C_DET was calculated by the following procedure. If a switch completes a circuit containing only two capacitors C_1 and C_2, they will both change from their initial voltages, V_{01} and V_{02} respectively, to final voltage V_1. Then the capacitance of one capacitor can be calculated from the capacitance of the other capacitor

and the voltage measurements because of the principle of conservation of charge Q:

$$\begin{aligned} Q_0 &= Q_1 \\ C_1 V_{01} + C_2 V_{02} &= C_1 V_1 + C_2 V_2 \\ C_1 V_{01} - C_1 V_1 &= C_2 V_1 - C_2 V_{02} \\ C_1 &= C_2 \frac{V_1 - V_{02}}{V_{01} - V_1}. \end{aligned} \tag{4.26}$$

The capacitance of the DET was calculated from Equation (4.26) using the capacitance of the capacitor bank (110 nF), and the voltages immediately before and after the DET transferred energy to the capacitor bank during the gait cycle tests with a 5 s gait period yielding $C_{\text{DET}} = 133\,\text{nF}$.

4.5 Results and discussion

The benchtop test results validate the DET AFO concept and point to paths for improvement. The DET AFO can provide dorsiflexion assistance, and charging the DET assembly reduces the effort that would be required from the plantarflexor muscles to stretch the DET assembly during push off. However, these capabilities are hampered by the effects of viscoelasticity and friction. The DET AFO's overall energy consumption was low enough that it could run for about 6000 steps on a 10 W h battery. The charge recovery system reduced the energy needed from the high-voltage DC-DC converter, but it increased overall energy consumption due to the power drawn by the relays. Though the overall AFO concept was sound, a future iteration of the AFO could perform much better with hardware improvements.

4.5.1 Dorsiflexion and plantarflexion

The DET AFO can provide dorsiflexion assistance (Figure 4.9). In the dorsiflexion test, the DET strap rapidly raised the lever arm and settled at 7.04°. In the delayed dorsiflexion test, the DET strap raised the lever arm and settled at 4.83°. Then, it was raised to the upper hard stop by hand and released, and it settled at 10.3°. Though the DET strap did not return the lever arm to its 10° starting angle on its own, these tests showed that the AFO can provide dorsiflexion assistance because the DET strap raised the weighted lever arm more than 25°.

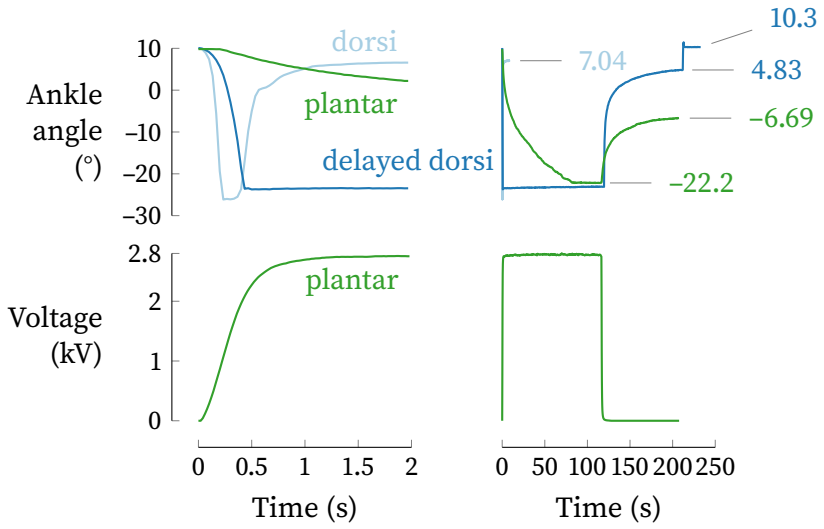

Figure 4.9: The DET assembly raised the weighted lever arm after it was manually lowered during the dorsiflexion tests, so the AFO can provide dorsiflexion support. When the DET assembly was charged to 2.8 kV during the plantarflexion test, it lowered the weighted lever arm to −22.2°, so charging the DET assembly reduces the effort that would be required from the plantarflexor muscles to stretch the DET assembly. The left panels show the first 2 s of the tests, and the right panels show the whole tests.

The DET AFO's dorsiflexion assistance is hampered by the effects of viscoelasticity and friction (Figure 4.9). The presence of friction explains why the DET strap was unable to raise the arm to the upper hard stop. Friction resisted the rising motion of the arm until the DET strap no longer exerted enough tension to overcome weight and friction and the arm came to rest below the upper hard stop. The lever arm rested at both [4.83 and 10.3]°, which is consistent with the effect of friction on a spring-mass system. A spring-mass system like the test setup has only one equilibrium position—a position where the spring force balances the weight of the mass—if the system is ideal (even with viscous damping). Friction causes a spring-mass system to have an equilibrium zone: a range of positions where the system can rest because friction is greater than the difference between the spring force and the weight of the mass. Viscoelasticity hampered the DET strap's ability to raise the lever arm in two ways. First, the motion of the rising lever arm asymptotically decays because this motion is governed by viscoelastic creep, so viscoelasticity slows the dorsiflexion assistance. Second, the lever arm did not rise as high after being held down longer because of viscoelastic stress relaxation, which reduced the tension exerted by the DET strap on the lever arm and thus its ability to overcome friction.

Charging the DET strap will make plantarflexion easier than it would be with the DET strap discharged. If the DET strap were discharged, the plantarflexor muscles would need to exert effort to stretch it during plantarflexion. In the plantarflexion test, the electric field pressure and the weight of the mass stretched the DET strap enough to lower the lever arm to −22.2° when the strap was charged to 2.8 kV (Figure 4.9). Thus, this motion would require no effort from the plantarflexor muscles if the DET strap were given enough time to stretch due to weight and field pressure. Even when the DET strap is not given enough time to stretch due to weight and field pressure, the DET's transduction work will offset the external mechanical work necessary for stretching, so the plantarflexor muscles will need less extra effort to stretch the DET strap than they would if the strap were discharged.

In the gait cycle tests (Figure 4.10), which better represent actual operating conditions than the dorsiflexion and plantarflexion tests, the lever arm traversed a portion of the ankle range of motion. In these tests, the lever arm started at the upper hard stop (10°), lowered when the DET strap was charged, and raised when the strap was discharged. The arm ended each cycle lower than it started, so it crept downward with successive cycles. However, after the first few cycles, the change in angle in each cycle stabilized and became consistent across cycles. In the trials with a 5 s gait period, the charge and discharge times were much shorter than times allowed for motion in the dorsiflexion and plantarflexion tests. Consequently, the lever arm traversed only a portion of the ankle's range of motion because its speed was limited by viscoelasticity and friction. In the trials with a 1 s gait period, the charge and discharge times were so short that the AFO's electronics could not fully charge and discharge the DET strap, which further reduced the range of motion. The amount that the arm lowered represents the angular range that would require no effort from the plantarflexor muscle. Motion beyond that range would require some effort from the plantarflexor muscles, but not as much as would be required with the DET strap discharged. Though the arm drifted lower with successive cycles, this effect is less pronounced for faster motion as seen by comparing the dorsiflexion and delayed dorsiflexion tests (Figure 4.9). The faster motion of the more realistic 1 s gait period tests indeed shows less drift, and would probably show even less if the electronics were able to fully discharge the DET in each cycle.

The sound of the DET assembly was not measured explicitly, but it was not audible to the ear over the ambient room noise under normal operation such as when trial data was being collected. During development, it occasionally produced faint crackling or whistling noises, but these were associated with DET breakdown, either incipient or imminent.

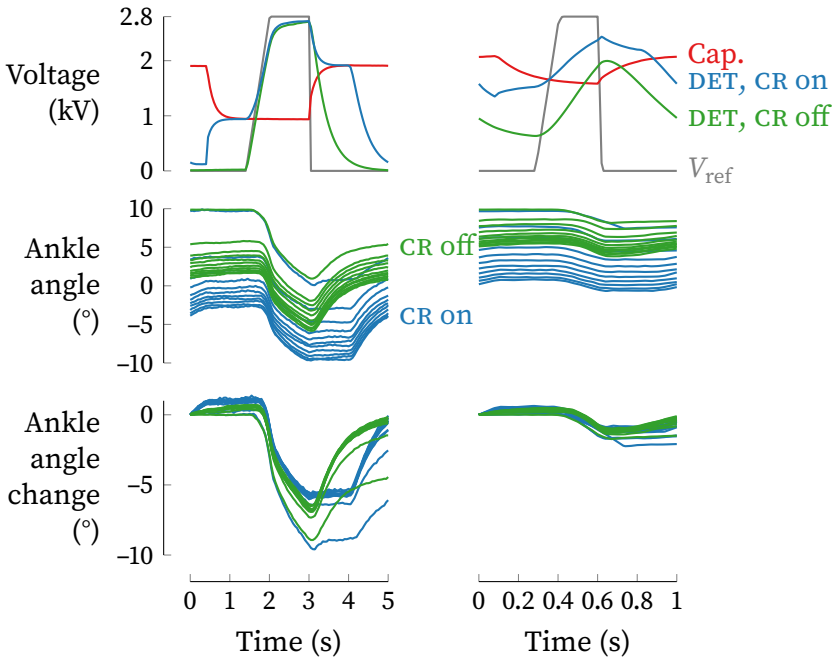

Figure 4.10: In the gait cycle tests, the voltage and ankle angle trajectories followed regular patterns. The voltages converged to the trajectories depicted here after the first four cycles. The ankle angle crept downward (lower angle) with subsequent cycles, but the ankle angle change was fairly consistent across cycles. Results from trials with a 5 s gait period are shown on the left, and results from trials with a 1 s gait period are shown on the right. CR means charge recovery.

4.5.2 Energy consumption

In the gait cycle tests, the DET and capacitor bank voltages followed consistent patterns even though the mechanical motion had not settled to a steady cycle. After the first four cycles, the voltages converged on the trajectories depicted in Figure 4.10. When charge recovery was off, the converter charged the DET, and then it was drained through the drain resistor. When charge recovery was on, the capacitor bank partially charged the DET, and then the converter charged it to its peak voltage. Then, the charge recovery system recovered a portion of the electrical energy stored on the DET, and the rest was drained through the drain resistor. Because the DET was not completely charged and discharged during the gait cycle tests with a 1 s gait period, data from these trials will not give an accurate understanding of the DET AFO's energy consumption, so all of our energy consumption results are based on the gait cycle tests with a 5 s gait period.

The DET AFO should be able to run on a battery for more than 6000 steps (Table 4.3). The AFO's electronics consumed 10.3 J per cycle without charge recovery in the gait cycle

Table 4.3: Energy consumed per cycle in the gait cycle tests with 5 s gait period, and resulting battery life assuming a 10 W h battery capacity

Charge recovery	Energy (J)				Battery life (steps)
	Total	Relays	Other	Converter	
off	10.30	0.74	6.08	3.48	6991
on	11.78	3.40	6.08	2.29	6114
change	1.48	2.66	0.00	-1.18	-877

Power (W)	
Relay	Other
0.74	1.22

tests with a 5 s gait period. A battery with a 10 W h capacity contains enough energy to power the AFO for 6991 steps at that energy consumption rate. Actual operating conditions should greatly reduce the energy consumed each cycle. In actual operating conditions, the gait period will be about 1 s instead of 5 s (once the issues preventing operating in 1 s cycles are resolved), so the energy consumed by the relays and other electronics should be about a fifth of the values reported in Table 4.3 because these energy values are linear functions of the gait period. The majority of the energy consumed each cycle was consumed by the relays and other electronics. Therefore, in actual operating conditions, a battery may be able to power the AFO for many more than 6000 steps.

The charge recovery system contributed 12 % of the energy required to charge the DET (Table 4.4) but this benefit was outweighed by the extra energy needed to run the relays. In the gait cycle tests, the AFO consumed more energy with charge recovery turned on than with it off (Table 4.3). This increase occurred because when charge recovery is on, there is a relay closed during more of the gait cycle than there is with charge recovery off (92 % versus 20 %). This additional relay activity added 2.66 J to the AFO's energy consumption. Charge recovery decreased the energy consumed by the converter by 1.18 J, but this benefit was outweighed by the extra energy needed to activate the relays for charge recovery.

Table 4.4: Energy used to charge the DET in the gait cycle tests with a 5 s gait period

	Energy		
Charge recovery	Stored in DET (mJ)	From capacitor bank (mJ)	(%)
off	487	0	0
on	491	59	12

4.5.3 Improving performance

The viscoelasticity that slowed dorsiflexion and plantarflexion could be mitigated by applying higher voltages or changing the DETs' elastomer. The effect of viscoelasticity on dorsiflexion may not be significant during actual operation because the DET assembly would be stretched and released quickly (Figure 4.1) like in the dorsiflexion test (Figure 4.9). The effect of viscoelasticity on plantarflexion could be compensated for by "overdriving" the DET assembly with a higher voltage for the brief push off period.[109] This approach may be practical because DETs can withstand higher voltages for brief periods.[110] Alternatively, the effects of viscoelasticity could be dramatically reduced by redesigning the DETs around a silicone elastomer, which would have much less viscoelasticity than the VHB 4905 currently used.[90,91] VHB 4905 has a glass transition range from −50 °C to 60 °C.[111] At room temperature, the operating condition for the experiments in this work, VHB 4905 has highly dissipative stress-strain behavior with $\tan\delta \approx 1$.[111] This dissipation prevents potential energy (either gravitational when the mass was raised or elastic when the arm was lowered) from being converted into kinetic energy of the moving mass and thus hinders rapid movement. In contrast, silicone elastomers suited for DETs typically have glass transitions below −100 °C, so at room temperature, they are in their rubbery state with viscous effects that are nearly negligible, with $\tan\delta \approx 0.01$.[91] With these properties, the DETs would dissipate almost no potential energy so the kinetic energy of the mass would be much greater, and the lever arm would raise and lower much faster.

Using a silicone instead of VHB 4905 would also mitigate two other detrimental effects of viscoelasticity: temperature-dependent behavior and a "warm-up" time. The stress-strain behavior of VHB 4905 is highly temperature-dependent[112] within its glass transition range: it softens with increasing temperature and stiffens with decreasing temper-

ature. In contrast, silicones suited for DETs stay in their rubbery state for a wide temperature range around room temperature and have stress-strain behavior that is much less temperature-dependent. The viscoelastic nature of VHB 4905 means that in real-world use, if the DET assembly was allowed to relax to its rest length, such as might occur if the AFO was doffed and set aside over night, then when the AFO was donned, the DET assembly would exert a stronger dorsiflexion force than normal until it relaxed into its operating length. This effect would mean the wearer would have to exert additional plantarflexion effort during the relaxation period, which is on the order of a few minutes. This effect could be mitigated by storing the DET assembly on a frame that held it at the operating length when not in use. Alternatively, using an appropriate silicone for the DET elastomer would almost entirely eliminate the issue because the silicone's stress-strain behavior would have minimal dependence on strain history due to the material's low value of $\tan\delta$.

The energy consumption of the DET AFO could be reduced by improving the charge recovery system.* The charge recovery system's energy consumption could be lowered by replacing the relays with high-voltage transistors, which would consume much less power to activate. Additionally, the energy saved by the charge recovery system could be increased by adding inductance or decreasing DET electrode resistance to make the charge transfer more effective. Currently, the charge recovery system has only 1.35 H of inductance. According to Equation (4.12), the charge recovery system should have

$$L > \frac{R_s^2 C}{4} = \frac{(860\,\mathrm{k\Omega})^2 \cdot 60.2\,\mathrm{nF}}{4} = 11.1\,\mathrm{kH} \tag{4.27}$$

to be underdamped, which would allow it recover more than 25 % of the electrical energy stored in the DET assembly.† Alternatively, if the DET electrode resistance was made negligible by using metallic electrodes, and only the parasitic resistance of the inductor bank (2.7 kΩ) affected the charge transfer, then

$$L > \frac{R_s^2 C}{4} = \frac{(2.7\,\mathrm{k\Omega})^2 \cdot 60.2\,\mathrm{nF}}{4} = 0.11\,\mathrm{H} \tag{4.28}$$

would make the system underdamped. Further, substituting $R_s = 2.7\,\mathrm{k\Omega}$, $L = 1.3\,\mathrm{H}$, $C_{\mathrm{DET}} = 133\,\mathrm{nF}$, and $g = 0.8721$ into Equations (4.23) and (4.24) yields an energy recovery of 48 %.

*Of course, the AFO's energy consumption could also be improved by refining the low-voltage circuitry that consumes a significant amount of energy itself.

†For this calculation, R_s was determined from the RC time constant obtained from a logarithmic curve fit of the voltage decay while the DET assembly discharged across R_{dr}.

Refining the AFO's design could reduce the AFO's mass significantly. The mass of the DET assembly is merely 26 % of the entire AFO mass (Table 4.2). The majority of the mass is in the electronics and knee brace, and these components were not optimized. The electronics would probably have less mass if consolidated into a single circuit board, and the knee brace's mass could probably be reduced by replacing the off-the-shelf brace with a custom design tailored for the needs of the AFO.

Adding additional DETs to the assembly would strengthen it to bear the full weight of a foot. In these tests, the DET assembly supported approximately 49 % of the ankle torque caused by foot weight, which would be useful to a foot drop patient with partial dorsiflexor function. For the full support required by foot drop patients with no dorsiflexor function, the DET assembly could be strengthened by adding additional DETs in parallel mechanically. Doing so would scale the assembly's strength linearly with the number of additional parallel DET layers, and would be only a minor design revision. The additional DETs would increase the assembly's capacitance and decrease its resistance, so the power supply and charge recovery components would have to be reselected accordingly.

4.6 Conclusion

Our DET AFO design promises to assist with foot drop with less mass, energy consumption, and noise than electric and pneumatic powered AFOs. It can provide dorsiflexion support, and reduce the effort required from plantarflexor muscles to stretch the DET assembly. Its energy consumption was low enough that it might be practical to power the AFO for 6000 steps on a small battery. Its direct drive design eliminates the need for a bulky transmission, and it could be refined to be lighter and more compact than it currently is. The design's architecture uses the foot's weight as a biasing load for the DET in keeping with the design principles of § 2.2. This approach helps minimize the mass and volume of the AFO because it eliminates the need for a biasing mechanism. It also gives the AFO the ability to provide passive, compliant support for the ankle. Though human subject testing is needed for full validation, the benchtop tests reported in this paper give a promising proof of the concept.

CHAPTER 5

CONCLUSION

Dielectric elastomer transducers (DETs) offer a promising path forward for powered prostheses and orthoses. They promise to make powered prostheses and orthoses mechanically simpler, quieter, and possibly lighter and more energy efficient because of the benefits of artificial muscle designs. The challenges of working with viscoelasticity and high voltages experienced in this work can be overcome with refinements of the device and DET designs. These refinements are practical now or will be in the next two years. Therefore, it is important to continue work on the details of designing powered prostheses and orthoses to use DETs so that powered prostheses and orthoses will be practical devices soon.

5.1 Benefits of artificial muscles

Despite prototyping concessions, the devices in this work display some of the benefits of artificial muscle design. Specifically, both the DET variable-stiffness actuator (VSA) and the DET ankle-foot orthosis (AFO) are mechanically simpler than their electric-motor-powered counterparts due to their direct drive designs and the inherent compliance of DETs. Further, the DETs of both devices operate quietly. The AFO also has potential to consume less energy and have less mass than electric motor powered AFOs once its design is refined. These benefits validate the artificial muscle design approach and encourage further development of DET-powered prostheses and orthoses.

Both devices built during this work are inherently compliant and use DETs in a direct drive configuration, which reduces their mechanical complexity. In the DET VSA, the DETs are used to create the compliance of the actuator, and they were connected directly to the load. Accordingly, the VSA's variable-stiffness mechanism has only one component motion in contrast to the four component motions of the state-of-the-art VSAs discussed in § 3.1. Because the DETs of the DET AFO are compliant and directly connected to the load, the AFO is also compliant. Because of its compliance, the AFO allows its wearer to plantarflex (albeit with additional muscle effort) when the AFO is unpowered while still providing dorsiflexion support. In contrast, a rigidly actuated AFO would lock the ankle in place when unpowered. The AFO's direct drive design eliminates the need for conversion of rotation to linear motion, and its inherent compliance eliminates the need for sliding

elastic mechanism components making it mechanically simpler than the electric motor powered AFOs discussed in § 4.1 so that its mechanical complexity is comparable to the pneumatic AFOs also discussed in that section.

The fundamental characteristics of DETs quiet both the VSA and AFO, but give mixed results for energy consumption. The sound produced by the DETs was not formally measured for either device during testing, but practically, no noise was noted by the researchers during normal operation such as when trial data were being collected. During development, however, faint crackles or whistles could be heard from DETs when failure was incipient or imminent. Due to DET leakage current, the VSA consumes energy to remain in a softened state unlike state-of-the-art VSAs, but this drawback may be negligible in applications that require the VSA to remain stiff most of the time. The VSA also consumes energy to soften, but much of this energy could be recovered with a properly-designed charge recovery system, an interesting area for future work. The total energy consumption of the AFO is low compared to state-of-the-art devices, and little of it was directly consumed by the DETs. Once the support electronics are refined, an AFO following design guidelines laid out in this work should have excellent battery life and could lead to a successful wearable device.

Neither of the designs in this work have obvious mass or volume reductions compared to state-of-the-art devices, partially due to their use of rigid frames. The VSA's mass and volume are comparable to those of other VSAs that store similar amounts of mechanical energy in their variable-stiffness mechanisms,[76] so it has no obvious advantage in this aspect. The VSA requires a rigid frame because of its electric motor, and the cone diaphragm DETs require rigid frames to maintain the prestretch of the underlying dielectric elastomer material, VHB 4910. Even if the cone diaphragm DETs were redesigned with another elastomer that did not require prestretch, the cone diaphragm design probably requires a stiff frame to maintain its shape for proper operation. The individual DETs used in the AFO are flexible and can be used without a rigid frame similarly to other width-constrained DETs used for a tactile display.[113] However, for ease of prototyping, the AFO's DET assembly has rigid end connectors and electrical insulation that limits it, in its current configuration, to uniaxial stretching (like a prismatic joint). Further, more than a third of the AFO's mass is in its knee brace, which also had a rigid frame. Again, this component was selected to facilitate prototyping, and a refined shank attachment may be able to greatly reduce the mass of a future AFO based on DETs.

5.2 Challenges of using DETs

The implementation of DETs in the devices in this work was challenging, but these challenges can be overcome with design refinements and improved technology. The viscoelastic nature of VHB 4910* inhibits purely elastic energy return from the VSA (§ 3.4.4 and Figure 3.10) and actuation stretch of the AFO (§ 4.5.1 and Figure 4.9). These effects can be partially compensated for by control or mitigated more thoroughly by using a different elastomer for the DETs. The biggest challenge in this work was DET reliability; electrical breakdowns were common and permanently destroyed DETs that suffered electrical breakdown. This challenge can be surmounted by using the dielectric-grade elastomers now being produced for use in DETs. The high voltages (>2 kV) required to create significant transduction effects in the DETs complicated the design of the power electronics for the AFO. However, these complications could be resolved or reduced by revising the power supply design or using DETs that work at lower voltages. The challenges of mediating viscoelastic responses and handling high voltages should be accounted for when designing DET-powered prostheses and orthoses, but they do not prohibit such development.

5.2.1 Viscoelasticity

The fundamental cause of viscoelastic behavior in polymers is their molecular structure, which consists of a network of intertwined polymer chains.[95] Like springs, these chains uncurl and lengthen when stress is applied to the polymer and curl and retract when stress is removed resulting in the elastic component of polymer stress-strain behavior. These chains are also sterically hindered by the electron clouds of side chains interacting with other parts of the same chain or other chains leading to time-dependent behavior. Essentially, the chains catch on and then slide past each other due to the steric entanglement caused by inter- and intramolecular forces creating a viscous stress-strain behavior like that of a mechanical damper. The combination of these two effects, called viscoelasticity, is a stress-strain behavior that is dependent on both strain and strain history,[83] yet allows the material to return to its original shape given enough time if the total stresses and strains are sufficiently low. This stress-strain behavior can be modeled as the force-displacement behavior of a network of springs and dashpots such as the Kelvin, Voigt, Maxwell, Wiechert, or standard linear solid models.

*Both VHB 4910 and VHB 4905 are the same elastomer. The difference is that VHB 4910 is 1 mm thick, and VHB 4905 is 0.5 mm thick. In this chapter, VHB 4910 will refer to both products.

Viscoelastic behavior dissipates energy during deformation. The integral of a stress-strain curve represents the volumetric mechanical energy absorbed or released due to the change of strain. The stress-strain curve of a viscoelastic material has greater stress when the material is being deformed from its natural shape and lower stress when the material returns to its natural shape. This stress difference makes the integral of the deforming motion larger than that of the returning motion, so a viscoelastic material absorbs more mechanical energy than it releases during cyclic loading. The difference between the values of energy absorbed and returned is the energy dissipated as heat. The dissipation phenomenon of viscoelasticity is modelled by the dashpots in spring-and-dashpot models of viscoelasticity. This dissipative behavior is evident in the force-displacement trajectories of the DET VSA (Figures 3.5, 3.6 and 3.9).

A polymer's viscoelastic dissipation is greatest in the polymer's glass transition range, which is the range of temperatures between its glassy zone and its rubbery zone. In the glassy zone, the polymer's temperature is low enough that the polymer chains cannot slide past each other due to steric hinderance, so the polymer is stiff. In the rubbery zone, the polymer's temperature is high enough that Brownian motion allows the chains to easily slide past each other, so the polymer is soft. In both zones, viscoelastic dissipation is small because the chains either do not slide past each other, or they slide past each other very easily. In the glass transition range, the chains can slide past each other, but it takes a significant amount of energy to overcome the steric hinderance of the motion.

A measure of viscoelastic dissipation is $\tan\delta$, which is the ratio of a material's loss and storage moduli.[83] This measure peaks for temperatures in a polymer's glass transition range when its energy dissipation is at its greatest.

The viscoelastic behavior of VHB 4910 causes undesirable behaviors in the DET VSA and the DET AFO. VHB 4910 has a glass transition range from −50 °C to 60 °C.[111] At room temperature, the operating condition for the experiments in this work, $\tan\delta \approx 1$ for VHB 4910[111] so its dissipation was high for this work's experimental conditions. Accordingly, the VSA's DETs dissipated a portion of the energy they absorbed rather than returning it. Also, a portion of the gravitational potential energy of the mass suspended by the AFO was dissipated in the AFO's DETs rather than being converted to kinetic energy, and this lack of kinetic energy slowed the plantarflexion motion. Viscoelastic dissipation also slowed the AFO's dorsiflexion by dissipating the elastic energy stored in the DETs rather than allowing it to convert into the kinetic energy of the rising mass. Further, because VHB 4910 is viscoelastic, its behavior is temperature-dependent,[112] so both the VSA and AFO will have

temperature-dependent stress-strain behavior. At lower temperatures, they will stiffen, and at higher temperatures they will soften.

Note that in some applications, VHB 4910's energy dissipation could be desirable.[114] Energy dissipation through damping can increase the control bandwidth of robots with compliant joints (such as those powered by VSAs) by reducing the joint oscillations caused by compliance.[89] It can also be useful for DET devices intended as brakes or shock absorbers, such as for helping a flying robot perch[115] or a jumping robot land,[116] which are intended to dissipate energy.

Active voltage control can compensate for some performance issues. Once parameter-fitting is performed, spring and dashpot models predict viscoelastic behavior with sufficient accuracy that they can be used for precise position control. This technique works well for closed-loop feedback control,[33] and for open-loop feedforward control.[109] Modeling can even account for the temperature-dependent effects of viscoelasticity.[112] Such approaches could speed up the AFO's plantarflexion by briefly applying higher voltages to it to overcome the damping effect of viscoelasticity. However, they would not be able to speed up the AFO's dorsiflexion because this behavior is passive. Control could also reduce the hysteresis of the VSA's force-displacement curves (Figure 3.9), but this effect wouldn't actually change the amount of energy dissipated by the VHB 4910. Rather, it would mask the dissipation by supplying the dissipated energy through the control input rather than taking it from the load. However, the effectiveness of compensation by control is limited by actuator saturation limits based on the power supply capabilities and the breakdown strength of the elastomer. Further, these models may not work well for operating conditions outside the range over which parameters were fitted.

The performance issues could be mitigated almost entirely by replacing VHB 4910 with an elastomer that has a small $\tan\delta$ value (i.e., little viscoelastic dissipation) over the application's temperature range. Doing so would address the source of the problem and allow the VSA to efficiently store and return energy and the AFO to move rapidly. To be well-suited for DET use, an elastomer should have (in addition to a small $\tan\delta$ value) a high failure strain, a low Young's modulus, a high relative permittivity, and a high dielectric strength. A high failure strain makes it possible for the elastomer to undergo large strains due to the applied electric field or the load. A low Young's modulus makes the elastomer's restoring forces smaller compared to the electrostatic forces, which gives the electrical input more control over the load. A high relative permittivity makes electrostatic force larger for a given applied electric field, and a high dielectric strength means the DET is able to withstand higher electric fields. Many types of elastomers have been

studied and evaluated for use in DETs including silicones, fluorosilicones, polyurethanes, and acrylics.[34,35,117]

For work focused on DET devices and applications, commercially available silicone film and laminate marketed for DETs may be the best alternative to DETs based on VHB 4910. Silicones suitable for DETs[91] typically have $\tan\delta \ll 1$, because their glass transitions occur well below room temperature. They also typically have high failure strain and low Young's modulus. However, they are usually held back by low relative permittivity values. Despite this weakness, comparisons of silicones to VHB 4910 indicate that silicones are good choices for DETs because they display rapid mechanical response that is independent of temperature over a wide temperature range.[90,118] Further, silicone-based DETs can achieve very high cycle life and reliability. Likely because of these characteristics, a silicone was used in the formerly available Danfoss Polypower film,[119] which was marketed for DET products and used in research projects.[28,118,120] Wacker Chemie AG currently manufactures and markets silicone films for use in DETs under its ELASTOSIL brand,[121] which has been used in many research projects.[39,122–125] These silicones will also be used in Wacker's forthcoming (available in 2021) NEXIPAL line of silicone laminates that adds electrodes to the silicone.[126] The use of prefabricated elastomer films or even films laminated with electrodes would save an enormous amount of time and effort compared to fabricating them in a research lab. Further, the commercial films will likely be of much higher quality than those produced in a lab making them much less susceptible to dielectric breakdown.

5.2.2 DET reliability

The largest challenge in this work was obtaining reliable operation from DETs. It was common for a freshly-fabricated DET to have a dielectric breakdown when it was first energized. In fact, this occurred for about 25 % of the DETs made for the VSA and AFO after fabrication processes and DET designs were optimized. Further, DETs that withstood operating voltage once did not necessarily withstand it when energized later.

This work did not investigate the causes of these failures in detail, but they are probably caused by dielectric breakdown due to randomly distributed defects in the VHB 4910 elastomer. VHB 4910 is meant to be an adhesive tape, not a dielectric, so its manufacturer likely does not manufacture it to dielectric quality. Accordingly, VHB 4910 has defects such as bubbles or contaminants that have been shown to weaken the dielectric strength of the material.[127] Another study showed that when electrodes cover only a small area,

VHB 4910 is capable of withstanding much higher electric fields (>400 V/μm)[81] than those at which breakdown normally occurs for realistic DETs.[82] This finding reinforces the idea that random defects decrease the dielectric strength of VHB 4910: large electrode areas are more likely to cover a defect, so they are associated with lower dielectric strengths.

The likelihood of breakdown for VHB 4910 can be reduced with changes to operating conditions or DET design. As mentioned in § 3.4.7, long lifetimes for DETs are possible by tailoring the electrode formulation, operating in an environment with low humidity (<5 % relative humidity), or operating with low electric fields.[88] Encapsulating a DET with dielectric oil can also greatly improve its dielectric strength.[128] Also, designing the DET to keep the electrode edges away from interfaces with rigid components separates mechanical and electrical stress concentrations and improves dielectric strength.[58,70,129] The DETs used in the DET VSA included lips of polyimide tape under the electrode edges for this reason (§ 3.2 and Figure 3.2).

Ultimately, the real solution to these issues is to use an elastomer film that does not have defects in the first place. The aforementioned ELASTOSIL film is manufactured with dielectric use in mind, so it is manufactured in a clean room environment, and care is taken to avoid defect and thickness variations.[121,130] This is another reason for work focused on DET devices and applications to use commercially available silicone films.

5.2.3 High voltages

The DETs used in this work required 2 kV to 5 kV to produce significant transduction effects (motion or softening), and these voltage levels complicated the design of the power electronics for the AFO. One of the oft-cited drawbacks of DETs is the need to work with high voltages. However, there is now an ample selection of high-voltage components readily available from suppliers including resistors, capacitors, transistors, optoisolators, and compact DC-DC converters that makes the design of DET power systems tractable. This section will discuss the challenges experienced in this work regarding controlling and switching high voltages in the AFO's power supply to help improve future DET power system designs.

A regulated DC-DC converter could reduce development time of a high-voltage power supply. The AFO's power supply used a feedback control loop around the high-voltage DC-DC converter to control its output voltage. This approach required some time to tune controller gains, and in the end, a PD (proportional-derivative) controller provided good

tracking results (Figure 4.10, top left). However, the slew rate of DC-DC converter's output appeared to have been a factor in the system's inability to track the voltage reference in the faster operating cycle trials (Figure 4.10, top right). Further, good tracking performance required the microcontroller code to be streamlined to run the control loop at a high frequency, and ultimately, the system ran at about 1 kHz. Also, closed loop control required high-frequency readings of the DC-DC converter's output voltage, which was additional work. All of this effort could have been eliminated by using a regulated DC-DC converter instead of the proportional model we chose. A regulated converter would run the control loop internally, so the microcontroller would only need to feed it the reference voltage signal. However, compact, regulated DC-DC converters were limited to 1 W at the time the power supply was designed, which is much less that the 10 W available from our proportional model. This year, a new line of regulated, compact, high-voltage DC-DC converters was released, the XP Power HRL30 series that features 30 W of output, and may have a greater slew rate from the powered-down state. This development could greatly simplify the design of mobile power supplies for DETs in the future.

The bigger challenge for the power supply design proved to be the switching of high voltages. An early iteration attempted to use high-voltage transistors (IXYS IXGF30N400) for connecting the DET to the charge recovery system. Due to the high-side configuration of the transistors, gate drivers were needed to operate the transistors. The gate drivers that were selected (Power Integrations 1SC0450E2B0-45) proved impractical because they added too much size and complexity to the circuit. So, we chose to use high-voltage relays instead, which proved much easier to operate. However, this choice had the unfortunate effect of making the charge recovery system counterproductive due to the energy consumed to operate the relays as described in § 4.5.2. A bigger issue was that the relays produced large voltage spikes (hundreds of volts) when they switched high voltages. These spikes proved impossible to isolate, and they caused smaller voltage spikes (10 V to 20 V) to appear in the low-voltage circuitry. These spikes interfered with the reading of the voltages from the high-voltage circuit and the reading of the power supply's emergency shutdown switch. Eventually, work-arounds were implemented, but future designs would probably be better served to use high-voltage transistors instead of high-voltage relays. It may be possible to avoid the difficulties of high-voltage gate drivers by using the transistors in a low-side configuration.

Ultimately, the challenges of working with high voltages will diminish as DET and electronics technology improve. Improved electronics technology will result in high-voltage

components with better performance and capabilities such as the regulated DC-DC converters mentioned above. Improved DET technology will results in lower operating voltages as processes are improved for fabricating thinner elastomers. Already, some works have demonstrated operation of DETs below 1 kV.[94,125]

5.3 The path forward

DETs offer a promising means to develop powered prostheses and orthoses without the shortcomings of electric motors. In this work, some of the benefits of artificial muscle design were observed in the DET VSA and DET AFO. Additional benefits could be obtained with refinements to the designs. Though working with DETs entails challenges, those experienced in this work appear to be surmountable within the next two to five years as silicone laminates become commercially available and high-voltage electronics technology improves. Therefore, future work should continue to solve the challenges of powering prostheses and orthoses with DETs so that powered prostheses and orthoses can become practical for real-world use.

BIBLIOGRAPHY

[1] Dominik Simon Pieringer et al. “Review of the actuators of active knee prostheses and their target design outputs for activities of daily living”. In: *International Conference on Rehabilitation Robotics (ICORR)*. London: IEEE, 2017, pp. 1246–1253.

[2] Weiguang Huo et al. “Lower Limb Wearable Robots for Assistance and Rehabilitation: A State of the Art”. In: *IEEE Systems Journal* 10.3 (2016), pp. 1068–1081.

[3] Jonathan W. Hurst and Alfred A. Rizzi. “Series Compliance for an Efficient Running Gait”. In: *IEEE Robotics & Automation Magazine* 15.3 (2008), pp. 42–51.

[4] Samuel K. Au, Jeff Weber, and Hugh Herr. “Biomechanical Design of a Powered Ankle-Foot Prosthesis”. In: *IEEE International Conference on Rehabilitation Robotics*. IEEE, 2007, pp. 298–303.

[5] Samuel K. Au, Jeff Weber, and Hugh Herr. “Powered Ankle-Foot Prosthesis Improves Walking Metabolic Economy”. In: *IEEE Transactions on Robotics* 25.1 (2009), pp. 51–66.

[6] Ryan D. Bellman, Matthew A. Holgate, and Thomas G. Sugar. “SPARKy 3: Design of an active robotic ankle prosthesis with two actuated degrees of freedom using regenerative kinetics”. In: *IEEE RAS & EMBS International Conference on Biomedical Robotics and Biomechatronics*. Scottsdale: IEEE, 2008, pp. 511–516.

[7] Jerry Pratt, Ben Krupp, and Chris Morse. “Series elastic actuators for high fidelity force control”. In: *Industrial Robot* 29.3 (2002), pp. 234–241.

[8] Jerry E. Pratt and Benjamin T. Krupp. “Series Elastic Actuators for legged robots”. In: *Proceedings of SPIE*. Ed. by Grant R. Gerhart, Chuck M. Shoemaker, and Douglas W. Gage. Vol. 5422. 2004.

[9] Marius Stücheli, Marianne Schmid Daners, and Mirko Meboldt. “Benchmark of the Compactness Potential of Adjustable Stiffness Mechanisms”. In: *Journal of Mechanisms and Robotics* 9.5 (2017), p. 051009.

[10] Toby Elery et al. “Design and Validation of a Powered Knee-Ankle Prosthesis with High Torque, Low-Impedance Actuators”. In: *IEEE Transactions on Robotics* conditiona (2020).

[11] Ge Lv, Hanqi Zhu, and Robert D. Gregg. “On the Design and Control of Highly Backdrivable Lower-Limb Exoskeletons: A Discussion of Past and Ongoing Work”. In: *IEEE Control Systems Magazine* 38.6 (2018), pp. 88–113.

[12] Hanqi Zhu et al. “Design and Validation of a Partial-Assist Knee Orthosis with Compact, Backdrivable Actuation”. In: *IEEE International Conference on Rehabilitation Robotics (ICORR)*. Toronto: IEEE, 2019, pp. 917–924.

[13] Sangok Seok et al. “Design principles for energy-efficient legged locomotion and implementation on the MIT Cheetah robot”. In: *IEEE/ASME Transactions on Mechatronics* 20.3 (2015), pp. 1117–1129.

[14] Homayoon Kazerooni. “Exoskeletons for Human Performance Augmentation”. In: *Springer Handbook of Robotics*. Ed. by Bruno Siciliano and Oussama Khatib. Berlin, Heidelberg: Springer, Berlin, Heidelberg, 2008. Chap. 33, pp. 773–793.

[15] K. Alex Shorter et al. “A portable powered ankle-foot orthosis for rehabilitation”. In: *The Journal of Rehabilitation Research & Development* 48.4 (2011), pp. 459–472.

[16] Yong-Lae Park et al. “Design and control of a bio-inspired soft wearable robotic device for ankle-foot rehabilitation.” In: *Bioinspiration & Biomimetics* 9.1 (2014), p. 016007.

[17] Ronald Van Ham et al. “Compliant actuator designs”. In: *IEEE Robotics & Automation Magazine* 16.3 (2009), pp. 81–94.

[18] Jun Zhang et al. “Robotic Artificial Muscles: Current Progress and Future Perspectives”. In: *IEEE Transactions on Robotics* 35.3 (2019), pp. 761–781.

[19] Seyed M. Mirvakili and Ian W. Hunter. “Artificial Muscles: Mechanisms, Applications, and Challenges”. In: *Advanced Materials* 30.6 (2018), p. 1704407.

[20] John D.W. Madden. “Dielectric Elastomers as High-Performance Electroactive Polymers”. In: *Dielectric Elastomers as Electromechanical Transducers*. Elsevier, 2008. Chap. 2, pp. 13–21.

[21] Bertrand Tondu. “What Is an Artificial Muscle? A Systemic Approach.” In: *Actuators* 4.4 (2015), pp. 336–352.

[22] Hugh M. Herr and Roy D. Kornbluh. “New horizons for orthotic and prosthetic technology: artificial muscle for ambulation”. In: *Proceedings of SPIE (EAPAD)*. Vol. 5385. 2004, pp. 1–9.

[23] Amit P. Mulgaonkar, Roy Kornbluh, and Hugh Herr. “A new frontier for orthotics and prosthetics: Application of dielectric elastomer actuators to bionics”. In: *Dielectric Elastomers as Electromechanical Transducers*. Ed. by Federico Carpi et al. 2008. Chap. 19, pp. 189–206.

[24] Nicholas Kellaris et al. “Peano-HASEL actuators: Muscle-mimetic, electrohydraulic transducers that linearly contract on activation”. In: *Science Robotics* 3.14 (2018), eaar3276.

[25] Eric Acome et al. “Hydraulically amplified self-healing electrostatic actuators with muscle-like performance”. In: *Science* 359.6371 (2018), pp. 61–65.

[26] Ujjaval Gupta et al. “Soft robots based on dielectric elastomer actuators: a review”. In: *Smart Materials and Structures* 28.10 (2019), p. 103002.

[27] Federico Carpi, Andrea Mannini, and Danilo De Rossi. “Dynamic Splint-Like Hand Orthosis for Finger Rehabilitation”. In: *Biomedical Applications of Electroactive Polymer Actuators*. Ed. by Federico Carpi and Elisabeth Smela. Chichester, UK: John Wiley & Sons, Ltd, 2009. Chap. 24, pp. 443–461.

[28] Federico Carpi et al. “Enabling Variable-Stiffness Hand Rehabilitation Orthoses with Dielectric Elastomer Transducers”. In: *Medical Engineering & Physics* 36.2 (2014), pp. 205–211.

[29] Ahad Behboodi. “An Artificial Skeletal Muscle for Use in Pediatric Rehabilitation Robotics”. Ph.D. dissertation. University of Delaware, 2019.

[30] Christopher R. Kelley and Jeffrey L. Kauffman. “Tremor-Active Controller for Dielectric Elastomer-Based Pathological Tremor Suppression”. In: *IEEE/ASME Transactions on Mechatronics* Early Acce (2020).

[31] Shahram Pourazadi et al. “On the electrical safety of dielectric elastomer actuators in proximity to the human body”. In: *Smart Materials and Structures* 26.11 (2017).

[32] Zhigang Suo. “Theory of Dielectric Elastomers”. In: *Acta Mechanica Solida Sinica* 23.6 (2010), pp. 549–578.

[33] Gianluca Rizzello. “Modeling, Control and Self-Sensing of Dielectric Elastomer Actuators”. Ph.D. dissertation. Polytechnic University of Bari, 2016.

[34] L. J. Romasanta, M. A. Lopez-Manchado, and R. Verdejo. “Increasing the performance of dielectric elastomer actuators: A review from the materials perspective”. In: *Progress in Polymer Science* 51 (2015), pp. 188–211.

[35] James Biggs et al. “Electroactive Polymers: Developments of and Perspectives for Dielectric Elastomers”. In: *Angewandte Chemie - International Edition* 52.36 (2013), pp. 9409–9421.

[36] Samuel Rosset and Herbert R. Shea. “Flexible and stretchable electrodes for dielectric elastomer actuators”. In: *Applied Physics A* 110 (2013), pp. 281–307.

[37] Roy Kornbluh. “Fundamental configurations for dielectric elastomer actuators”. In: *Dielectric Elastomers as Electromechanical Transducers*. Ed. by Federico Carpi et al. 2008. Chap. 8, pp. 79–90.

[38] Jean-Sebastien Plante and Steven Dubowsky. “On the properties of dielectric elastomer actuators and their design implications”. In: *Smart Materials and Structures* 16.2 (2007).

[39] Micah Hodgins and Stefan Seelecke. “Systematic experimental study of pure shear type dielectric elastomer membranes with different electrode and film thicknesses”. In: *Smart Materials and Structures* 25.9 (2016).

[40] Micah Hodgins, Alexander York, and Stefan Seelecke. “Experimental Comparison of Bias Elements for Out-Of-Plane DEAP Actuator System”. In: *Smart Materials and Structures* 22.9 (2013), p. 094016.

[41] Marcus Rosenthal et al. “Designing components using smartMOVE electroactive polymer technology”. In: *Proceedings of SPIE (EAPAD)*. Ed. by Yoseph Bar-Cohen. Vol. 6927. 2008, p. 692704.

[42] Brett Kennedy, Chris Melhuish, and Andrew Adamatzky. “Biologically Inspired Robots”. In: *Electroactive Polymer (EAP) Actuators as Artificial Muscles: Reality, Potential, and Challenges*. 2nd ed. Bellingham, WA: SPIE, 2004. Chap. 17, pp. 583–619.

[43] Roy Kornbluh et al. “Application of Dielectric Elastomer EAP Actuators”. In: *Electroactive Polymer (EAP) Actuators as Artificial Muscles: Reality, Potential, and Challenges*. Ed. by Yoseph Bar-Cohen. 2nd ed. Bellingham: SPIE, 2004. Chap. 16, pp. 529–581.

[44] Manuel Cestari, Daniel Sanz-Merodio, and Elena Garcia. “A New and Versatile Adjustable Rigidity Actuator with Add-on Locking Mechanism (ARES-XL)”. In: *Actuators* 7.1 (2018).

[45] Edgar Bolívar et al. “Towards a Series Elastic Actuator with Electrically Modulated Stiffness for Powered Ankle-Foot Orthoses”. In: *IEEE International Conference on Automation Science and Engineering*. Fort Worth: IEEE, 2016, pp. 1086–1093.

[46] Stefan O. Schrade et al. “Development of VariLeg, an exoskeleton with variable stiffness actuation: First results and user evaluation from the CYBATHLON 2016”. In: *Journal of NeuroEngineering and Rehabilitation* 15 (2018).

[47] Rafael R. Torrealba, Samuel B. Udelman, and Edgar D. Fonseca-Rojas. “Design of variable impedance actuator for knee joint of a portable human gait rehabilitation exoskeleton”. In: *Mechanism and Machine Theory* 116 (2017), pp. 248–261.

[48] Ronald Pelrine and Roy D. Kornbluh. “Electromechanical Transduction Effects in Dielectric Elastomers: Actuation, Sensing, Stiffness Modulation and Electric Energy Generation”. In: *Dielectric Elastomers as Electromechanical Transducers*. Ed. by Federico Carpi et al. Elsevier Science, 2008. Chap. 1, pp. 3–12.

[49] Ronald Pelrine. “Variable Stiffness Mode: Devices and Applications”. In: *Dielectric Elastomers as Electromechanical Transducers*. Ed. by Federico Carpi et al. Elsevier Science, 2008. Chap. 14, pp. 141–145.

[50] Jean-Philippe Lucking Bigué and Jean-Sébastien Plante. “Experimental Study of Dielectric Elastomer Actuator Energy Conversion Efficiency”. In: *IEEE/ASME Transactions on Mechatronics* 18.1 (2013), pp. 169–177.

[51] Guggi Kofod. “The static actuation of dielectric elastomer actuators: how does pre-stretch improve actuation?” In: *Journal of Physics D: Applied Physics* 41.21 (2008), p. 215405.

[52] Gilles Marckmann and Erwan Verron. “Comparison of Hyperelastic Models for Rubber-Like Materials”. In: *Rubber Chemistry and Technology* 79.5 (2006), pp. 835–858.

[53] Paul Steinmann, Mokarram Hossain, and Gunnar Possart. “Hyperelastic models for rubber-like materials: Consistent tangent operators and suitability for Treloar’s data”. In: *Archive of Applied Mechanics* 82 (2012), pp. 1183–1217.

[54] Mokarram Hossain and Paul Steinmann. “More hyperelastic models for rubber-like materials: consistent tangent operators and comparative study”. In: *Journal of the Mechanical Behavior of Materials* 22.1-2 (2013), pp. 27–50.

[55] Kwangmok Jung et al. “Micro inchworm robot actuated by artificial muscle actuator based on nonprestrained dielectric elastomer”. In: *Proceedings of SPIE (EAPAD)*. Ed. by Yoseph Bar-Cohen. Vol. 5385. 2004, pp. 357–367.

[56] Gabor Kovacs et al. “Robotic arm”. In: *Dielectric Elastomers as Electromechanical Transducers*. Ed. by Federico Carpi et al. Elsevier Science, 2008. Chap. 27, pp. 279–289.

[57] Curtis M Ihlefeld and Zhihua Qu. “A Dielectric Electroactive Polymer Generator-Actuator Model: Modeling, Identification, and Dynamic Simulation”. In: *Proceedings of SPIE (EAPAD)*. Ed. by Yoseph Bar-Cohen. Vol. 6927. 2008, 69270R.

[58] Atsuo Orita and Mark R. Cutkosky. “Scalable Electroactive Polymer for Variable Stiffness Suspensions”. In: *IEEE/ASME Transactions on Mechatronics* 21.6 (2016), pp. 2836–2846.

[59] Hyouk Ryeol Choi et al. “Biomimetic Soft Actuator: Design, Modeling, Control, and Applications”. In: *IEEE/ASME Transactions on Mechatronics* 10.5 (2005), pp. 581–593.

[60] Gabor Kovacs and Lukas Düring. “Contractive tension force stack actuator based on soft dielectric EAP”. In: *Proceedings of SPIE (EAPAD)*. Vol. 7287. 2009, 72870A.

[61] Siavash Rezazadeh et al. “Robot Leg Design: A Constructive Framework”. In: *IEEE Access* 6 (2018), pp. 54369–54387.

[62] Elliott J. Rouse, Luke M. Mooney, and Hugh M. Herr. “Clutchable series-elastic actuator: Implications for prosthetic knee design”. In: *The International Journal of Robotics Research* 33.13 (2014), pp. 1611–1625.

[63] Kevin C. Galloway, Jonathan E. Clark, and Daniel E. Koditschek. “Variable Stiffness Legs for Robust, Efficient, and Stable Dynamic Running”. In: *Journal of Mechanisms and Robotics* 5.1 (2013), p. 011009.

[64] Martin Grimmer and André Seyfarth. “Stiffness Adjustment of a Series Elastic Actuator in an Ankle-Foot Prosthesis for Walking and Running: The Trade-Off Between Energy and Peak Power Optimization”. In: *IEEE International Conference on Robotics and Automation*. Shanghai: IEEE, 2011, pp. 1439–1444.

[65] Victor Grosu et al. “Design of Smart Modular Variable Stiffness Actuators for Robotic-Assistive Devices”. In: *IEEE/ASME Transactions on Mechatronics* 22.4 (2017), pp. 1777–1785.

[66] Bram Vanderborght et al. “Variable Impedance Actuators: A Review”. In: *Robotics and Autonomous Systems* 61.12 (2013), pp. 1601–1614.

[67] Amir Jafari, Hung Quy Vu, and Fumiya Iida. “Determinants for Stiffness Adjustment Mechanisms”. In: *Journal of Intelligent and Robotic Systems* 82 (2016), pp. 435–454.

[68] David J. Braun, Vincent Chalvet, and Abhinav Dahiya. “Positive–Negative Stiffness Actuators”. In: *IEEE Transactions on Robotics* 35.1 (2018), pp. 162–173.

[69] Stuart Diller, Carmel Majidi, and Steven H. Collins. “A Lightweight, Low-Power Electroadhesive Clutch and Spring for Exoskeleton Actuation”. In: *IEEE International Conference on Robotics and Automation*. Stockholm: IEEE, 2016, pp. 682–689.

[70] Sanjay Dastoor and Mark R. Cutkosky. “Design of Dielectric Electroactive Polymers for a Compact and Scalable Variable Stiffness Device”. In: *IEEE International Conference on Robotics and Automation*. Saint Paul: IEEE, 2012, pp. 3745–3750.

[71] Jason Newton et al. “Modeling and Characterization of Stiffness Controlled Robotic Legs Using Dielectric Elastomers”. In: *Proceedings of SPIE (EAPAD)*. Ed. by Yoseph Bar-Cohen. Vol. 8340. SPIE, 2012, 83400Z.

[72] Steffen Hau et al. “Design and Control of a High-Speed Positioning System Based on Dielectric Elastomer Membrane Actuators”. In: *IEEE/ASME Transactions on Mechatronics* 22.3 (2017), pp. 1259–1267.

[73] Giovanni Berselli et al. “Implementation of a Variable Stiffness Actuator Based on Dielectric Elastomers: A Feasibility Study”. In: *ASME Conference on Smart Materials, Adaptive Structures and Intelligent Systems*. Stone Mountain: ASME, 2012, pp. 497–506.

[74] Ronald Pelrine and Roy D. Kornbluh. “Dielectric Elastomers as Electroactive Polymers (EAPs): Fundamentals”. In: *Electromechanically Active Polymers. Polymers and Polymeric Composites: A Reference Series*. Ed. by Federico Carpi. Springer, Cham, 2016. Chap. 30, pp. 671–686.

[75] Ludo C. Visser, Raffaella Carloni, and Stefano Stramigioli. “Energy-Efficient Variable Stiffness Actuators”. In: *IEEE Transactions on Robotics* 27.5 (2011), pp. 865–875.

[76] Amir Jafari, Nikos Tsagarakis, and Darwin Caldwell. “Energy Efficient Actuators with Adjustable Stiffness: A Review on AwAS, AwAS-II and CompACT VSA Changing Stiffness Based on Lever Mechanism”. In: *Industrial Robot: An International Journal* 42.3 (2015), pp. 242–251.

[77] Gianluca Rizzello et al. “Modeling of the Effects of the Electrical Dynamics on the Electromechanical Response of a DEAP Circular Actuator with a Mass–Spring Load”. In: *Smart Materials and Structures* 24.9 (2015), p. 094003.

[78] Steffen Hau et al. “Performance prediction and scaling laws of circular dielectric elastomer membrane actuators”. In: *Journal of Mechanical Design* 140 (2018), p. 113501.

[79] Dake Wang. “The Most Energy Efficient Way to Charge the Capacitor in a RC Circuit”. In: *Physics Education* 52.6 (2017), p. 065019.

[80] Tianhu He, Xuanhe Zhao, and Zhigang Suo. “Dielectric Elastomer Membranes Undergoing Inhomogeneous Deformation”. In: *Journal of Applied Physics* 106 (2009), p. 083522.

[81] Jiangshui Huang et al. “The Thickness and Stretch Dependence of the Electrical Breakdown Strength of an Acrylic Dielectric Elastomer”. In: *Applied Physics Letters* 101 (2012), p. 122905.

[82] Guggi Kofod et al. “Actuation Response of Polyacrylate Dielectric Elastomers”. In: *Journal of Intelligent Material Systems and Structures* 14.12 (2003), pp. 787–793.

[83] Wolfgang G. Knauss, Igor Emri, and Hongbing Lu. “Mechanics of Polymers: Viscoelasticity”. In: *Springer Handbook of Experimental Solid Mechanics*. Ed. by W Sharpe. Boston: Springer US, 2008. Chap. 3, pp. 49–95.

[84] L. Di Lillo et al. “Measurement of Insulating and Dielectric Properties of Acrylic Elastomer Membranes at High Electric Fields”. In: *Journal of Applied Physics* 111.2 (2012), p. 024904.

[85] *Capacitance Leakage Current Measurement Techniques Using the B2985A/87A*. Tech. rep. Keysight Technologies, 2018.

[86] Matthias Kollosche et al. “Complex Interplay of Nonlinear Processes in Dielectric Elastomers”. In: *Physical Review E* 85.5 (2012), p. 051801.

[87] Karali Patra and Raj Kumar Sahu. “A Visco-Hyperelastic Approach to Modelling Rate-Dependent Large Deformation of a Dielectric Acrylic Elastomer”. In: *International Journal of Mechanics and Materials in Design* 11 (2015), pp. 79–90.

[88] Roy D. Kornbluh et al. “Long-lifetime All-polymer Artificial Muscle Transducers”. In: *MRS Proceedings* 1271 (2010), 1271–JJ03–01.

[89] Matteo Laffranchi, Nikos G. Tsagarakis, and Darwin G. Caldwell. “Analysis and Development of a Semiactive Damper for Compliant Actuation Systems”. In: *IEEE/ASME Transactions on Mechatronics* 18.2 (2013), pp. 744–753.

[90] Roy D. Kornbluh and Ronald Pelrine. “High-Performance Acrylic and Silicone Elastomers”. In: *Dielectric Elastomers as Electromechanical Transducers*. Ed. by Federico Carpi et al. Elsevier Science, 2008. Chap. 4, pp. 33–42.

[91] Frederikke B. Madsen et al. “The Current State of Silicone-Based Dieletric Elastomer Transducers”. In: *Macromolecular Rapid Communications* 37 (2016), pp. 378–413.

[92] Herbert Shea et al. “Dielectric Elastomers as EAPs: How to Start Experimenting with Them”. In: *Electromechanically Active Polymers. Polymers and Polymeric Composites: A Reference Series.* Ed. by Federico Carpi. Springer, Cham, 2016. Chap. 34, pp. 767–787.

[93] Mitja Babič et al. “An Electronic Driver for Improving the Open and Closed Loop Electro-Mechanical Response of Dielectric Elastomer Actuators”. In: *Mechatronics* 20.2 (2010), pp. 201–212.

[94] Alexandre Poulin, Samuel Rosset, and Herbert R. Shea. “Printing Low-Voltage Dielectric Elastomer Actuators”. In: *Applied Physics Letters* 107.24 (2015), p. 244104.

[95] Julian Vincent. “Basic Elasticity and Viscoelasticity”. In: *Structural Biomaterials*. 3rd ed. Princeton University Press, 2012. Chap. 1, pp. 1–28.

[96] Jeremy Farley. “Controlling drop foot: Beyond standard AFOs”. In: *Lower Extremity Review* (2009).

[97] Joaquin A. Blaya and Hugh Herr. “Adaptive Control of a Variable-Impedance Ankle-Foot Orthosis to Assist Drop-Foot Gait”. In: *IEEE Transactions on Neural Systems and Rehabilitation Engineering* 12.1 (2004), pp. 24–31.

[98] Alexander W. Boehler et al. “Design, implementation and test results of a robust control method for a powered ankle foot orthosis (AFO)”. In: *IEEE International Conference on Robotics and Automation*. IEEE, 2008, pp. 2025–2030.

[99] Steven H. Collins, M. Bruce Wiggin, and Gregory S. Sawicki. “Reducing the energy cost of human walking using an unpowered exoskeleton”. In: *Nature* 522 (2015), pp. 212–215.

[100] Matthew B. Yandell, Joshua R. Tacca, and Karl E. Zelik. “Design of a Low Profile, Unpowered Ankle Exoskeleton That Fits Under Clothes: Overcoming Practical Barriers to Widespread Societal Adoption”. In: *IEEE Transactions on Neural Systems and Rehabilitation Engineering* 27.4 (2019), pp. 712–723.

[101] Junji Furusho et al. “Development of Shear Type Compact MR Brake for the Intelligent Ankle-Foot Orthosis and Its Control; Research and Development in NEDO for Practical Application of Human Support Robot”. In: *IEEE International Conference on Rehabilitation Robotics*. IEEE, 2007, pp. 89–94.

[102] Wolfgang Svensson and Ulf Holmberg. “Ankle-Foot-Orthosis Control in Inclinations and Stairs”. In: *IEEE Conference on Robotics, Automation and Mechatronics*. IEEE, 2008, pp. 301–306.

[103] J. Perry, J. M. Burnfield, and Lydia Cabico. *Gait Analysis: Normal and Pathological Function*. 2nd ed. Thorofare, NJ: Slack, 2010.

[104] David A. Winter. *Biomechanics and motor control of human gait: normal, elderly and pathological*. 1991.

[105] Ho Cheong Lo et al. “Transferring electrical energy between two dielectric elastomer actuators”. In: *Sensors and Actuators, A: Physical* 212 (2014), pp. 123–126.

[106] Ho Cheong Lo. “Converters for Milliwatt Dielectric Elastomer Generators”. Ph.D. dissertation. University of Auckland, 2015.

[107] Ashok K. Singal. “The Paradox of Two Charged Capacitors – A New Perspective”. In: *Physics Education* 31.4 (2015).

[108] Ryan Little. “Manufacturing Methods for Medium-Volume Production of Planar Dielectric Elastomer Actuators”. Master’s thesis. The University of Texas at Dallas, 2020.

[109] Alexandre Poulin and Samuel Rosset. “An open-loop control scheme to increase the speed and reduce the viscoelastic drift of dielectric elastomer actuators”. In: *Extreme Mechanics Letters* 27 (2019), pp. 20–26.

[110] Toma Kobayashi and Stoyan K. Smoukov. “Pulsed actuation avoids failure in dielectric elastomer artificial muscles”. In: *International Journal of Smart and Nano Materials* 5.4 (2014), pp. 217–226.

[111] Junjie Sheng et al. “Thermal, Mechanical, and Dielectric Properties of a Dielectric Elastomer for Actuator Applications”. In: *Journal of Macromolecular Science, Part B* 51.10 (2012), pp. 2093–2104.

[112] Zisheng Liao et al. “On thermo-viscoelastic experimental characterisation and numerical modelling of VHB polymer”. In: *International Journal of Non-Linear Mechanics* 118 (2020), p. 103263.

[113] Christian Bolzmacher, James Biggs, and Mandayam Srinivasan. “Flexible dielectric elastomer actuators for wearable human-machine interfaces”. In: *Proceedings of SPIE (EAPAD)*. Vol. 6168. 2006, p. 616804.

[114] Roy D. Kornbluh et al. “Rubber to rigid, clamped to undamped: toward composite materials with wide-range controllable stiffness and damping”. In: *Proceedings of SPIE*. Ed. by Eric H. Anderson. Vol. 5388. 2004, pp. 372–386.

[115] Sanjay Dastoor and Mark Cutkosky. “Variable impedance due to electromechanical coupling in electroactive polymer actuators”. In: *IEEE/RSJ International Conference on Intelligent Robots and Systems*. 2011, pp. 774–779.

[116] Sanjay Dastoor et al. “Jumping Robot with a Tunable Suspension Based on Artificial Muscles”. In: *Biomimetic and Biohybrid Systems, Living Machines 2012, Lecture Notes in Computer Science, vol 7375*. Ed. by Tony Prescott et al. Springer, Berlin, Heidelberg, 2012, pp. 95–106.

[117] Paul Brochu and Qibing Pei. “Advances in dielectric elastomers for actuators and artificial muscles”. In: *Macromolecular Rapid Communications* 31.1 (2010), pp. 10–36.

[118] Christa Jordi et al. “Performance evaluation of cutting-edge dielectric elastomers for large-scale actuator applications”. In: *Smart Materials and Structures* 20 (2011), p. 075003.

[119] Mohamed Benslimane, Hans-Erik Kiil, and Michael Tryson. “Electromechanical properties of novel large strain PolyPower film and laminate components for DEAP actuator and sensor applications”. In: *Proceedings of SPIE (EAPAD)*. Ed. by Yoseph Bar-Cohen. Vol. 7642. 2010, p. 764231.

[120] Heather Lai. “Induced damping and its relationship to beneficial energy harvesting in dielectric elastomers with application to walking”. Ph.D. dissertation. Wayne State University, 2013.

[121] *Outstanding silicone properties in a new shape: ELASTOSIL film*. promotional document. Wacker Chemie AG. URL: https://www.wacker.com/h/medias/6924-EN.pdf.

[122] Marc Hill, Gianluca Rizzello, and Stefan Seelecke. “Development and validation of a fatigue testing setup for dielectric elastomer membrane actuators”. In: *Smart Materials and Structures* 28.5 (2019), p. 055029.

[123] E.-F. Markus Henke, Katherine E. Wilson, and Iain A. Anderson. “Entirely soft dielectric elastomer robots”. In: *Proceedings of SPIE (EAPAD)*. Ed. by Yoseph Bar-Cohen. Vol. 10163. Portland, 2017, 101631N.

[124] Nitesh Arora, Pramod Kumar, and M. M. Joglekar. “A Modulated Voltage Waveform for Enhancing the Travel Range of Dielectric Elastomer Actuators”. In: *Journal of Applied Mechanics* 85.11 (2018), p. 111009.

[125] Tobias Pointner and Michael Wegener. “Low voltage driven dielectric membrane actuators integrated into fast switching electronic circuit boards”. In: *Smart Materials and Structures* 28.8 (2019), p. 084002.

[126] *NEXIPAL silicone laminates: powerful performance - layer on layer*. promotional document. Wacker Chemie AG. URL: https://www.wacker.com/h/medias/7743-EN.pdf.

[127] John D. Vogan. “Development of Dielectric Elastomer Actuators for MRI Devices”. Master’s thesis. Massachusetts Institute of Technology, 2004.

[128] Thanh-Giang La et al. “High stress actuation by dielectric elastomer with oil capsules”. In: *Proceedings of SPIE (EAPAD)*. Vol. 9056. 2014, p. 90560X.

[129] Runan Zhang et al. “Novel Arrangements for High Performance and Durable Dielectric Elastomer Actuation”. In: *Actuators* 5.3 (2016).

[130] *ELASTOSIL Film 2030*. product webpage. Wacker Chemie AG. URL: https://www.wacker.com/h/en-us/c/elastosil-film-2030/p/000038005.

BIOGRAPHICAL SKETCH

David Allen is a native of the north Dallas area, where he was homeschooled through high school, graduating in 2008. He began his engineering education at Collin College and then transferred to The University of Texas at Dallas (UTD) in 2012. He graduated with his bachelor's degree *Summa Cum Laude* in 2014.

Desiring a career in robotics, David continued on at UTD for graduate school and earned his master's degree in 2016 and his doctoral degree in 2020. His research addressed designing powered prostheses and orthoses to use an artificial muscle technology. After graduation, he pursued an engineering career in industry.

CURRICULUM VITAE

David P. Allen

david.allen@utdallas.edu
linkedin.com/in/dallen5221

Summary of qualifications

Modeling and simulation experience: developed MATLAB models and simulations for exoskeleton and polymer actuator research yielding a patent application

Excellent teamwork and leadership skills: mentored seven undergraduate reseachers, collaborated in research team, and led senior design team using systems engineering processes

Strong verbal and written communication skills: conveyed behavior of polymer actuators created with additive manufacturing in three publications and two international conference presentations

Education
The University of Texas at Dallas (UTD)

Degrees in Mechanical Engineering

Ph.D.	GPA 3.857	2020
M.S.	GPA 3.818	2016
B.S.	GPA 4.000	2014

Research assistant
UTD, 2015–present

Collaborated with experts and used Solidworks, MATLAB, and ANSYS for modeling and simulation of hybrid polymer actuator to make design decisions resulting in patent application

Mentored junior team members in experiment design, polymer modeling, and data analysis for design of polymer actuators and an ankle exoskeleton

Used written communication and data visualization skills in MS Office and LaTeX to analyze actuator performance and novel electrode design in three publications

Communicated complex ideas to audiences ranging from high schoolers to technical experts in more than ten internal and three external PowerPoint presentations

Used additive manufacturing (3D printing) techniques to improve repeatability of manufacturing processes for polymer actuators

Teaching assistant
UTD, 2014–2015

Taught students to model and simulate devices using MATLAB and Solidworks and program microcontrollers with C++ contributing to 89 % of students passing

Coordinated with team for additive manufacturing of student project components

Senior design team leader
UTD, 2014

Led team that used CREO for modeling two chess piece robots and for simulating stresses in their additively manufactured components

Managed team using systems engineering processes: defined functional baseline, developed concepts, scheduled in MS Project, and met required and stretch goals

Research intern
UTD, 2012

Developed haptics and computer vision software in C++ for simulating augmented reality robotic surgery using OpenCV

Customer service representative
DBI, 2008–2012

Resolved conflicts with customers and managed product returns contributing to the company's 99 % positive feedback rating on eBay

Patent application

"Variable Stiffness Actuator with Electrically Modulated Stiffness." R.D. Gregg, E.A. Bolívar, D.P. Allen, W. Voit. U.S. patent app. 16/111,072. 2018

Publications and presentations

"Mechanical Simplification of Variable-Stiffness Actuators Using Dielectric Elastomer Transducers." D.P. Allen, E. Bolívar, S. Farmer, W. Voit, R.D. Gregg.

Published in *Actuators*. 2019, *8*, 44. DOI: 10.3390/act8020044

"Stretchable Conductive Fabric Simplifies Manufacturing of Low-Resistance Dielectric Elastomer System Electrodes." D.P. Allen, S.E. Farmer, R.D. Gregg, W. Voit.

Presented at *SPIE Electroactive Polymers and Devices XX*
Published in *Proceedings of SPIE*, 2018, vol. 10594, pages 1059412. DOI: 10.1117/12.2292108

"Towards a Series Elastic Actuator with Electrically Modulated Stiffness for Powered Ankle-Foot Orthoses." E. Bolívar, D. Allen, G. Ellson, J. Cossio, W. Voit, R. Gregg.

Presented at 2016 *IEEE International Conf. on Automation Science and Engineering*
Published in conference proceedings, pages 1086–1093. DOI:10.1109/COASE.2016.7743525